Light to Shape the Future: From Photolithography to 4D Printing

*Jesús del Barrio and Carlos Sánchez-Somolinos**

Over the last few decades, the demand of polymeric structures with well-defined features of different size, dimension, and functionality has increased from various application areas, including microelectronics, biotechnology, tissue engineering, and photonics, among others. The ability of light to control over space and time physicochemical processes is a unique tool for the structuring of polymeric materials, opening new avenues for technological progress in different fields of application. This article gives an overview of various photochemical reactions in polymers, photosensitive materials, and structuring techniques making use of light, and highlights most recent advances, emerging opportunities, and relevant applications.

1. Introduction

The production of structures with well-defined features at the micro- and submicrometer scales is key to a multitude of scientific areas and industries spanning from microelectronics to tissue engineering. Since the 1970s, the semiconductor industry has led the development of topographically patterned surfaces with submicrometer resolution and set the trend toward producing increasingly complex patterned films and miniaturized devices, which are required in modern information and communication technologies.[1] In addition to semiconductor device fabrication, a host of applications for patterned thin films and structured polymeric systems have been identified over the last two decades in areas including optics, energy harvesting, biotechnology, and medicine.[2]

Our ability to structure polymeric materials has grown tremendously and the palette of materials and techniques to achieve a quick and reliable production of patterns with increasing resolution is quite extensive. This boom has been largely sustained by the development of specific photonic technologies, such as advanced light sources or spatial light modulators, photosensitive materials, and, more importantly, our growing knowledge of the interaction between light and matter. Indeed, the ability to control a chemical reaction with light in a remote fashion is a powerful concept. Light irradiation can initiate a photochemical process that otherwise would not occur at ambient conditions. This property lies at the origin of the temporal control afforded by simply turning the light source on and off. Moreover, patterned illumination or the use of focused light beams enables control of not only when, but also where a photoinduced transformation occurs. The photochemical processes occurring in many polymers and resists can be effectively manipulated by fine-tuning the intensity and frequency of light. However, these are just two of the primary properties of light, and there are specific photoresponsive systems that enable the generation of ordered structures by adjusting the polarization of light, in addition to intensity and frequency.

In this review, an overview of photochemical reactions, photosensitive polymers, and light-based structuring techniques is provided. As this field is too broad to be covered in depth in one single article, some recent examples and applications, as well as emerging opportunities and trends, are highlighted throughout the discussion. Section 2 is focused on light-induced reactions and photosensitive materials. The fundamentals of photochemical reactions and their implementation in polymer science have been overviewed in many excellent books and reviews.[3] In Section 2, rather than being comprehensive, emphasis is given to those photochemical processes lying at the basis of those structuring techniques that are later discussed in Section 3. Some of these techniques, including conventional mask lithographies, interference lithographies, direct laser writing (DLW) with one- or two-photon processes, or stereolithographic techniques, make use of light as a structuring tool.

There is an additional group of techniques where light is employed to set a structure created beforehand through a

Dr. J. del Barrio
Departamento de Química Orgánica
Facultad de Ciencias
Instituto de Ciencia de Materiales de Aragón (ICMA)
CSIC–Universidad de Zaragoza
50009 Zaragoza, Spain

Dr. J. del Barrio
Instituto Universitario de Investigación en Nanociencia de Aragón
Universidad de Zaragoza
50018 Zaragoza, Spain

Dr. C. Sánchez-Somolinos
Departamento de Física de la Materia Condensada
Facultad de Ciencias
Instituto de Ciencia de Materiales de Aragón (ICMA)
CSIC–Universidad de Zaragoza
50009 Zaragoza, Spain
E-mail: carlos.s@csic.es

Dr. C. Sánchez-Somolinos
CIBER in Bioengineering, Biomaterials and Nanomedicine (CIBER-BBN)
28029 Madrid, Spain

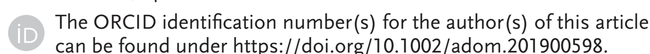
The ORCID identification number(s) for the author(s) of this article can be found under https://doi.org/10.1002/adom.201900598.

© 2019 The Authors. Published by WILEY-VCH Verlag GmbH & Co. KGaA, Weinheim. This is an open access article under the terms of the Creative Commons Attribution-NonCommercial-NoDerivs License, which permits use and distribution in any medium, provided the original work is properly cited, the use is non-commercial and no modifications or adaptations are made.

The copyright line was changed on 17 July 2019 after initial publication.

DOI: 10.1002/adom.201900598

© 2019 The Authors. Published by WILEY-VCH Verlag GmbH & Co. KGaA, Weinheim

process that does not necessarily employ light irradiation. For example, in extrusion-based 3D printing of photopolymerizable materials, a system achieves a structured state after being extruded through an orifice. The photopolymer is digitally deposited and a subsequent light-induced curing step allows the material to maintain the structured shape-sustaining state. Some additional techniques that require a light-enabled fixing process include UV-assisted nanoimprinting lithography (NIL) or the inkjet printing of photosensitive materials.

A special focus is placed on materials responding to light polarization in Section 4. While most photoinduced processes depend on the wavelength and intensity of light, some photosensitive polymeric materials are able to capture the information associated with the polarization state of light, thus enabling an additional degree of control on the material morphology.[4] This feature can result in optical or mechanical anisotropic properties. Recent advances in the field of photoinduced alignment of polymeric materials with application in optics, nanolithography, and soft actuators will also be highlighted.

Jesús del Barrio completed his Ph.D. degree at the University of Zaragoza, Spain, in 2010 in the area of photoresponsive polymers for optical applications. He then moved to the UK to work on supramolecular materials with Professor Oren A. Scherman at the University of Cambridge. In 2014, he took up a position as a research scientist at the Schlumberger Gould Research Center in Cambridge, UK. Since 2017, he has been a Ramón y Cajal Research Fellow at the University of Zaragoza. His work encompasses both fundamental and applied research in soft matter systems, dynamic polymeric materials, and supramolecular chemistry.

Carlos Sánchez-Somolinos, Ph.D. in Physics (University of Zaragoza, Spain), is currently a Tenured Scientist of the Spanish National Research Council (CSIC) and Deputy Director at the Institute of Materials Science of Aragon (ICMA). He leads the Advanced Manufacturing Laboratory at ICMA. His expertise and current scientific objectives are focused on the development of materials and their processing through the use of advanced microstructuring techniques in the search of surfaces or functional systems of interest in the areas of optics, biomedicine, and soft robotics. He is coordinator of the H2020 FET-OPEN European Project PRIME.

2. Photoinduced Reactions

The chemical reactivity, including photochemical transformations, of a given molecule is intimately linked to its electron distribution. When a ground-state molecule or chromophore AB (**Scheme 1**) becomes excited to AB* upon light irradiation, a photochemical reaction may initiate leading to an intermediate species I, which then undergoes either a photophysical or photochemical transformation (Scheme 1).[3a]

The excited species, AB*, may react or lose its excess energy in a variety of ways, as depicted in **Scheme 2**. Those pathways that imply a chemical transformation include i) isomerization, ii) direct reaction, and iii) dissociation. Pathway (i) is associated with the *E*–*Z* isomerization of specific molecules containing a double bond. In this case, the double bond becomes in effect a single bond in the excited state, thus permitting, for example, rotation. In pathway (ii), the excitation energy is used to promote a reaction that otherwise would not be possible from the ground electronic state. For pathway (iii), the energy of the absorbed photon induces the break-up of a covalent bond of the excited species.

Other pathways include, but are not limited to, iv) intermolecular energy transfer, v) intramolecular energy transfer, vi) luminescence, vii) physical quenching, viii) and ionization. The pathways in Scheme 2 for loosing excitation are all primary processes that, in some cases, are accompanied by the generation of new products. Such products can subsequently be involved in secondary thermal reactions. As mentioned earlier, only pathways (i), (ii), and (iii) lead to primary photochemical processes, and these will be discussed in more detail in Sections 2.1, 2.2, and 2.3, respectively. In Section 2.4, we highlight a few examples of the so-called photoinitiated click reactions. These are useful and highly efficient bond-forming processes with growing popularity that, while not being strictly photosensitive, have been tuned in such a way that spatiotemporal control is achieved.

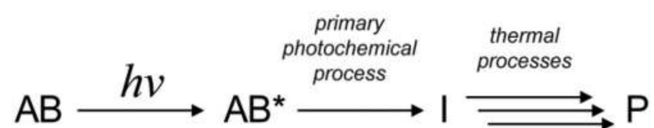

Scheme 1. A general paradigm of organic photochemistry. The absorption of a photon ($h\nu$) by AB generates and electronically excited state AB*. The primary chemical reaction of AB* produces a thermally equilibrated ground-state reactive intermediate, I, which subsequently reacts, via one or more thermally induced secondary processes, leading to the observed product, P.

2.1. Isomerization

A wide variety of isomerization processes can be induced photochemically, including those associated with azines and stilbenes. Particularly important is the isomerization of azobenzenes, such as compound **1** in **Figure 1**, which has been employed to produce highly ordered structures in a host of polymeric materials.[5]

Azobenzene (**1** in Figure 1a) is composed of two phenyl rings linked together through an azo double bond (−N=N−)

© 2019 The Authors. Published by WILEY-VCH Verlag GmbH & Co. KGaA, Weinheim

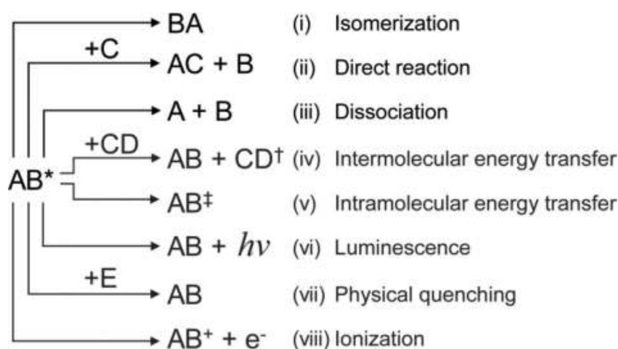

Scheme 2. Several pathways for loss of electronic excitation. Excited electronic states are indicated with symbols *, †, and ‡. Pathways (i), (ii), and (iii) imply a chemical transformation.

and can exist either in the thermodynamically stable *trans* state or in the metastable *cis* isomerization state. While the *trans* isomer exhibits a rigid and planar rodlike geometry, the *cis* isomer is nonplanar with a −C−N=N−C− dihedral angle approaching 173°.[6] The electronic absorption maximum of azobenzenes can be shifted from the UV to the red-visible region by the appropriate selection of the ring substituents. More interestingly, azobenzenes cleanly and reversibly isomerize between the *trans* and the *cis* isomeric states. This property together with the fact that azobenzenes are a relatively robust and chemically stable class of chromophores has prompted extensive studies in a number of research areas, including holography, surface patterning, and maskless photolithographies.[7] Azobenzene has been derivatized in a number of ways and there exist a wide range of interesting molecular systems, including polymers, dendrimers, surfactants, macrocycles, and liquid crystals (LCs), into which azobenzenes have been incorporated.[7d,8]

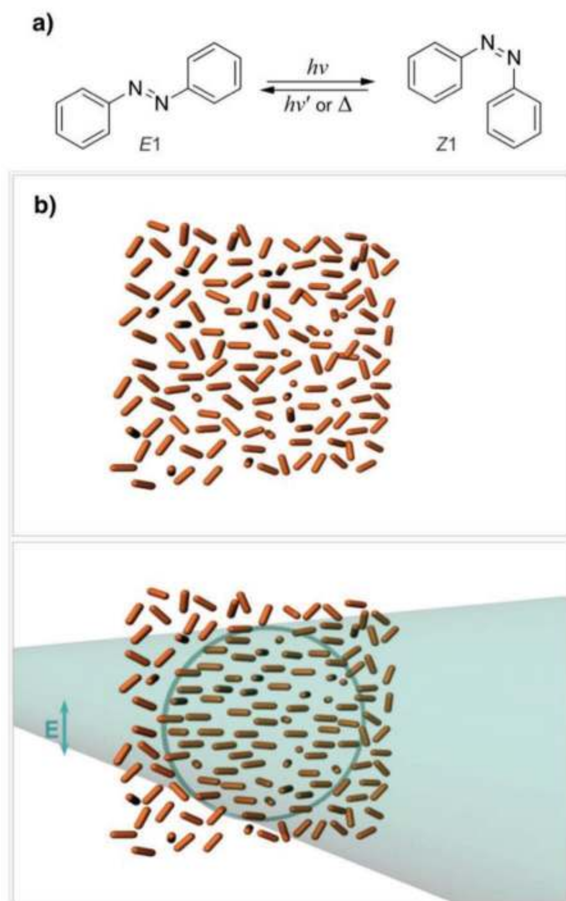

Figure 1. a) The *E–Z* isomerization of azobenzene. b) Photoinduced alignment of azobenzene moieties (Weigert effect). Reproduced with permission.[7a] Copyright 2009, The Royal Society of Chemistry.

As mentioned earlier, the introduction of ring substituents alters the properties of azobenzenes. These chromophores can be classified into one of the three types—azobenzene type, aminoazobenzene type, and pseudo-stilbene type—according to the relative positions of the electronic absorption bands associated with the n–π^* and π–π^* transitions.[9] Compound **1** in Figure 1 belongs to the azobenzene-type molecules, which exhibits a high-intensity π–π^* absorption band in the UV region and a low-intensity n–π^* absorption band in the visible region. A substitution pattern of electron-donating groups in the *ortho* or *para* positions, such as that of 4-aminoazobenzene, induces a redshift of the π–π^* absorption band; therefore, the absorption bands of aminoazobenzene-type molecules are typically overlapped. This effect, which is associated with an increase in the energy of the π orbital and a decrease in the energy of the π^* orbital, is further enhanced in azobenzene molecules of the pseudo-stilbene type. These compounds commonly present a push–pull-type substitution pattern with electron-acceptor (such as a nitro group) and electron-donor (e.g., an amino group) groups at the 4 and 4′ positions. The relative differences in the energy of the relevant orbitals of azobenzene molecules determine not only their electronic absorption but also their rates of isomerization and the composition of the photostationary states (see below).

The azobenzene isomerization can proceed via a rotation or an inversion mechanism about the −N=N− bond, although it is still a subject of debate.[10] The conversion of the *trans* to the *cis* isomer reduces the distance between the 4 and 4′ positions from 9.0 to 5.5 Å.[11] In addition to increasing the bulkiness of the molecule, the switch of the *trans* to the *cis* isomer is also accompanied by an increase in the dipole moment—the *trans* isomer of compound **1** has no dipole moment, whereas the dipole moment of the *cis* isomer is ≈3 D.[12]

Similarly to the *trans* isomer, the *cis* isomer also exhibits a π–π^* absorption band in the UV region and a n–π^* absorption band in the visible region; however, the n–π^* absorption band of the *cis* isomer is more intense than that of the *trans* isomer. The π–π^* absorption band of the *cis* isomer is blueshifted and less intense than that of the *trans* isomer. The irradiation of azobenzenes with light of the appropriate frequency induces the interconversion of the *trans* and *cis* isomers with minor fatigue, provided the illumination conditions are moderate. Azobenzene molecules in the *cis* state can thermally relax and return to the *trans* state. While the light-induced reactions take place on scales of a few picoseconds, the *cis*-to-*trans* thermal relaxation happens on the range of milliseconds to days, depending on the substituents of the chromophore and the molecular environment.[13] It is important to note that the large changes of the molecular geometry, free volume requirements, and dipole

© 2019 The Authors. Published by WILEY-VCH Verlag GmbH & Co. KGaA, Weinheim

moment associated with the *cis*-to-*trans* isomerization have vast implications in specific macroscopic properties of the materials into which azobenzene has been incorporated.[14] The isomerization process has a significant effect not only at the closest environment of azobenzenes but also across multiple length scales. Light can alter, for example, the degree of order of liquid crystal systems or even induce their isotropization.[15]

Since the absorption bands of the *trans* and the *cis* isomers are relatively broad and typically overlap, it is possible to trigger both the *trans*-to-*cis* and *cis*-to-*trans* isomerization processes with light of the appropriate frequency. Under these conditions, azobenzene molecules undergo a number of *trans–cis–trans* isomerization cycles in an iterative fashion, which induces a stochastic reorientation of the molecules in the exposed media.[16] The selection rules of the absorption process dictate that the transition probability is proportional to $\cos^2\theta$, where θ is the angle formed by the direction of the electric field of light and the direction of transition dipole moment of the absorbing species.[17] In the case of the *trans* isomer of azobenzenes, the transition dipole moment is parallel to the long molecular axis. Therefore, the exposure of a randomly oriented population of azobenzenes to linearly polarized light (LPL) initiates a cyclic *trans–cis–trans* isomerization process during which the orientation of the long molecular axis of the *trans* azobenzenes varies in each isomerization cycle. After a number of cycles, some of the *trans*-azobenzenes become preferentially oriented with their long molecular axis perpendicular to the polarization direction of light, and stop reorienting as they do not absorb photons in this orientation. In the absence of rotational diffusion, this photoinduced orientation remains even if the light irradiation continues. The overall process results in a population of azobenzenes with a large fraction of molecules preferentially oriented in a direction orthogonal to the direction of the polarization of light. This phenomenon, schematically shown in Figure 1b, is known as the Weigert effect.[18] Such a molecular orientation gives origin, in the relatively condensed state of polymer films where thermal rotation diffusion is limited, to strong birefringence in the areas exposed to polarized light, since the *trans* isomer exhibits anisotropic molecular polarizability. The photoinduced order can easily be reverted or reconfigured, and a new alignment can be induced by simply rotating the linear polarization direction. The system can be reverted to the isotropic state by using nonpolarized or circularly polarized light.[19] The possibility of photoinducing anisotropy has been extensively studied and a wide range of azobenzene-containing polymers and liquid crystals have been proposed as technology materials for reversible optical data storage and volume holography.[20,21] Additional photoinduced effects and the generation of orientational patterns in azobenzene-containing films and related applications will be discussed in Section 4.

2.2. Direct Reaction

In addition to isomerization, an electronically excited species resulting from the absorption of radiation can promote a reaction—an activation barrier can be surpassed after excitation or a reaction occurs as a result of a new electronic rearrangement—that is not possible for the ground electronic state (Scheme 2). The excited species can react with a separate molecule in an *intermolecular* process. An *intramolecular* process can also occur if one functional group of the excited molecule reacts with another group of the same species. Such process leads to a rearrangement (see below).

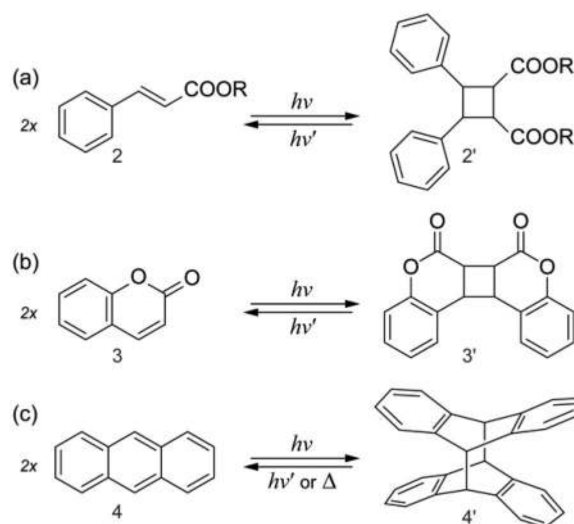

Figure 2. The reversible photoinduced cycloaddition of a) cinnamate, b) coumarin, and c) anthracene.

Cycloaddition reactions are one notable group of *intermolecular* bond-forming processes that have been extensively employed in organic and polymer synthesis.[22] One of the most widely applied cyclization reactions is the [2 + 2] photodimerization of cinnamates (**Figure 2**a).[23] Such a reaction has been commonly used for the generation of insoluble cross-linked systems having therefore these materials application as photoresists.[24] The library of cinnamate-functionalized materials has been significantly expanded in the last few decades and cross-linked cinnamate-containing polymers have been used in a wide range of areas and applications including hydrogel and elastomer systems and photoalignment layers for liquid crystals (see Section 4).[25]

Another light-induced bond formation reaction is the [2 + 2] photodimerization of coumarin derivatives (Figure 2b). Such a process, which yields the corresponding cyclobutane dimer, takes place upon irradiation with light of $\lambda > 300$ nm, and can be reverted by using UV light with a shorter wavelength. Similarly to cinnamate materials, coumarin-containing polymers have been exploited in both cross-linked systems and liquid crystal photoalignment.[26]

The photodimerization of anthracene is another well-known photochemical reaction. Anthracene and many anthracene derivatives have the ability to photodimerize via a [4 + 4] cycloaddition under excitation with UV light ($\lambda \approx 366$ nm) (Figure 2c).[27] The resulting dimers can be reverted either thermally at a temperature higher than 180 °C or photochemically with UV light irradiation of $\lambda < 300$ nm. The photochromic properties of anthracence derivatives are associated with the reduction in the degree of the conjugation of these systems upon dimerization and a significant change in molecular

© 2019 The Authors. Published by WILEY-VCH Verlag GmbH & Co. KGaA, Weinheim

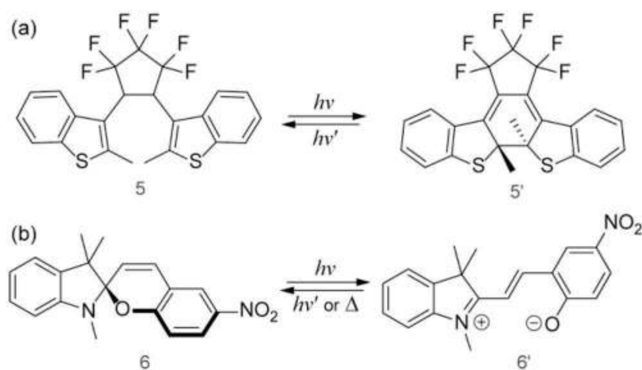

Figure 3. The reversible photoinduced electrocyclization of a) diarylethene and b) spiropyran derivatives.

geometry. This behavior has been exploited in the design of optical, electronic, and magnetic switches in polymers, liquid crystals, and crystalline materials.[28] The clean and reversible switching between unimers and dimers offers an excellent opportunity to remotely control the degree of cross-linking in polymeric networks, which can be employed for producing ordered structures and patterns.[29]

In contrast to the *intermolecular* bond-forming processes associated with cinnamate, coumarin, and anthracene derivatives, *intramolecular* rearrangements can also occur after light excitation. Diarylethenes (**5** in **Figure 3**), spiropyrans (**6** in Figure 3), spirooxazines, and fulgides/fulgimides are capable of undergoing photoinduced electrocyclizations that, broadly, can be seen as *intramolecular* rearrangements (Figure 3). The molecular changes accompanying the light-induced processes in electrocyclic photochromic compounds can propagate across multiple length scales providing an opportunity to selectively modify some of the bulk properties—such as the refractive index and glass transition—of the materials into which photochromic molecules have been incorporated.[30] Recently, diarylethenes, spirothiopyrans, and spirooxazines have also enabled the production of patterns with features on the micro- and nanoscale by employing various laser patterning techniques.[31]

2.3. Dissociation

As mentioned earlier, light absorption can also induce the break-up of a covalent bond of specific excited species. Such a bond-breaking process may be classified into one of the following categories: i) deprotection, ii) generation of radical species, and iii) the formation of ionic reactive intermediates. It should be mentioned that the dimerized species of coumarin, cinnamate, and anthracene derivatives, mentioned in the previous section, can revert to their individual components by undergoing a retrocyclization (Figure 2). This, in essence, is an additional dissociation reaction. For the sake of clarity, this section will focus exclusively on those bond-breaking reactions associated with deprotection reactions or the generation of radical or ionic species, which are the basis for a wide variety of technologies and structuring strategies in polymer science.

2.3.1. Photoinduced Deprotection for Polymer Structuring

The chemistry of photolabile groups is varied and rich and numerous phototriggered caging reactions have been shown to provide spatiotemporal control over, for example, the release of chemicals and the functionalization of surfaces.[32] One of the most common photolabile groups are *o*-nitrobenzyl derivatives, which photocleave at the *ortho* position to generate a new functionality including alcohols and acids (**Figure 4**a).[33] The implementation of the photoinduced bond breaking of *o*-nitrobenzyl derivatives in polymer chemistry was proposed by Anseth and coworkers who developed hydrogels for cell culture composed of a poly(ethylene glycol) cross-linked network with nitrobenzyl ether–derived linkages at specific positions of the network.[34] Such a cross-linked system exhibits a selective degradation upon exposure to UV and blue light. Photolysis can also be triggered with infrared (IR) light through two-photon absorption (TPA) processes. The photoinduced deprotection of *o*-nitrobenzyl polymeric derivatives has been shown to be a versatile strategy to build up and control complex functionalities in hydrogel media such as the selective release of drugs.[35] Anseth and coworkers have recently employed a photocaged aldehyde that, upon light-triggered uncaging, revealed a reactive benzaldehyde functionality. Such a functional group is capable of reacting in aqueous media at neutral pH with hydrazine derivatives to generate hydrazones. This concept was employed to produce patterned hydrogel structures by exposing a mixture of caged aldehyde and hydrazine-terminated poly(ethylene glycol) star-shaped polymers to a light pattern.[36]

Thomas and coworkers have reported the use of UV and visible light to alter the solubility of layer-by-layer polymer films.[37] Their approach relies on the photoinduced uncaging of specific masked anionic functionalities of a cationic polyelectrolyte of the layer-by-layer films. The uncaging of the anionic carboxylate functionalities at neutral pH shifts the charge balance of the polymeric material and induces, in a selective fashion, solubility of the film. The solubilization and functionalization of polymer films and gels with spatiotemporal control can also be achieved through NIR light–induced deprotection of carboxylic acid groups caged as 6-bromo-7-hydroxycoumarin ester (Figure 4b), or thioester groups.[38] This is a desirable feature if the polymeric system is to be used for biological applications,

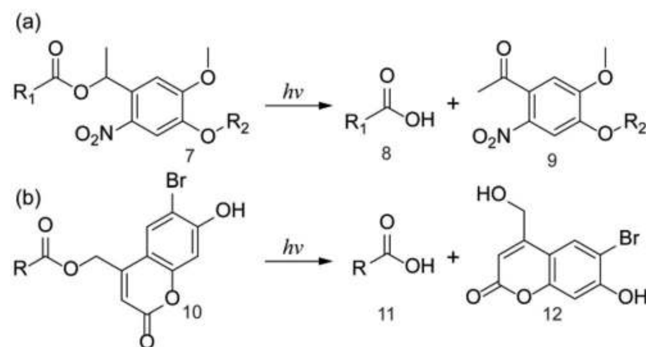

Figure 4. Selected examples of photoinduced deprotection reactions associated with a) *o*-nitrobenzyl and b) 6-bromo-7-hydroxycoumarin ester groups.

 © 2019 The Authors. Published by WILEY-VCH Verlag GmbH & Co. KGaA, Weinheim

since living tissues have a transparency window between 650 and 950 nm.

2.3.2. Photoinduced Generation of Radical Species

Radical-mediated chemical transformations, and, in particular, photocuring processes, are one of the most widely exploited reactions in polymer science and industry, including lithography, printing, coatings, and adhesives.[39] The uniqueness of the photoinitiated radical polymerization lies in its property of rapidly transforming a liquid monomer system into a solid material with almost no release of organic volatile compounds. While the field of photoinitiated radical polymerization is too vast to review comprehensively here, this section is meant to provide some generalities and to highlight some selected recent developments. In free-radical photopolymerization, there are two main pathways of generating free radicals from an excited species: i) homolytic cleavage, also called the Norrish type I process, which is associated with type I photoinitiating systems, and ii) hydrogen abstraction, or Norrish type II process, related to type II photoinitiating systems (**Figure 5**).[40]

Homolytic cleavage leading to the formation of free radicals is typically associated with the use of benzyl ketals (including Irgacure 184, Irgacure 651, and Irgacure 369). Acyl phosphine oxides such as TPO and Irgacure 819 are also utilized. In all of them, the unimolecular α-bond cleavage step generates two reactive radicals. Hydrogen abstraction from an organic species by a photochemically excited ketone, such as benzophenone, is a well-known reaction in photochemistry.[41] This bimolecular reaction is uncommon in photoinitiation unless the photosensitive ketone is employed in combination with an electron-donor species, such as an amine (Figure 5b). Alternatively, amino-substituted benzophenones, such as Michler´s ketone, thioxanthones (such as **16** in Figure 5b), anthraquinones, and camphorquinone derivatives, can also be used (Figure 5b).[42]

Type I photoinitiating systems exhibit relatively high quantum yields, but their operational window is limited to the UV or blue region. Type II photoinitiating systems (such as that in Figure 5b), by contrast, exhibit a wider range of working wavelength spanning the UV and visible light spectrum. It is worth noting that the use of visible light is a convenient curing mechanism for a wide variety of applications including dental repairs and coatings.[43] Type II systems, however, exhibit a limited efficiency compared to those of type I.

Regardless of the type of radical photoinitiator, these are added at a relatively low weight percent to a low molecular weight acrylate or methacrylate monomer to obtain photopolymerizable formulations. The use of oligomeric multifunctional reactive species, such as pentaerythritol tetraacrylate (**23** in **Figure 6**), facilitates rapid cross-linking. Some other formulations are capable of undergoing photopolymerization in the absence of photoinitiator, for example, some maleimide–vinyl ether systems.[44] This feature enables the curing of thick films and the avoidance of colored subproducts, which are generally associated with the decomposition of the photoinitiator. Thiol–ene and thiol–yne formulations, which also have the ability of photopolymerizing in the absence of a photoinitiator, exhibit some additional advantages including reduced both oxygen inhibition and polymerization shrinkage relative to acrylate-based formulations (Section 2.4).[45]

The free-radical photopolymerization of acrylate and methacrylate monomers follows the mechanism of any chain polymerization reaction. In the first step, free radicals are produced by the light-induced bond cleavage of the photoinitiator. When the highly reactive radicals come in close proximity with a monomer, they can react by breaking the olefinic bond, which results in the generation of a larger radical species. This newly formed radical can again appear in proximity of an additional monomer; these two species react, one more time, by breaking the olefinic bond. The reaction of monomers and a growing polymer chain continues in this manner until the process is terminated by a reaction between two radical species (polymer chain radical species or fragments of the photoinitiator). The resulting system is a mixture of polymer chains of different molecular weights or, if multifunctional monomers are employed, a cross-linked network. In the latter case, the final cross-linked material is insoluble in organic solvents and normally exhibits a relatively high glass transition and notable resistance to thermal treatments.

Free-radical photopolymerization is one of the most prominent reactions to structure polymers as will become evident in Section 3. In most of the cases, the photoinitiator is excited with light in its absorption band; however, excitation can also be carried out by using a TPA process in which the excited electronic state of the photoinitiator is achieved by the simultaneous absorption of two low-energy IR photons. By using tightly focused beams, the excitation of the photoinitiator by TPA processes can be confined to a very small volume at the focal point, thus enabling the 3D structuring of photopolymers at sub-100 nm resolution (see Section 3).

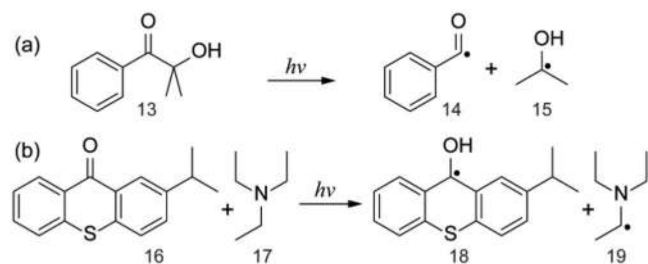

Figure 5. Generation of radical intermediates via a) Norrish type I and b) Norrish type II processes.

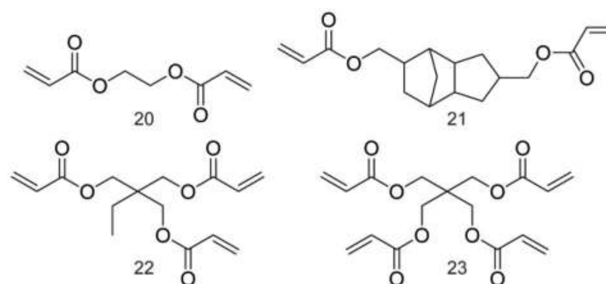

Figure 6. Selected examples of multifunctional acrylate monomers.

© 2019 The Authors. Published by WILEY-VCH Verlag GmbH & Co. KGaA, Weinheim

Two-photon polymerization (TPP) based on TPA processes is rapidly expanding and advances are sustained and built on technical developments and research efforts on innovative resists and initiators. High excitation power and long exposure times are typically associated with the use of traditional photoinitiators, on account of their limited TPA cross-section. This is impractical as polymeric structures are damaged during fabrication. In the field of TPP, in the last few decades, there have been significant efforts toward the synthesis of soluble photoinitiators with both high TPA cross-section and high initiation efficiency, pursuing fast writing speeds and low TPP threshold values.[46] Suitable initiators for TPA typically present spatially separated electron-donating and electron-accepting functional groups connected through an extended π-conjugated planar core. This configuration reduces the energy of the excited states of the initiator and increases its dipolar transitions, resulting in a higher probability for multiphoton absorption processes.[47]

2.3.3. Photoinduced Generation of Cationic and Anionic Species

While free-radical photopolymerization has been widely applied in numerous technological products and applications, it suffers from specific drawbacks including oxygen inhibition, significant polymerization-induced shrinkage, and shrinkage stress—which compromises their use in applications requiring parts of precise shape and size—and, sometimes, insufficient conversion. The photoinitiated cationic polymerization, developed by Crivello and coworkers, came to solve some of these problems associated with the free-radical photopolymerization.[48] The presence of oxygen, in contrast to the free-radical polymerization, does not inhibit the cationic polymerization, which facilitates their use in industrial environments. It is worth pointing out that while moisture can inhibit the cationic polymerization, under reasonably dry conditions, termination rates are low and, therefore, the polymerization occurs to an adequate level. Additionally, volume shrinkage in the photoinitiated cationic polymerization is produced to a much lesser extent in comparison to the free-radical photopolymerization. Also, while free-radical polymerization is restricted to monomers with olefinic bonds (acrylates and methacrylates, typically), a large group of compounds of different chemical nature can be polymerized by photoinitiated cationic polymerization including epoxides, vinyl ether derivatives, acetals, and sulfides. Such monomers exhibit, in general, low toxicity, viscosity, and volatility, which are desirable aspects for many industrial applications. One interesting feature of the cationic photopolymerization is that once the active cationic species are produced, upon exposure to light, the polymerization proceeds even in the dark. This way, high levels of conversions are achieved, which is beneficial in a number of applications including coatings and adhesives.

One classical example of a cationic photoinitiator is an aryl iodonium salt with a non-nucleophilic counterion (such as **24** in **Figure 7**). These compounds decompose after photoexcitation, via homolytic and heterolytic bond cleavage, into a mixture of aryl cations, aryl iodine radical cations, and other radical species (Figure 7a). Such a mixture of reactive species further reacts with the solvent or monomer molecules generating a Brønsted acid, which initiates the polymerization. Photoinduced acid

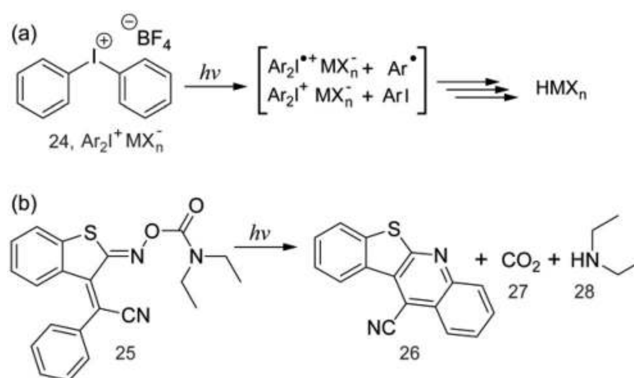

Figure 7. Photoinduced generation of a) cationic and b) anionic species.

generators (PAGs), such as aryl iodonium and aryl sulfonium salts, have been widely used in cationic photopolymerization. These “onium” salts exhibit a good thermal stability; however, their spectral working window is limited to the UV range. With the advent of advanced fabrication techniques, the search for initiators capable of working at increasingly longer wavelengths is growing in importance. Onium salts with extended π-conjugated structures provide only limited benefits with respect to visible light–induced initiation.[49] An alternative strategy to trigger the cationic polymerization with visible light employs a combination of a type I or II radical initiator and a cationic initiator, often an onium salt, through what is known as a free-radical promoted cationic polymerization process. In such a system, an appropriate radical photoinitiator generates, upon visible light, free radicals that are oxidized by the onium salt into the corresponding cationic species, triggering the cationic polymerization.[50]

The photoinitiated anionic polymerization, in comparison to the cationic and the free-radical photopolymerization, has not been so widely developed, which is partly associated with the lack of appropriate photoinitiators.[3c] Uchida and coworkers have reported the anionic coordination polymerization of epoxides based on a catalyst system comprising titanium tetraisopropoxide phenol, which was generated photochemically.[51] The polymerization of cyanoacrylates—which is widely used in the adhesives industry—is normally triggered by anionic species. Only a very few photoinitiating systems capable of promoting the light-induced polymerization of cyanoacrylates have been reported to date and include metal-organic[52] and all-organic species (Figure 7b).[53] Photolabile caged nucleophiles have also been employed to structure materials based on the thiol-Michael reaction.[54]

2.4. Photoinitiated Click Reactions

Since being coined by Sharpless at the beginning of this century, the concept of click chemistry has attracted a surmount attention of chemists and materials scientists,[55] and there is a clear trend toward developing strategies to impart spatiotemporal control over efficient bond-forming processes. While not being strictly photosensitive, there are many excellent examples of click reactions that have been tweaked to enable photocontrol

© 2019 The Authors. Published by WILEY-VCH Verlag GmbH & Co. KGaA, Weinheim

over their initiation. This step, in many cases, is associated with a primary reaction in which radical species are produced after the light-induced dissociation of an excited species. Owing to their growing importance in polymer science, we highlight in this section a few selected examples of photoinitiated click reactions, including CuAAC, Diels–Alder, thiol–ene, and thiol–yne coupling chemistries.

The Cu(I)-catalyzed variant of the Huisgen 1,3-dipolar cycloaddition between azide derivatives and terminal alkynes (CuAAC) is arguably one of the most quoted examples of a click reaction. Reported independently in 2002 by Sharpless and coworkers and Meldal and coworkers,[56] the CuAAC reaction has been widely explored for a number of material science applications. For such a cycloaddition reaction, the Cu(I) catalyst is typically generated in situ by the reduction of Cu(II) to Cu(I). Alternatively, the CuAAC can also be catalyzed by various Cu(I) salts. Although not evident when CuAAC reaction conditions are considered, the implementation of light-controlled reactivity via CuAAC has been realized by various ways. Ritter and König reported the use of a redox flavin-based catalytic system for the photoinduced reduction of Cu(II) to Cu(I), which subsequently catalyzed a CuAAC reaction.[57] Alternatively, the active Cu(I) species can be generated from Cu(II) via a photoinduced electron-transfer reaction.[58] Popik and coworkers reported the photoinduced generation of cyclooctynes, from cyclopropenones, which undergo a Cu-free cycloaddition in the presence of an appropriate azide derivative.[59] Anseth, Bowman, and coworkers have taken advantage of the radical-mediated photochemical reduction of Cu(II) to Cu(I) to generate patterned hydrogel structures (**Figure 8**a).[60] The reactive mixtures were composed of tetraazide and dialkyne poly(ethylene glycol) compounds, copper sulfate, and a photoinitiator. Upon UV light exposure, the photogenerated radicals efficiently reduce Cu(II) to Cu(I), which catalyzes the network formation between the end-functionalized poly(ethylene glycol) compounds. Patterned hydrogel fabrication and chemical modification were enabled with the assistance of a photomask. The concept of the photoinitiated CuAAC has been pushed further by the groups of Bowman, Kloxin, and other laboratories around the world in a wide variety of directions and cross-linked materials, elastomers, foams, and shape memory polymers (SMPs) have been produced by exposing bulk mixtures of multifunctional azides and alkynes to either UV or visible light.[61]

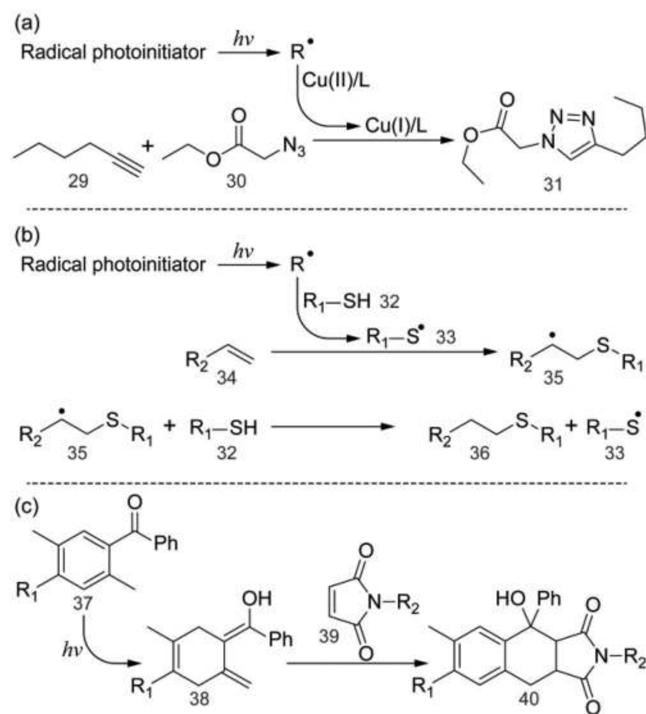

Figure 8. Selected examples of "photoinitiated" click reactions: a) CuAAC, b) thiol–ene, and c) Diels–Alder.

The reaction between thiols and olefinic bonds can proceed via an anionic chain reaction, known as thiol-Michael addition, or a radical-mediated step growth mechanism, which is commonly termed as thiol–ene.[62] Both types of reactions exhibit many of the features of a click reaction that include achieving quantitative yields, creating only by-products that can be easily removed without chromatography, being insensitive to ambient oxygen or water, and simple to perform in a benign or easily removable solvent. Also, both the thiol-Michael and the thiol–ene reactions can be initiated by light if appropriate formulations are employed but, considering its radical-mediated mechanism (Figure 8b), the thiol–ene coupling is better suited to fully exploit the benefits of photopolymerization.

Although thiol–ene reactions can be photopolymerized in the absence of a photoinitiator molecule,[63] the presence of a small amount of a photoinitiator, such as 2,2-dimethoxy-2-phenylacetophenone, in the reactive mixture is very common. In addition to the photoinitiator molecule, thiol–ene resists include multifunctional monomers in their formulation that typically lead to rapid network formation. In comparison to free-radical photopolymerization, the photoinitiated thiol–ene reaction has a lower oxygen inhibition. Thiol–ene networks also tend to be less brittle than those based on (meth)acrylates. This feature is associated with the step growth mechanism of thiol–ene systems itself that produces, in comparison to the free-radical polymerization of (meth)acrylates, more homogeneous networks based on relatively flexible thioether linkages. Such networks are relatively more efficient at dissipating stress and minimize, to some extent, crack propagation.[64]

Bowman and coworkers have reported on both the mechanism of thiol–ene network formation and the patterning, via nanoimprint lithography, of cross-linked films. The authors employed a liquid resist composed of oligomeric multifunctional alkynes and vinyl monomers.[65] It was later demonstrated that, by choosing the appropriate stoichiometry of thiol and vinyl functionalities, it is possible to produce patterned films containing free thiol groups, which enable the selective functionalization of the surface of the film by a subsequent thiol–ene reaction.[66] Other groups have further stretched the potential of the photoinitiated thiol–ene reactions and fabricated functional microstructures, microfluidic devices, organic semiconductor networks, and, as discussed in Section 3, hydrogels by employing various patterning techniques such as photolithography, stereolithography (SLA), and TPP techniques.[67]

The benign reaction conditions, the tolerance to aqueous environment, and the possibility of employing unreacted functional groups for anchoring specific molecules (dyes, bioactive

 © 2019 The Authors. Published by WILEY-VCH Verlag GmbH & Co. KGaA, Weinheim

compounds, etc.), through a postpatterning thiol-Michael coupling, make the thiol–ene reaction ideally suited for applications in biomaterials science.

The coupling of thiols to terminal alkynes, or thiol–yne reaction, and the thiol–ene coupling share many similar features.[68] The fact that two thiols, in the thiol–yne reaction, can react with one alkyne group yields cross-linked materials with higher glass transition than those based on thiol–ene chemistry.[69] Cross-linked elastomeric materials, structured hydrogels, patterned surfaces, and monolithic polymer columns, among other systems, have been produced by means of photoinduced thiol–yne coupling reactions.[70]

The Diels–Alder reaction is a [4 + 2] cycloaddition reaction of a conjugated diene and a substituted dienophile, an alkene or an alkyne, which yields a substituted cyclohexene derivative.[71] Alkenes and alkynes with electron-withdrawing substituents make the unsaturated groups more electron poor and are thus suitable dienophiles to react with a diene. The product resulting from a Diels–Alder reaction is thermally unstable and can undergo a reverse reaction, a retro-Diels–Alder reaction, at higher temperature to regenerate the starting diene and dienophile species. Owing to the reversible nature of the Diels–Alder reaction, thermally responsive polymer networks and self-healing systems have been designed.[72] Similarly to the CuAAC, the Diels–Alder reaction cannot be initiated by means of light irradiation. Instead, specific strategies have been devised to impart photocontrol over Diels–Alder cross-linked polymer systems.

Bowman and coworkers have shown that a dynamic and thermally reversible Diels–Alder network can be rendered irreversible by photoinducing a thiol–ene reaction between the Diels–Alder adducts and the thiol species of a reactive network.[73] Such a cross-linked material was employed as a resist, and 3D structures were written using two-photon techniques, which was followed by a developing step. The supporting material, unexposed to light, was easily depolymerized into a mixture of low-viscosity monomers by heating up the system.

Barner-Kowollik and coworkers have reported an alternative strategy to achieve a phototriggered Diels–Alder reaction, which is based on the photoinduced generation of hydroxy-*o*-quinodimethane species from *o*-methyl phenyl ketones. The photoenolization of *o*-methyl phenyl ketones and aldehydes is a well-known organic chemistry reaction. Photoexcitation induces an intramolecular hydrogen abstraction, which results in the formation of a biradical. A subsequent rearrangement yields the *E* photoenol, which undergoes an efficient stereospecific *endo*-addition with an appropriate dienophile (Figure 8c).[74] This protocol has been implemented in the preparation of polymers with well-defined architectures, the inscription of 3D microstructures by means of multiphoton polymerization, and the surface patterning of microscaffolds.[75]

3. Structuring Techniques for Light-Sensitive Polymers

This section provides an overview of the most relevant structuring techniques for light-sensitive polymers. On one hand, some of these techniques make use of structured or focused light to selectively modify the photosensitive materials. Beyond the most traditional mask-wise photolithographic techniques, other maskless techniques such as interference lithography (IL) or light-assisted direct writing techniques have been explored in order to create patterns and 3D structures using light-sensitive soft materials. On the other hand, another set of techniques involves the structuring of light-sensitive materials by means of processing methodologies not using light, this being employed just to fix the generated structure. Among these technologies, UV-assisted NIL, making use of a mold to structure the polymer precursor, as well as additive manufacturing (AM) techniques such as inkjet printing and extrusion-based 3D printing techniques, digitally depositing photopolymerizable materials with a high degree of precision, will also be surveyed. **Table 1** lists all these structuring technologies indicating main types of materials used, typical resolution and geometries, main advantages and limitations, and main application areas. The choice of a specific structuring technology is dictated by cost, patterning speed, type of structure/topography, resolution, and compatibility with the target final application that might sometimes require the inclusion of functionalities.

3.1. Mask Photolithography

In the most traditional photolithographic process, the image of a mask, having a pattern of transparent and opaque areas, is transferred to the photosensitive material to create the desired polymeric structure on the target substrate (**Figure 9**a). This can be done by putting the mask in direct contact with a photoresist film, or in close proximity to it, and then irradiating it with collimated actinic light. Alternatively to contact or proximity photolithography, the image of the mask can be projected onto the film by using an appropriate optical projection system. Illumination of the photoresist leads to a change in the solubility of the irradiated polymer, so exposure of the film to an appropriate solvent selectively removes certain areas of the film. In particular, for negative photoresists, illumination in the exposed areas triggers polymerization and/or cross-linking reactions decreasing the solubility of the exposed material. The use of selective solvents can eliminate the material in the non-exposed regions leaving a topographic structure with raised features that resemble those corresponding to the transparent regions of the photolithographic mask. On the other hand, for positive photoresists, illumination typically produces either decomposition reactions in the exposed areas, leading to a decrease in the molecular weight of the systems, or changes in the polarity of the materials.[76] Regardless of the origin of the solubility change, an adequate solvent selectively removes the material in the exposed areas.

Mask photolithography has been crucial in the development of the microelectronics industry. The image of the mask with the structure of an integrated circuit (IC) is transferred to a thin photoresist layer applied on top of a silicon wafer, through the previously described process, leading to a polymeric surface relief structure. This is used as a material mask to transfer the pattern of the IC to the underlying silicon wafer modifying it through different postprocesses such as oxidation or doping with other species, spatially tailoring in this way its electrical properties.[77] By performing multiple steps on the same wafer, the complete structure of the IC is implemented. In the

© 2019 The Authors. Published by WILEY-VCH Verlag GmbH & Co. KGaA, Weinheim

Table 1. Structuring techniques for light-sensitive polymers.

Structuring technology	Geometry; Resolution (limited by)	Materials used (properties)	Advantages	Drawbacks	Application areas
Mask photolithography	Arbitrary features in the plane determined by the mask; 10–1000 nm (diffraction)	Acrylate, epoxide, chemically amplified resists	High throughput, large area (wafer scale), low density of defects	Diffraction limited, expensive equipment	Microelectronics, optics
Interference lithography	Periodic features in the volume determined by the beam interference; 50–1000 nm (lattice size determined by geometry and wavelength)	Acrylate, epoxide photoresists	Large area (determined by beam interference area), defects free	Only periodic structures are accessible	Optics, sensing
Stereolithography	Arbitrary 3D features, digital technology; 1–100 µm (diffraction)	Acrylate, epoxide photoresists (low viscosity)	Arbitrary structures, digital structuring	Low speed, low throughput	Prototyping, medical, microfluidics, soft robotics
Two-photon absorption-based DLW	Arbitrary 3D features, digital technology; 20–100 nm (optics and photoresists)	Acrylate, epoxide, hybrid organic–inorganic photoresists	Digital structuring, not limited by diffraction	Low speed and small building volume	Biomedical, sensing
UV-assisted NIL	Arbitrary features in the plane determined by the mask; 5–1000 nm (mold resolution)	Acrylate, epoxide photoresists (low viscosity)	Parallel process, R2R compatible, high throughput, low cost	Complex mold fabrication, mold durability	Microelectronics, sensing, optoelectronics
Inkjet printing	Arbitrary features in the plane, digital technology; 10–100 µm (droplet size)	Acrylate, epoxide-based inks (viscosity and surface tension)	High throughput despite being a serial process (multinozzle printheads), multimaterial, digital structuring	Low resolution	Graphics, photonics
Extrusion-based 3D printing	Arbitrary 3D features, digital technology; 10–500 µm (filament size)	Acrylate-based inks (yield stress)	Multimaterial, digital structuring	Slow printing, low resolution, low throughput (serial process)	Prototyping, biomedical, soft robotics

high-volume semiconductor manufacturing industry, the continuous demand of denser packaging of components and faster integrated circuits with reduced cost has driven research to double the number of transistors of an IC every 2 years approximately, as postulated by Gordon Moore already in 1965.[78] This trend, turned into the roadmap of the semiconductor industry, has been successfully attained over the last five decades, thanks to the continuous improvements in resolution achieved with optical photolithographies.

This resolution *R*, defined as the width of the printed line, is inherently limited by the diffraction of light, and is given by the following expression:

$$R = \frac{k_1 \lambda}{\mathrm{NA}} \tag{1}$$

where λ is the wavelength of the actinic radiation employed, k_1 is an empiric coefficient, with a lower limit value of 0.25,[79] that depends on the photoresist, the illumination system, and the mask pattern, and NA is the numerical aperture of the optical system, being equal to $n\cdot\sin(\Theta)$ with n the refractive index of the medium on top of the photoresist and Θ the largest incident angle formed by the actinic light with the normal of the photosensitive film.

Another inherent limitation in these systems is the depth of focus (DoF), defined as the amount of focus change along the optical axis, in which the image of the mask has suitable quality, and given by the following equation:

$$\mathrm{DoF} = \frac{k_2 \lambda}{\mathrm{NA}^2} \tag{2}$$

k_2 being a process-dependent empirical coefficient. The DoF imposes restrictions on the thickness of the photoresist and also on the position of the thin film related to the image formation plane.

Advances in resolution have been achieved by improving the photoexposure optical systems, the photoresists, and the materials processing procedures. Concerning the optical system, one of the primary strategies to improve resolution is reducing the excitation wavelength (see Equation (1)). Sequential changes toward shorter wavelengths in the excitation have been made pursuing improved resolutions, from the visible g-line at 436 nm and the UV i-line at 365 nm (mercury lamp), to deep UV (DUV) at 248 nm (KrF excimer laser), 193 nm (ArF excimer laser), and even shorter wavelengths such as 157 nm (F_2 laser) or extreme UV (EUV) at 13.5 nm. Increasing of the numerical aperture of the optical system in projection systems has also led to significant improvements in resolution. Besides the use of objectives with higher working angles (higher NA objectives), the use of immersion liquids (e.g., water) to increase the refractive index of the medium, between the lens and the photoresist layer, has also been industrially employed to increase resolution of the patterned features. Air and nitrogen have refractive indexes around 1, while high-purity water has a refractive index of 1.44 and keeps acceptable levels of absorption at 193 nm, thus providing an increase of NA of 44% and therefore a

© 2019 The Authors. Published by WILEY-VCH Verlag GmbH & Co. KGaA, Weinheim

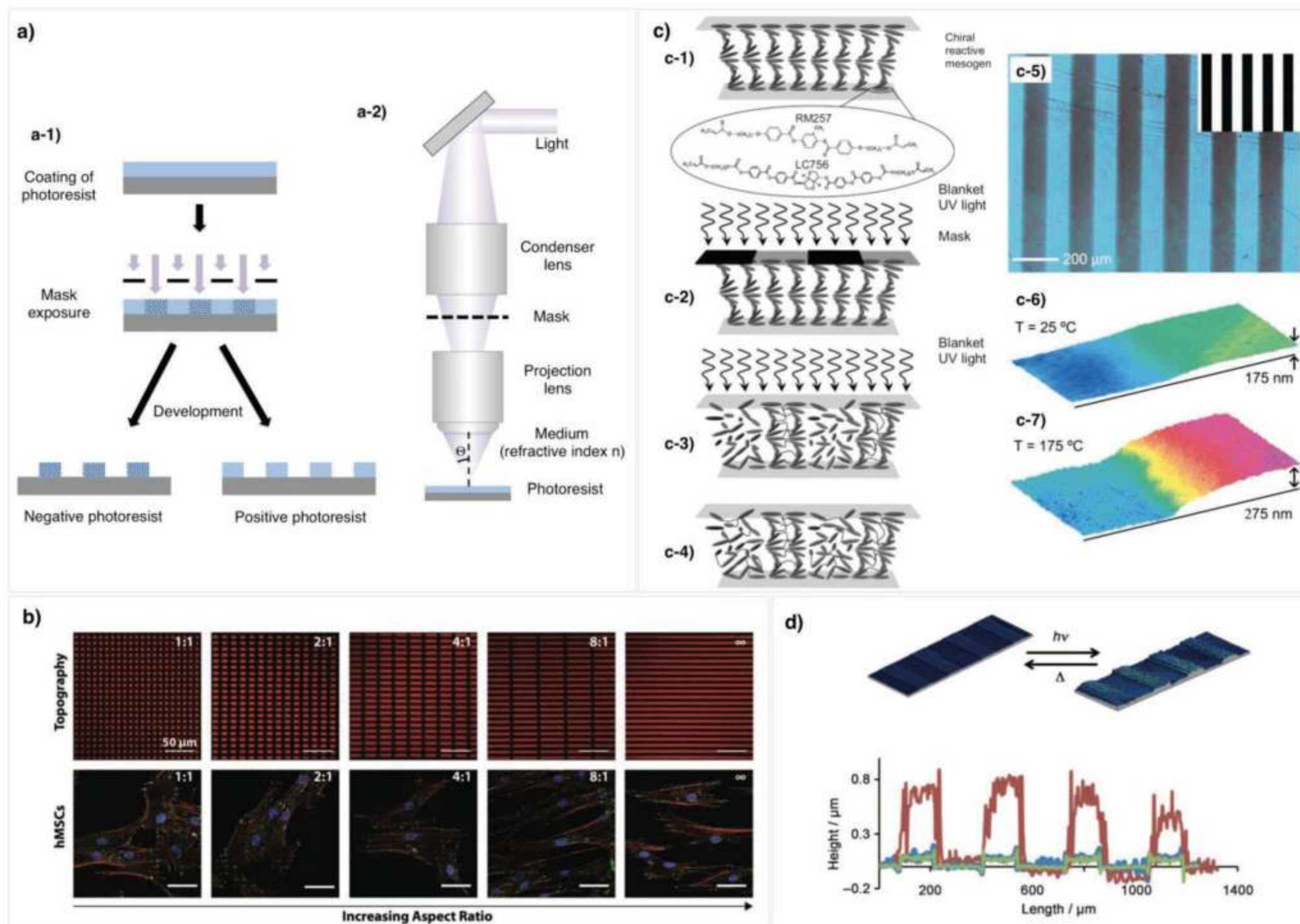

Figure 9. Mask photolithography. a) Schematic illustration of a-1) a mask photolithographic process (contact/proximity) and a-2) an optical projection system. b) Cell guidance studies: Cells exhibit elongation and preferential alignment on substrate topographies produced by UV photolithography. Topographic features (top row) with increased feature aspect ratio (from left to right) induce more pronounced cellular elongation and alignment (as qualitatively shown in the bottom row). Reproduced with permission.[95] Copyright 2013, Wiley-VCH. c) Temperature-responsive surfaces: c-1 to c-4) Schematic representation of the sample fabrication process. Briefly, a cholesteric reactive mesogen is planarly aligned (c-1) and exposed through a mask in the chiral nematic phase fixing this orientation (c-2). A second exposure is carried out without a mask above the clearing point (c-3) locking a disordered state in the rest of the film. The film contains chiral nematic and isotropic regions (c-4) as shown by polarization optical microscope (c-5). Heating between 25 and 175 °C leads to changes in topography (c-6 and c-7, respectively). Adapted with permission.[101] Copyright 2006, Wiley-VCH. d) Light-responsive surfaces: Topography of a patterned chiral nematic-homeotropic film containing light-responsive azobenzene molecules. Surface profile of the initial profile (blue), during UV illumination (red), and after removal of the illumination (green). Reproduced with permission.[102a] Copyright 2012, Wiley-VCH.

notable associated resolution enhancement with this simple change.

Significant increase of the resolution can also be achieved through multiple-patterning techniques, consisting in successive exposures using laterally displaced mask images,[80] beating the limits of resolution imposed by optical diffraction.[81] These approaches applied on advanced photoresists, which will be described later, have enabled to extend the lifetime of the 193 nm photolithography keeping the pace prescribed by Moore's law, reaching the current state-of-the-art resolutions of 10 nm for industrial production. To meet the ceaseless demands of the semiconductor industry that continuously seeks for higher resolution features, EUV lithography with light of 13.5 nm is quickly being developed. Plasma sources are used as they produce extremely high temperatures leading to the short wavelength of 13.5 nm. Significant challenges regarding the masks, the optics, and the materials (see below) are being addressed in order to make this technology available for mass production. Large advances have already been done and commercial photolithographic systems for development purposes, showing improved defectivity performance, are already available from ASML.[82]

Focusing on the materials and their processing, photoresists should fulfill several requirements including ability to form thin films with uniform thickness, appropriate sensitivity to relevant wavelengths, high-resolution capability, including the ability to create high aspect ratio (height to width) structure features, and resistance to harsh processing conditions such as ion, plasma, acid, or temperature treatments. First important examples of negative photoresists employed in mask photolithography were formulations based on free-radical initiated photo-cross-linking or photopolymerization for the blue and UV region.[83] Systems

© 2019 The Authors. Published by WILEY-VCH Verlag GmbH & Co. KGaA, Weinheim

comprising a free-radical photoinitiator together with vinyl- or acrylate-functionalized polymers or multifunctional monomers have extensively been used as they easily react upon light exposure, forming a highly cross-linked, mechanically and chemically resistant structure that becomes a negative pattern of the mask image.

Another important set of negative photoresists relies on polymers or monomers provided with epoxidic groups and PAGs such as the triphenylsulfonium hexafluoroantimonate onium salt.[48a,84] The photolysis of these systems leads to the production of acids that catalyze the cationic polymerization of epoxide monomers.[83a] Different from free-radical polymerization, this process is not sensitive to oxygen inhibition and photoresists are thermally more stable. Aiming to reach high-resolution photolithographic systems, monomers bearing multiple reactive groups were investigated, leading to highly cross-linked systems upon polymerization. A prominent example is the glycidyl ether of bisphenol A, functionalized with eight epoxide groups and commonly known as SU-8. In combination with triarylsulfonium salts, it lead, upon irradiation with UV and a subsequent thermal annealing treatment, to highly cross-linked materials with excellent mechanical and chemical resistance as well as thermal stability, with a glass transition temperature (T_g) beyond 200 °C. Overall, the use of PAG in this highly functionalized resists has enabled the preparation of very sharp features with aspect ratio higher than 10:1.[85]

Onium salts were also specially relevant when DUV photolithographic systems using 248 and 193 nm light were introduced as the existing UV photoresists were too absorbent for these wavelengths and therefore inadequate to provide uniform excitation across the photoresist film thickness. The need of extremely sensitive resists drove the development of a family of chemically amplified resists (CARs) essentially comprising a polymer, solubility inhibitors, and a PAG. As a representative example, Frechet, Ito, and Willson first introduced a photoresist comprising poly[4-[(*tert*-butyloxycarbonyl)oxy]styrene], having an acid-labile *tert*-butyl carbonate (*t*-BOC) side group, and triphenylsulfonium hexafluoroantimonate onium salts that generate a strong acid upon exposure to DUV light.[86] Post-baking, to further facilitate the reaction and diffusion of the acid, produces the decomposition of the *t*-BOC groups leading to a polar polymer in the exposed areas. By adequate selection of the solvent used in the developing step, either positive or negative high-resolution images of the photolithographic mask can be achieved with these systems. CARs, the most widely used photoresist in DUV, have also been demonstrated to be suitable materials for EUV.[87] With feature sizes closer and closer to those of molecules involved, the use of resists based on disordered polymers brings new issues such as the lack of homogeneity and subsequent structure collapse. To solve these issues, highly ordered materials, such as calixarenes, or metal oxide-based resists are being considered as a promising strategy for next-generation EUV photoresists.[88]

The impressive development of the semiconductor industry has been propelled by the advances in photolithography, these being pushed in turn by the parallel progress in optical exposure systems, photoresists, and processing methodologies. Besides IC manufacturing, other application areas have benefitted from these developments in photolithographies. Surface relief structures obtained through these processes can be used, either directly or as intermediate structures for further processing.[89] Photolithographic techniques have been extensively employed in the generation of masters for mold replication,[90] in the fabrication of microfluidic chips,[91] and in the preparation of microlenses, Fresnel lenses, and diffractive or polarization elements.[92]

Mask photolithographies have also been used on chemically engineered photopolymers to generate platforms for cell culture studies. In living tissues, the extracellular matrix (ECM), which provides natural support to cells, strongly influences cellular behavior and biological functions.[93] Aspects such as cell morphology, orientation, migration, gene expression, or even differentiation are strongly influenced by the physicochemical information that cells gather from the environment.[94] As a result, the tailorability of photopolymerizable systems, in which monomers can be precisely adjusted, as well as the possibility to structure them with high spatiotemporal control, constitutes an excellent opportunity to mimic the different aspects of the ECM, including its (bio)chemical composition, structural and topographical features, and its mechanical properties.

Photolithography has been used to generate microstructures with topographic cues able to guide cell morphology, function, and fate. Even more, this surface topography can also be dynamically controlled. In this respect, Kirschner and Anseth made use of photodegradable hydrogels based on poly(ethylene glycol)-containing photolabile units to create surface relief microtopographies able to guide cellular elongation and alignment. Dynamic alteration of the topographies, by photoinduced degradation of the hydrogel, can also affect cell morphologies in real time (Figure 9b).[95]

Mask UV exposure of photopolymerizable systems has also been used to modulate the mechanical properties of hydrogels.[96] Methacrylated hyaluronic acid (MeHA) has been used to generate patterns of the elastic modulus in these materials by spatially varying the amount of actinic light through mask photolithography.[96b] This patterned mechanics leads to different responses with cells spreading out more in stiffer substrates. As both composition and mechanical properties of the ECM experience important changes in tissue development, tissue healing, or progression of diseases such as cancer,[97] there is a growing interest toward the development of biomimetic photopolymerizable hydrogels able to recapitulate these dynamic aspects of the ECM.[98]

Mask photopatterning has also been demonstrated to be a powerful tool to program shape morphing in stimuli-responsive systems. Patterning of the cross-linking density enables, for example, fine-tuning of the swelling behavior in hydrogels allowing the programming of deformations of 2D flat sheets into 3D shapes.[99] For example, Santangelo, Hayward, and coworkers developed a halftone lithographic method making use of a poly(*N*-isopropylacrylamide) copolymer with benzophenone pendant groups that can cross-link under actinic light irradiation to lead to temperature-responsive gel sheets. The halftone process, consisting in a double exposure, generates a lightly cross-linked continuous matrix with highly cross-linked dot regions. The heavily cross-linked dots swell less than the rest of the film, introducing internal stresses in the film that the system releases by escaping into the third dimension forming curved surfaces such as spherical caps, saddles, or cones.[99a]

© 2019 The Authors. Published by WILEY-VCH Verlag GmbH & Co. KGaA, Weinheim

Instead of cross-linking density spatial modulations, composition variations can also be patterned in hydrogels through mask photolithographic steps to create stress distributions leading to complex 3D shapes.[100]

Besides hydrogels, liquid crystalline polymeric coatings patterned by mask photolithography have demonstrated great potential as surfaces with responsive topographies. Regions with different orientation of the LC molecules, defined by the director **n**, over the area of the film, experience different expansion when exposed to an appropriate stimuli. As an example, a thin film of LC network showing chiral nematic and isotropic patterned regions presents relative changes between the height of the different areas on heating, due to their differences in thermal expansion coefficients. Cooling back to room temperature (RT) reverts the situation to its initial state. To achieve this orientational pattern, a photopolymerizable system comprising reactive mesogens showing a chiral nematic phase is initially oriented in a planar LC cell. Patterned irradiation with actinic light through a photomask fixes the planar orientation in the irradiated areas. A subsequent heating above the cholesteric-isotropic transition temperature induces the isotropization of the nonexposed regions and randomizes the orientation of the unreacted monomers, which are subsequently crosslinked by flood exposure (Figure 9c).[101] Extension of this principle to other orientational patterns and stimuli, such as light, has been further investigated by Broer, Liu, and coworkers (Figure 9d). Dynamic control of the surface topography over areas created with these mesogenic coatings can find exciting applications in areas such as responsive photonics, topology modulated friction, or switchable wettability.[102]

3.2. Interference Lithography

Instead of using the image of a physical mask, holographic or interference lithography makes use of patterns obtained from the interference of two or more laser coherent beams. Well-defined periodic patterns in two and three dimensions can be achieved by controlling angles and phase differences between beams, as well as their amplitudes and polarizations. To create these patterns, a laser beam is typically split into two or more beams that are redirected and made to overlap in the photosensitive material where the interference pattern is formed (**Figure 10**a). The traditional implementation of interference lithography consists in free-space setups involving bulky optical elements such as beam splitters and mirrors requiring a meticulous and time-consuming alignment that needs to be readjusted upon slight changes in the pattern periodicity or geometry (Figure 10a-1).[103] Besides, due to the optical path lengths involved, these systems are extremely sensitive to mechanical vibrations or environmental thermal fluctuations. Alternative IL schemes have been developed seeking for simpler, more robust, and versatile practical approaches. In this direction, different approaches to implement holographic lithography involving one single beam and robust optics setups have been developed. In a two-beam Lloyds' mirror interferential setup (Figure 10a-2), the overlapping of the portion of the beam direction reaching the sample and that being reflected in a contiguous mirror creates a sinusoidal intensity profile whose period can be tuned by changing the angle between sample and mirror. Beyond these sinusoidal patterns generated with two beams, more complex geometries can also be created by using modified Lloyd's interferometers that generate multiple interfering beams.[104] As an example, by adding a second mirror in the Lloyd's interferometer, an interference of the direct beam and the two reflections coming from each of the mirrors can generate a hexagonal intensity pattern. Hole or pillar defect-free patterns that extend over areas of several cm^2 can be created in a negative photoresist by using a single exposure, all with an easy alignment and with flexibility in the selection of the periodicity.[104a]

Analogously, interferential patterns can also be generated by using multifaceted prisms, such as the top-cut, four-sided prism (Figure 10a-3). A laser beam reaching the base of the prism is converted into five different beams. One of them directly passes through the top side of the prism with no deviation. The other four are deviated by total internal reflection at the four sides of the prism. The five beams, with well-defined angles and electric field intensity, recombine forming an interference pattern at the exit region of the prism. The phase difference between the different beams can be controlled by the insertion, in one of the beams, of a thin glass plate that can be rotated obtaining in this way interference patterns leading to complex photonic 3D structures, including diamond-like, all in one single exposure.

A higher degree of control of the angles, amplitudes, and phases of the different involved beams can be achieved by using masks with built-in phase changes. These masks consist in two orthogonally oriented binary gratings separated by a homogeneous film of controlled thickness and refractive index. The needed phase shift among the diffracted beams is introduced by this spacer layer enabling the fabrication of complex 3D photonic crystals such as woodpile structures in one single exposure.[105] Despite these masks being rather complicated to fabricate, requiring complex photolithographic process, they can be used many times and with minimal alignment, making this implementation of IL an interesting approach for industrial manufacturing of photonic structures. Digitally reconfigurable phase masks for holographic lithography can also be created by using a spatial light modulator (SLM). This element allows the arbitrary adjustment of the beam wavefront in real time enabling the precise control of amplitude, phase, and angles of the resulting beams. The beam reaching the SLM is transformed into multiple beams with well-controlled properties that, after their demagnification with a lens system, form an interference pattern with small feature size below the micrometer.[106]

Additional degrees of sophistication can be incorporated in the interference patterns by including supplementary optical elements. As an example, by using a simple two-beam interference setup, normally leading to 2D patterns in the plane, applied to a photoresist on top of a reflective substrate, complex 3D structures can be created. The reflection in the substrate generates an additional standing wave along the film thickness and thus a lamellae-like pattern along this same direction (Figure 10b). Although this interference pattern is usually avoided by the use of antireflective surfaces to get the pure interferential 2D figure,[107] it can also be advantageously employed to generate additional hierarchical features.

© 2019 The Authors. Published by WILEY-VCH Verlag GmbH & Co. KGaA, Weinheim

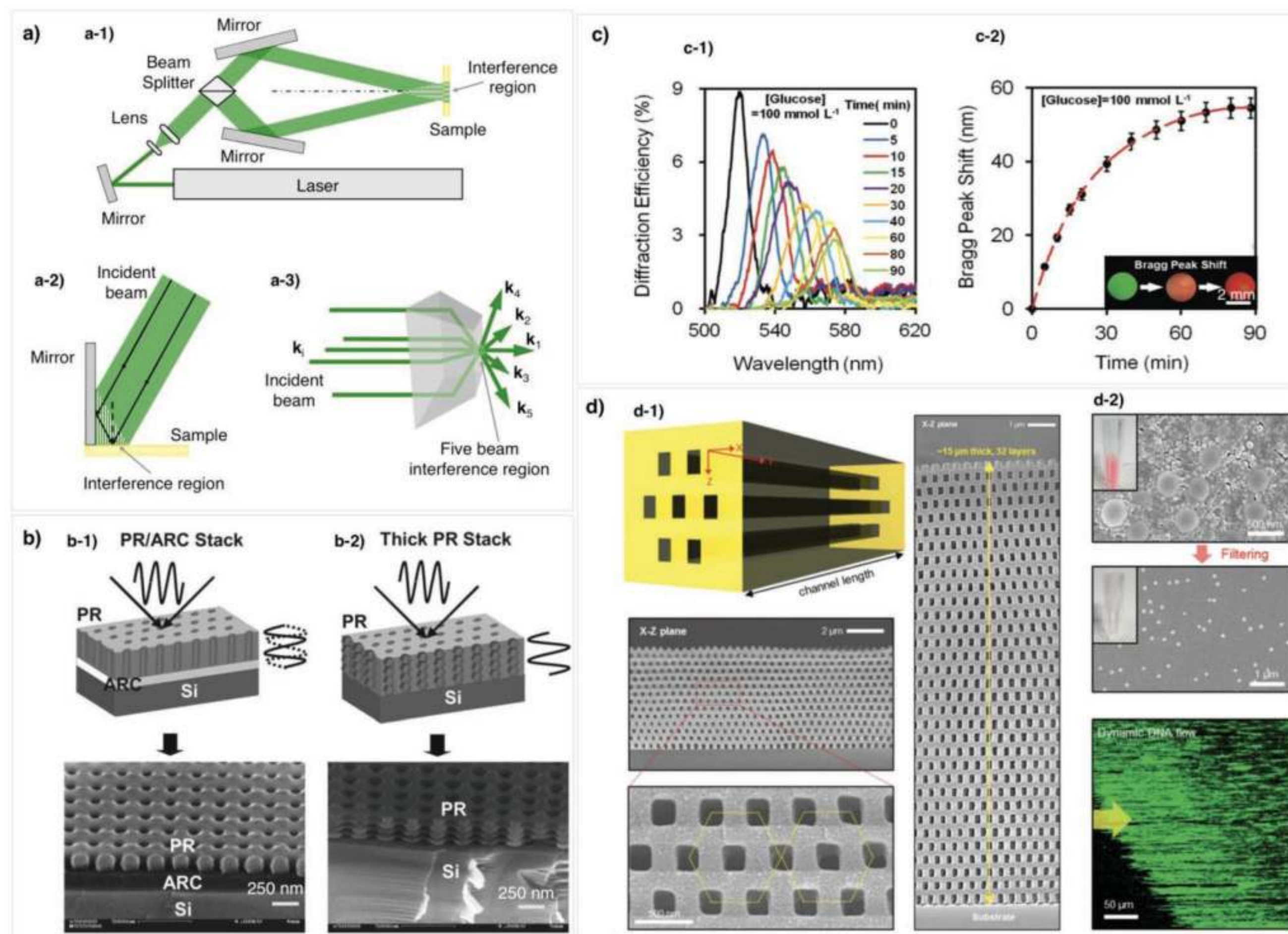

Figure 10. Interference photolithography. a) Schematics of a-1) free-space, a-2) two-beam Lloyd mirror, and a-3) top-cut prism IL setups. b) Hierarchical structures. Holographic lithography processes and scanning electron microscope (SEM) image of structures obtained with a two-beam Lloyd mirror interferometer using a photoresist (PR) layer on top of a substrate provided b-1) with an antireflecting coating (ARC) and b-2) without ARC. Reproduced with permission.[108] Copyright 2013, Wiley-VCH. c) Glucose sensors: c-1) Diffraction spectra of the structured hydrogel in response to glucose. c-2) Bragg peak shift as a function of time. Reproduced with permission.[112] Copyright 2018, Wiley-VCH. d) Nanochannel arrays: d-1) Schematic illustration and SEM images of ultralong nanochannel arrays generated using phase-mask IL on SU-8. d-2) The nanochannel arrays serve as filters for nanoparticles and force DNA stretching. Reproduced with permission.[113c] Copyright 2015, Wiley-VCH.

By using this simple approach, high aspect ratio, hierarchical 3D patterns can be prepared in one single exposure. This type of complex polymeric structures with controlled 3D geometry have been explored in the preparation of inorganic structures acting as photocatalyst-functionalized membranes for water decontamination,[108] or as biomimetic photonic structures that replicate those found in *Morpho* butterflies showing well-controlled structural colors.[109]

Overall, the regular periodic structures obtained with IL, with adjustable pattern structure and size over areas of several cm^2, have strong potential in different application areas such as energy storage[110] or sensing.[111] Yetisen and coworkers have recently demonstrated the use of photonic poly(acrylamide-*co*-poly(ethylene glycol) diacrylate) hydrogel structures generated by IL to fabricate glucose sensors. By applying silver halide chemistry on these periodic structures, AgBr nanocrystal multilayers are created. Functionalization of the hydrogel backbone with 3-(acrylamido)phenylboronic acid makes the photonic structure sensitive to the presence of glucose. The shifting of the Bragg reflection peak enables the quantification of the glucose content. This system is reversible and demonstrates great potential for medical diagnostics (Figure 10c).[112]

The ability to form these periodic structures on photoresist layers with no contact allows the easy integration in other devices. For example, the interconnected open-pore structure generated by IL has been integrated in microfluidic chips to implement size exclusion filters, passive mixers, and sensors.[113] Large stacks of nanochannels (up to 33 layers), with diameter on the order of tens of nanometers and length in the millimeter scale, have been integrated in microfluidic channels by using phase-mask interference lithography applied on SU-8 photoresist (Figure 10d). The subsequent chemical modification of the channel inner surface by metal oxide deposition allows to tune the diameter (50 nm) and turn it hydrophilic. The so-generated channels present excellent performance as filters for

 © 2019 The Authors. Published by WILEY-VCH Verlag GmbH & Co. KGaA, Weinheim

nanomaterials. Even more, when the diameter of the channels is comparable to the persistence length of DNA molecules, the flow inside the channels is able to force DNA stretching having this great potential in biological sequencing.[113c]

3.3. Light-Assisted Direct Writing

The most common implementation of this technique consists in a focused laser beam that scans a film of photosensitive polymer in a controlled fashion locally modifying the material. Typically, a laser beam is focused by an objective on a photosensitive film that is placed on top of a computer-controlled motorized stage. As a result, DLW techniques can digitally turn a computer-aided design (CAD) into a complex real and tangible structure. This technology thus enables the introduction of changes in design in a fast and reliable fashion, being a versatile and valuable tool for research and prototyping. This is in contrast to conventional photolithography that needs photolithographic masks whose fabrication process is complex, expensive, and time consuming. With writing speeds typically below few cm s^{-1}, however, the penetration of this technique in industry is quite limited. As in mask photolithographies, lateral resolution in DLW is limited by diffraction and determined by the optical characteristics of the beam (wavelength and polarization) as well as the numerical aperture of the focusing optics.[114] Another important limitation in DLW is again the depth of focus of the beam that, together with the lateral resolution and response characteristics of the photosensitive material, defines the exposed volume of the film.

3.3.1. One-Photon Photopolymerization Processes

When using photopolymers directly excited with light in the absorption band of their photoinitiating system, the amount of excited photoinitiator molecules, related many times to the polymerization reaction rate, follows a linear relationship with the light intensity. In these one-photon processes, the exciting beam is typically strongly attenuated by the linear absorption as light penetrates through the film. As a result, when dealing with focused beams, the focus has to be close to, ideally on, the surface to create structures with well-defined features. The fact that light out of the focus also contributes to the polymerization in these systems precludes the direct creation of well-defined 3D microstructures in the interior of the photoresist, this approach therefore being, in principle, limited to the generation of microstructured surfaces. These patterned layers have been employed in the preparation of photonic elements on flat substrates,[115] templates for replication,[116] and surface microstructures for cell–substrate interaction and cell guidance studies.[70b,117]

Despite curing in one-photon polymerization processes being limited to a thin layer of material, the fabrication of 3D microstructures directly writing with actinic light can still be undertaken. A complete family of light-based 3D manufacturing techniques relies on the successive layer-by-layer curing of photopolymer to create fully 3D structures. As in other AM methods, a CAD 3D model is digitally sliced into layers, each having the coordinates corresponding to the material points. Usually, computer-controlled stages move a photonic device (e.g., a laser together with its associated optics) that precisely fixes material at the target positions in each layer. For example, in vat photopolymerization techniques, a liquid photopolymer contained in a vat is selectively polymerized by light. Within vat technologies, SLA makes use of a focused laser beam that is steered across the surface of the photopolymerizable liquid to locally turn it into cross-linked material, fixing a complete solid layer of the object to be created to the supporting substrate (**Figure 11**a-1).[118] Sample and substrate are then both lowered down into the photoresist vat at a small predetermined distance, so a new layer of liquid photopolymer is on top of the cured material in such a way that it can be exposed again to light to generate another solid layer. This process can be iterated many times to create in this way 3D objects.

Relying on focused laser beams, SLA can easily provide resolutions of few micrometers in the *XY* plane using low-cost translation stages. In the *Z* direction, resolutions of tens of micrometers are typical, this being mainly determined by the penetration of light in the photopolymerizable liquid, a parameter that can be tuned by adding suitable absorbers that reduce the thickness of the photopolymerized layer. One of the major limitations of this technique is the speed of writing as the laser excites the photoresist in a serial manner, point by point. Digital light processing (DLP), a variation of SLA, makes use of a spatial light modulator to create the image of a complete layer at once significantly reducing writing time of the complete layer in comparison to laser-focused SLA systems. DLP systems typically use a digital micromirror device (DMD), usually employed in overhead projection systems. A DMD consists in an array of over 2 million aluminum micromirrors (10 µm side) arranged in a matrix, each of them being individually addressed to form images on a surface. Illumination in DLP systems is typically carried out from the bottom side of the vat, exposing the photopolymer through an optically clear plate provided with an antistick layer (Figure 11a-2). This minimizes adhesion of the photocured material preventing undesired deformation or collapse of the created object. By using low-cost optics, lateral resolution of these systems can easily be in the range of tens of micrometers although improved resolution in the micrometer range can be easily achieved.[119]

As resins employed in vat photopolymerization techniques typically rely on free-radical polymerization, inhibition by oxygen may occur when the curing layer is in direct contact with the atmosphere as it happens in focused beam SLA systems. Illumination from the bottom as described earlier in DLP systems typically eliminates this problem. In both cases, SLA and DLP, once a complete layer has been exposed to light, object displacement in the *Z* direction as well as renewal of the liquid photopolymerizable resin needs to be carried out. This step takes a significant amount of time, in which no new volume of object is generated, overall increasing the piece fabrication time. To improve this scenario, DeSimone and coworkers introduced continuous liquid interface production (CLIP) that leads to significant improvements as it simplifies the overall process and thus reduces the production time.[120] CLIP consists in a simple modification of a conventional DLP

© 2019 The Authors. Published by WILEY-VCH Verlag GmbH & Co. KGaA, Weinheim

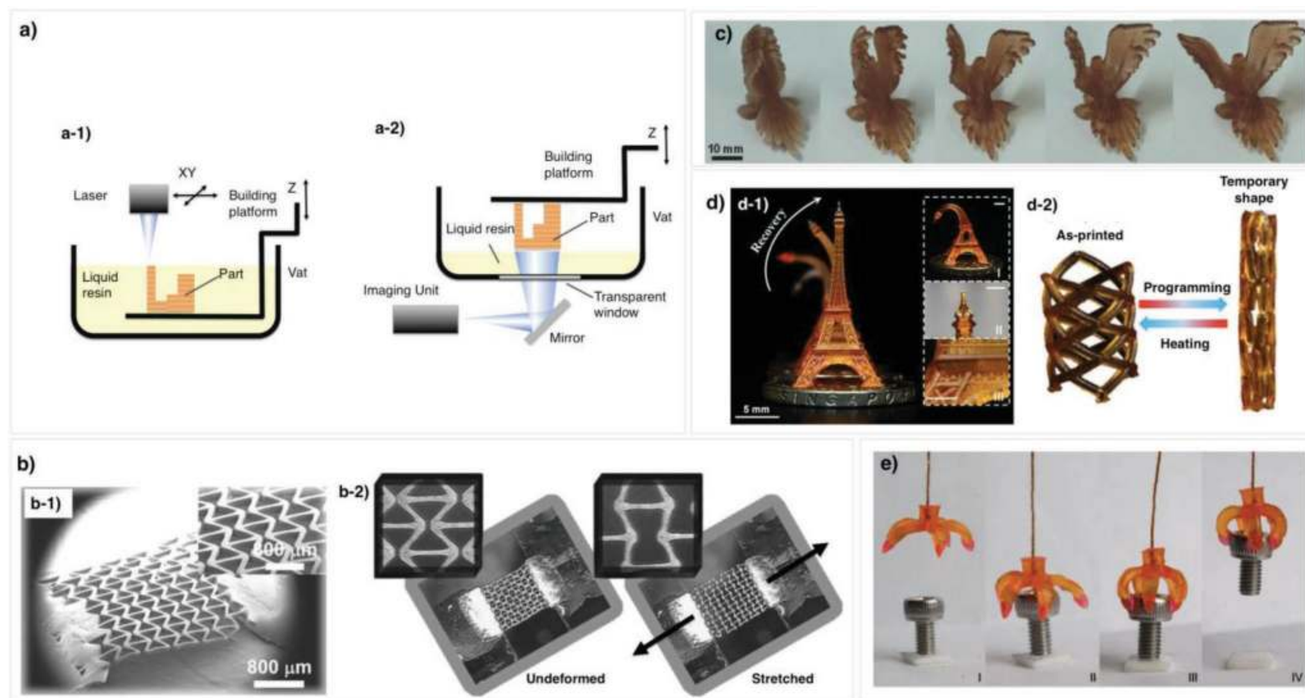

Figure 11. Stereolithographic techniques. a) Schematic illustration of a-1) SLA and a-2) DLP. b) Tunable mechanic structures: SEM images of b-1) a negative Poisson-ratio re-entrant honeycomb structure fabricated using a DMD microstereolithographic system on PEGDA, and b-2) its mechanical response on stretching. Adapted with permission.[128a] Copyright 2011, Wiley-VCH. c) Shape memory polymers: Polycaprolactone-based bird fabricated using SLA. The bird changes its shape from the deformed state at RT (left) to the original shape at 70 °C (right). Reproduced with permission.[131] Copyright 2016, Wiley-VCH. d-1) Eiffel tower model and d-2) stent fabricated by projection microstereolithography showing shape shifting on heating. e) SLA printed shape-shifting element with gripping ability. d,e) Adapted under the terms of a Creative Commons Attribution 4.0 International License.[132] Copyright 2016, The Authors, published by Springer Nature.

setup with bottom illumination (see Figure 11a-2). The conventional transparent window used in conventional DLP systems is substituted in CLIP by a transparent window made of an oxygen-permeable amorphous fluoropolymer (Teflon AF). As a result of the oxygen diffusion through this window, from the atmosphere to the photopolymerizable liquid, free-radical polymerization is strongly inhibited in a thin photoresin layer of few tens of micrometers, named as "dead zone," in contact with the window. Due to the existence of this dead zone, the generated 3D object advantageously does not stick to the bottom window of the vat. As a result, processing of the object can be carried out in a continuous, therefore faster, fashion as the photopolymer renewal step after photocuring of each layer, needed in conventional vat photopolymerization processes, is not required in CLIP.

In an attempt to further simplify the fabrication process, Taylor and coworkers have recently introduced computer axial lithography (CAL) that allows the printing of 3D shapes by illuminating a rotating volume of photoresin using a dynamically evolving light pattern.[121] The energy deposited at each point of the photoresin is the result of the addition of multiple exposures at different angles. The photoresin selectively solidifies at the points at which sufficient dose is accumulated. The existence of an energy threshold for polymerization in this technique relies on the oxygen inhibition of photoresins based on free-radical polymerization. Light reaching the resin generates radicals that are initially quenched by oxygen, inhibiting solidification; however, above certain energy dose, oxygen becomes depleted and cross-linking takes place. CAL manufacturing has demonstrated the generation of centimeter-scale 3D objects with feature resolution of 300 μm in less than 120 s. Printing of larger objects is foreseen to be feasible by tailoring the excitation wavelength in connection with the absorption of the photoresin. Advantageously, CAL manufacturing can make use of high-viscosity resins, which cannot be employed in layer-by-layer light-based 3D printing techniques (such as SLA or conventional DLP) as renewal of the resist, required between printing of successive layers, is not possible above certain viscosity threshold. Contrarily, in the framework of CAL manufacturing method, the use of high-viscosity resins can favor the direct printing of objects with overhanging features or disconnected parts, all with no additional support structures required, an aspect that cannot be achieved in current light-based 3D printing methodologies.

Overall, the previously mentioned light-based 3D printing techniques allow on-demand, relatively fast, flexible, and cost-effective preparation of complex 3D objects, with customized size and shape, minimal postprocessing, and including multiple materials (by sequential printing). With these unique characteristics, these 3D printing technologies have become an essential tool for rapid prototyping, being extensively adopted by academia and industry, across different application areas such as engineering, healthcare, biomedical, optics, aerospace, automotive, and robotics.[122] Beyond prototyping, 3D printing

© 2019 The Authors. Published by WILEY-VCH Verlag GmbH & Co. KGaA, Weinheim

technologies have currently a great challenge of incorporating functions into the printed objects. For this, new printable materials are required to accomplish specific functions beyond the purely structural or aesthetic ones.

Biocompatible photo-cross-linkable resins for SLA have been designed and prepared to generate scaffolds with controlled microstructure, porosity, topography, and (bio)chemistry trying to mimic the different aspects of the ECM of living tissues.[123] As an example, osteogenic cell signaling and tissue growth, which are strongly influenced by the scaffold porosity and interconnectivity, have demonstrated to be promoted in SLA-fabricated structures with optimized architecture.[124] Photoresins have also been tailored to replicate the mechanical properties of different ECMs. In this direction, photopolymerizable formulations based on polylactide, which after curing reach elastic moduli of about 3 GPa, have been optimized to create porous constructs by SLA with mechanical properties that approach those of bone.[125] Softer materials, aiming to emulate cartilage ECM in this case, have been generated using a photoresin based on poly(trimethylene carbonate) macromer. Bovine chondrocytes seeded in scaffolds obtained by SLA from this formulation spread on their surface and even promote the differentiated chondrocyte phenotype, increasing the applicability of these scaffolds in cartilage tissue engineering.[126]

Beyond the tunability of the elastic modulus, control of the Poisson ratio in tissue engineering scaffolds is also of great interest although it has been less studied. This property, which essentially describes the transversal deformation of a construct when it is axially strained, can be precisely controlled, in artificially built scaffolds, through the arrangement of their pores and their deformation mechanisms.[127] DLP has been applied on poly(ethylene glycol) diacrylate (PEGDA)-based photoresins to generate microstructured scaffolds with different geometries including conventional and re-entrant honeycomb structures showing positive and negative Poisson ratios, respectively (Figure 11b).[128] The possibility to accurately tune the mechanical properties makes these systems an interesting platform for mechanobiological studies.[128b]

Light-based 3D printing techniques have also been applied to responsive materials. While conventional 3D printing leads to immutable objects, the combination of 3D printing with responsive materials leads to complex 3D structures that change their shape, in a prescribed fashion, in response to certain stimulus. These shape-shifting 3D printed structures give rise to 4D printing that adds time as a fourth dimension.[129]

Hydrogels have been explored in combination with light-based structuring techniques to prepare shape-morphing films or objects. For example, Xie and coworkers have recently structured hydrogel films based on acrylate monomers with DLP to generate variable cross-linking density at the pixel level. On swelling, the so-created patterns differentially swell generating local stresses that make the 2D film turn into a well-defined 3D object.[130]

SMPs based on commercially available photocurable resins for SLA have also been investigated for the preparation of shape-shifting structures. Methacrylate-based polycaprolactone (PCL) semicrystalline macromers molten in a heated vat have been used by Zarek et al. to create 3D structures by SLA.[131] The resultant cross-linked structures, rigid at RT, become rubbery above 55 °C, the melting point of the PCL macromer. Deformations applied to the structures in the high-temperature elastomeric state can be fixed by cooling down the object below 55 °C while keeping the deformation. The load to generate the deformation can be removed once the system is cooled down to RT, and the deformation remains. Once this programming is completed, heating above 55 °C induces shape shifting (Figure 11c).

Photopolymers have been specifically developed seeking improvement of the thermomechanical response in SMPs. Methacrylate-based photoresins have been developed by Ge et al. to create high-resolution 3D structures by projection microstereolithography.[132] Tailored thermal and mechanical properties are achieved by adequate formulation of monomers including benzyl methacrylate, which acts as a chain extender, and poly(ethylene glycol)dimethacrylate, bisphenol A ethoxylate dimethacrylate, and di(ethylene glycol) dimethacrylate, working as cross-linkers. Values of the rubbery modulus from ≈1 MPa to ≈100 MPa, glass transition temperatures in the range from −50 to 180 °C, and failure strains above 300% have been demonstrated, significantly better than those attained with conventional photoresins. As a result, controlled shape shifting with large deformation and the implementation of shape-morphing 4D printed robotic devices such as active self-expandable stents or soft grippers with application in the medical field have been accomplished (Figure 11d,e).[132]

3.3.2. Two-Photon Photopolymerization Processes

Feature resolution of patterning techniques based on one-photon absorption is largely outperformed by TPP-based fabrication technologies. In these systems as outlined in Section 2.3.2, a femtosecond pulsed laser beam, typically in the NIR, is tightly focused with a high NA objective, to excite the photoresin through TPA processes, triggering photopolymerization (**Figure 12**a). As the TPA probability follows a quadratic dependence with the light intensity, the region in which the reaction can be initiated can be set to a very small region, well below the diffraction limit of light, in which the concentration of photons is high enough to trigger the photoreaction. As a result, TPP provides lateral resolution that can be on the order of tens of nanometers.[133] In addition to resolution, TPP offers additional advantages when compared to one-photon photopolymerization processes. Light typically used in TPP falls in the NIR region of the spectra where common photoresists present negligible linear absorption, so this light is normally transmitted through the material with no attenuation. As a result of the nonlinear nature of the TPP process, the probability of absorption of two photons is only high when enough energy is localized in a small volume pixel, named voxel, around the focal point. Out of the focus, the probability of TPP dramatically decreases, so cross-linking does not occur. By moving the focus within the bulk of the photoresist, truly 3D polymeric structures can be digitally defined with enhanced resolution in comparison to one-photon absorption–based techniques.[134] Despite these clear advantages, the small size of the voxels, typically on the order of 100 nm, together with the limited writing speed, of several cm s^{-1}, in these systems

© 2019 The Authors. Published by WILEY-VCH Verlag GmbH & Co. KGaA, Weinheim

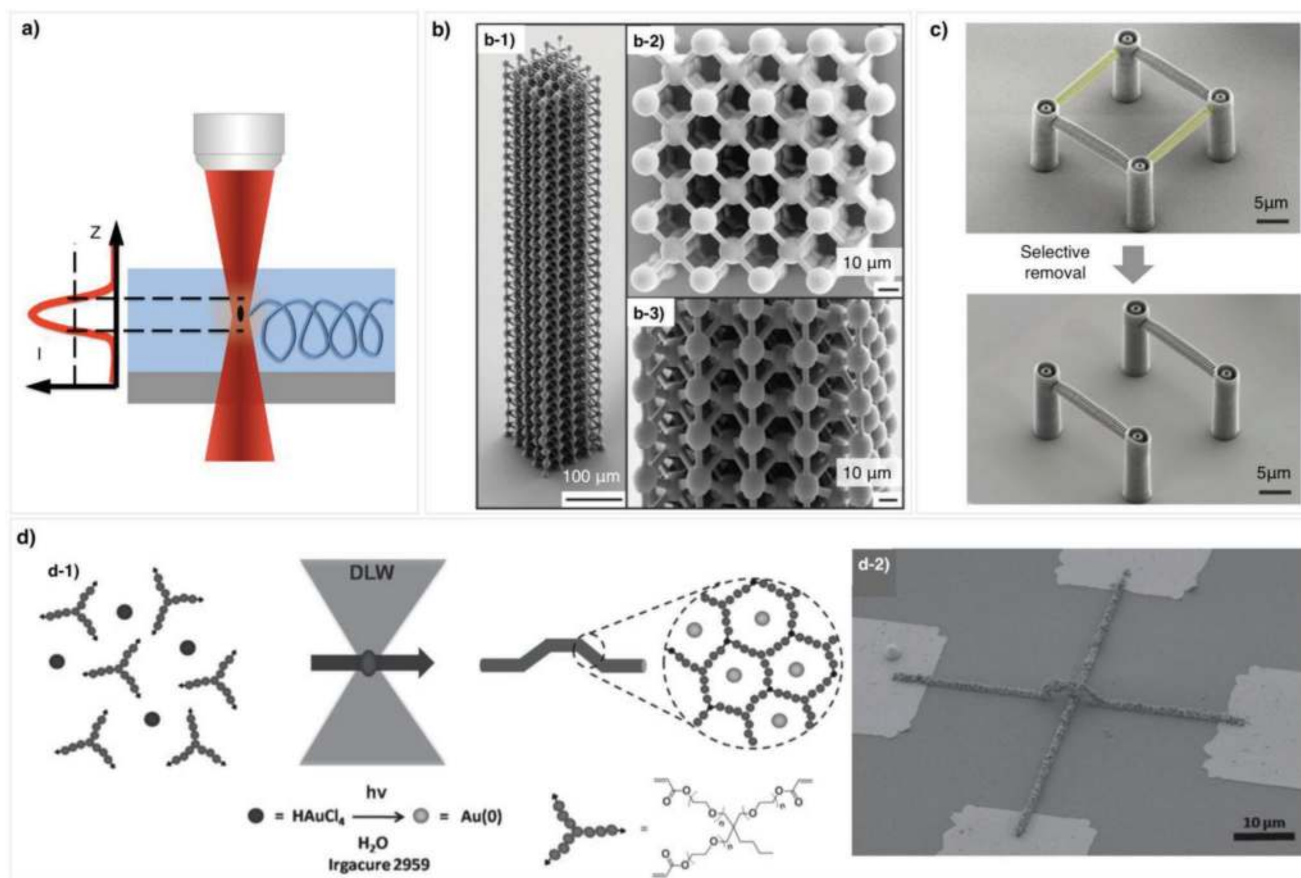

Figure 12. Two-photon polymerization. a) Schematic process of TPA-based DLW. A tightly focused beam triggers the reaction only in a very small volume (voxel) as TPA has a quadratic dependence with light intensity. b) High aspect ratio complex structures: SEM analysis of a 1 mm high 3D structure based on thiol–alkyne photoresist showing b-1) general, b-2) top, and b-3) side views. Reproduced with permission.[138] Copyright 2015, Wiley-VCH. c) Compound structures: Thiol–ene-based elements (stained yellow) are integrated in a structure generated using a conventional photoresist (in gray). Selective cleavage of the integrated thiol–ene-based elements leaves the primary structure unaffected. Adapted with permission.[67g] Copyright 2018, Wiley-VCH. d) Functional structures: d-1) Schematic illustration of the simultaneous photopolymerization and photoreduction of gold in the conductive photoresist and d-2) SEM image of electrical connections on the microscale. Reproduced with permission.[141b] Copyright 2016, Wiley-VCH.

precludes nowadays the direct fabrication of large samples using this technique.

Common photoresists used in TPP are based on free-radical polymerization of acrylates,[135] cationic ring-opening polymerization of epoxides, mainly SU-8,[136] or organic–inorganic hybrid systems.[137] Alternative chemistries for the preparation of 3D photonic microstructures have been undertaken based on photoinduced Diels–Alder reaction,[75b] and photoinduced thiol–ene[67c] and thiol–yne polymerization.[138] As a recent example, the group of Wegener and Barner-Kowollik developed novel photoresists based on a tetrafunctional thiol, a tetrafunctional alkyne, and a photoinitiator. The radical coupling of thiols and alkynes induced by TPA processes enables the preparation of structures as large as 1 mm with micrometric feature size with writing speed of 1 cm s^{-1} (see Figure 12b). Advantageously, this photoinduced chemistry leaves unreacted thiol and alkyne groups, so postmodification of the generated 3D structures can be performed by thiol-Michael addition and the copper-catalyzed azide alkyne cycloaddition.[138]

Most photopolymers used with TPP are negative resists that, after cross-linking and development, lead to stable structures that can only be removed under harsh cleavage conditions. This limits their use as templates for replication in other materials (e.g., inorganic) or as sacrificial supports for building other material structures with flying features, as the sacrificial elements are not always removed completely or damage is infringed to the final structure on development. Recently, the groups of Barner-Kowollik and Wegener have introduced novel chemoselective cleavable photoresists that enable removable 3D microstructures using mild chemical conditions. These photoresists, based on labile silane cross-linkers, together with a multifunctional acrylate and a two-photon photoinitiator,[139] allow the fabrication of stable 3D structures through TPP. The inclusion of different silanes enables the selective degradation of the microstructures using mild cleavage conditions, for example, $NaHCO_3$, K_2CO_3, or KF in methanol. In another example, commercially available chemicals are used to prepare thiol–ene-based formulations for TPP, leading to dimensionally

 © 2019 The Authors. Published by WILEY-VCH Verlag GmbH & Co. KGaA, Weinheim

stable complex 3D microstructures that can be later cleaved by exposing to ethanolamine. The same authors demonstrate the preparation of compound structures comprising permanent segments, prepared with conventional photoresists and cleavable elements that can be selectively eliminated afterward, serving as temporary supports to generate mechanically demanding structures (Figure 12c).[67g]

The possibility to digitally create 3D structures with features in the range of tens of nanometers offers great potential in different application areas. Periodic structures generated by TPA-based DLW have been directly used as photonic structures or as templates for the fabrication of inverse replicas.[136a,137,140] Functionalities can also be directly added in the photoresists or later in the final microstructure. In this way, the fabrication of electrically conductive structures with this level of resolution could have a large impact in microelectronics, nanophotonics, or plasmonics. Efforts to generate these conductive microstructures have been focused on the photoreduction of metallic salts that can be included directly in a photoresist (Figure 12d).[141] Formulations incorporating soluble silver trifluoroacetate in a SU-8 photoresist have been used to fabricate 3D microstructures with silver nanoparticles embedded in the polymeric matrix. This is achieved by TPA-based DLW and a thermal annealing at moderate temperatures.[141a] Alternatively, 3D microstructures can be functionalized in a later step. As an example, a maleimide functionalized π-conjugated polythiophene was used to functionalize 3D polymeric microstructures fabricated via TPA-based DLW.[75c]

In the biomedical field, TPA-based DLW has drawn large attention to create patterned substrates and structures for cell–substrate interaction and mechanobiological studies.[142] Polymeric surfaces textured with submicrometric linear ridges through this technique have been employed to perform cell–substrate interaction studies demonstrating improved axonal growth and guidance along the linear features as well as promotion of the differentiation of stem cells toward neurons.[143] Beyond surfaces, 3D scaffolds have served to carry out cell adhesion and migration studies.[144] Cell-laden systems based on methacrylated gelatin have demonstrated to be suitable systems for in situ cell encapsulation generating complex 3D tissue models.[144c] TPA-based DLW has also been extensively used in the preparation of 3D microstructures with controlled mechanical response (e.g., auxetic structures), constituting an interesting platform for mechanobiological studies.[136b,145]

Although the fabrication of hydrogel structures with TPA processes is typically done by photo-cross-linking the hydrogel precursors, patterning of hydrogels can also be carried by locally modifying an existing hydrogel. TPA has been used to produce a 3D modulation of the biophysical and biochemical hydrogel properties. This has been done, for example, on a system based on poly(ethylene glycol) provided with photolabile blocks by Anseth and coworkers, as already mentioned in Section 2.3.1.[34] Mesenchymal stem cells (MSCs) encapsulated in this material respond to the locally photoinduced hydrogel changes. While MSCs in the unexposed, and therefore densely cross-linked, regions, were round in shape, they showed spread morphology in the exposed areas in which the cleavage of the backbone at the photolabile blocks reduces the cross-linking density. Overall, this platform enables great spatiotemporal control of the physical interactions between the cells and the hydrogel.[34] In another example, poly(vinyl alcohol) norbornenes together with a proteolytic cross-linker have been used to create cell-laden hydrogels provided with cell-instructive cues, such as cell-adhesive motifs, that are immobilized by multiphoton excitation. This strategy enables precise control of cell migration, with great flexibility and precision in both space and time.[144d]

Liquid crystalline polymers have also been explored as photoresists for the generation of smart microstructures through TPP. Parmeggiani, Wiersma, and coworkers have demonstrated the fabrication of 3D liquid crystal elastomer (LCE) microstructures with controlled mesogen orientation. The observed anisotropic swelling of these microstructures, perpendicular to the preferential orientation direction, offers great potential in the fabrication of responsive structures for robotic applications.[146] More recently, 3D bimaterial hetero-microstructures incorporating temperature-responsive poly(*N*-isopropylacrylamide) have been created by TPP. The differential expansion of the materials leads to controlled deformation of the structures. Even more, by locally changing the photocuring dose, different thermal expansion is advantageously achieved, so heterostructures can be generated with one single photoresist. Thermal actuation has been demonstrated by globally heating the sample and its environment; however, light-induced heating of the sample can also be used to trigger the deformation gaining control in the actuation and shortening the response time.[147]

3.4. UV-Assisted NIL

UV-assisted NIL is one of the most important NIL techniques that is demonstrated to be a suitable approach for the low-cost, high-throughput generation of well-defined, high aspect ratio nanostructures over a large wafer area with resolutions below 10 nm. In UV-assisted NIL, a mold is pressed against a low-viscosity prepolymer, which is later UV photopolymerized. Once cured, the material is detached from the mold and its inverse topography is replicated in the polymerized material (**Figure 13**a).[148] Advances in the way to apply the photoresins, by using microdeposition techniques, as done in jet-and-flash imprint lithography (J-FIL), the modern version of step-and-flash imprint lithography, have notably improved defectivity. Resolutions on the order of 5 nm,[149] which compete with state-of-the-art mask-based photolithographies, have been achieved. UV-assisted NIL, compatible with nonflat and flexible substrates,[150] has demonstrated to be compatible with roll-to-roll (R2R) continuous production processes bridging the gap between basic research in the laboratory and real applications closer to the market of flexible electronics (Figure 13b).[151] Going toward an industrial process, photopolymerizable materials for UV-assisted NIL should show low viscosities, so the material can easily flow into the mold features with little pressure. Besides, photocuring should be preferably conducted at RT and be fast enough to be compatible with R2R production processes.

Acrylate materials have been extensively used as UV-assisted NIL resins as their properties can be finely tuned by the choice of already commercially available components; however, these

© 2019 The Authors. Published by WILEY-VCH Verlag GmbH & Co. KGaA, Weinheim

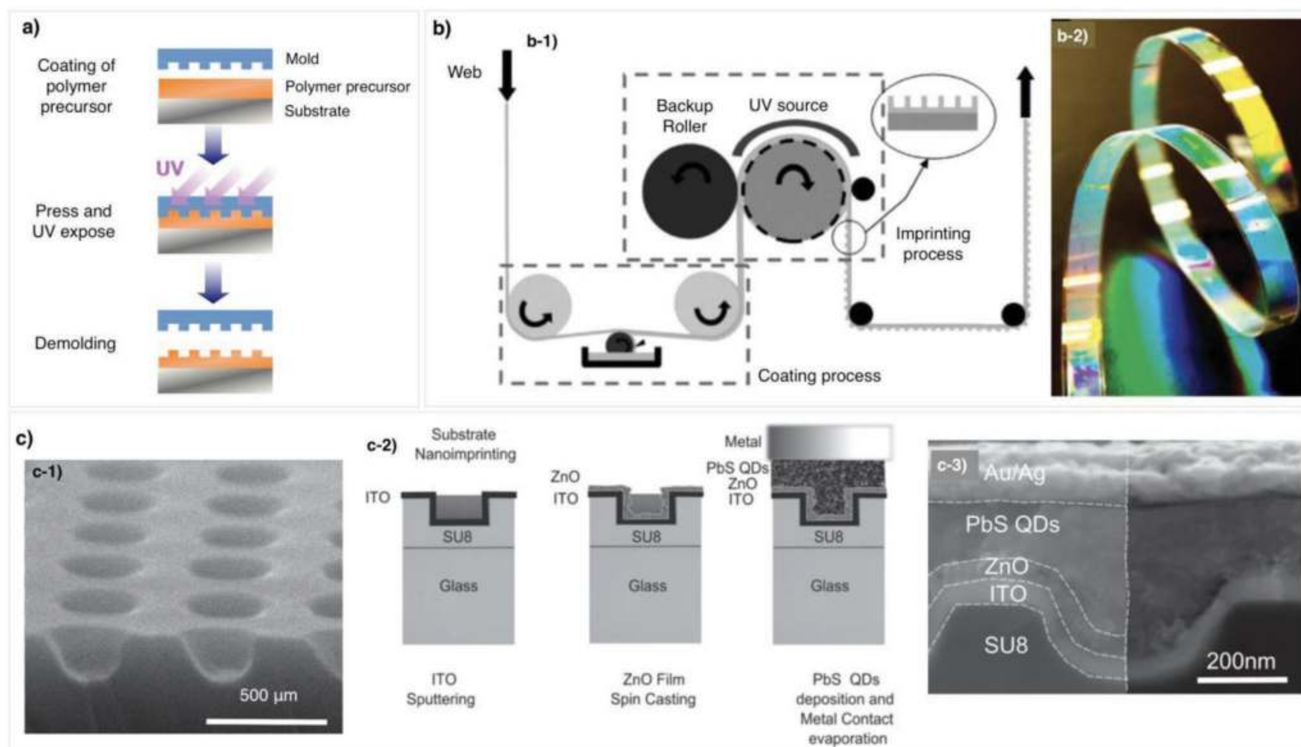

Figure 13. UV-assisted NIL. a) Schematic illustration of the UV-assisted NIL process. b) Roll-to-roll process: b-1) Schematic of the R2R process and b-2) PET stripe with a 700 nm period, 300 nm linewidth periodic pattern imprinted on an epoxysilicone photopolymer. Adapted with permission.[151b] Copyright 2008, Wiley-VCH. c) Enhancing performance of heterojunction solar cells: Based on an imprinted epoxy-based periodic structure (c-1), a heterojunction solar cell is constructed by (c-2) coating ITO by sputtering deposition, spin casting and sintering ZnO nanocrystals, layer-by-layer deposition of the PbS quantum dots, and evaporation of the metal contacts leading to the structure shown in (c-3). Reproduced with permission.[153] Copyright 2014, Wiley-VCH.

formulations present some limitations. Photocuring of these systems, based on free-radical polymerization, can be advantageously conducted at RT with fast curing rates; however, the presence of oxygen in the working atmosphere strongly inhibits the curing process complicating the use of these technologies in an industrial environment. Shrinkage upon polymerization, usually present in acrylate formulations, also has deleterious effects on the dimensional fidelity of the created structure.[152] Compared to acrylates, epoxide monomers have been used significantly less, despite they being not sensitive to oxygen, as they typically present higher viscosities, requiring the use of solvents to assist the molding step.[153] Trying to address all these issues, alternative chemistries have been employed such as vinyl ethers or thiol–ene prepolymers leading to high-resolution patterns through this technique. In particular, thiol–ene systems are quite attractive as they do not suffer from oxygen inhibition and the reaction can also be triggered even without initiator.[45,154] Jiang and coworkers have prepared hybrid resins consisting in polyhedral oligomeric silsesquioxane functionalized with mercaptopropyl groups together with mono- and multifunctionalized methacrylate monomers. These photopolymerizable systems have low viscosity (6–25 cP), good coating ability, fast photopolymerization rate, and acceptable volumetric shrinkage on the order of 5%, all these being suitable characteristics to achieve good pattern transfer in UV-assisted NIL. Besides, the hybrid organic–inorganic nature of the material confers high etching resistance for O_2 plasma, so this system can be used as a sacrificial layer for silicon nanopatterning. By using a double layer approach, with a poly(methyl methacrylate) layer in between the silicon and the photoresist, nanopatterns obtained by UV-assisted NIL in the photoresist can be successfully transferred to the underlying silicon substrate with enhanced aspect ratio.[154b]

The sub-10 nm resolution reached with UV-assisted NIL has attracted great interest in the semiconductor industry. Efforts are being devoted in this area toward the reduction of defects by improving the control of particles in the air, and the improvement of the throughput of wafers, now on the order of some tens of wafers per hour. Durability of the mold has also been improved through a good management of contaminants reaching 1000 replicas per mold.[155]

UV-assisted NIL has also demonstrated great potential in the preparation of micropatterned surfaces for cell–substrate interaction studies,[156] biomimetic surfaces with anisotropic friction-reducing properties,[157] and with controlled wettability.[158] Periodic structures generated by UV-assisted NIL have found also large interest as sensitive substrates for surface-enhanced Raman scattering detection,[159] or in the preparation of optical elements such as wire-grid polarizers,[160] antireflective surfaces,[161] and enhancement foils for photovoltaic or optoelectronic devices.[153,162] As an example, Konstantanos and coworkers demonstrated improvement of the photocurrent in

© 2019 The Authors. Published by WILEY-VCH Verlag GmbH & Co. KGaA, Weinheim

solution-processed solar cells by patterning the transparent conductive oxide electrode with an array of holes. This is fabricated by sputtering indium tin oxide onto an SU-8 nanoimprinted electrode that besides collecting the photogenerated carriers also diffracts light, partly trapping it within the thickness of the solar cell structure, all this without deterioration of the electrical characteristics of the system (Figure 13c). This results in a device, implemented by a low-cost approach, with a 17.5% enhancement of power conversion efficiency with respect to the unstructured system.[153]

3.5. Inkjet Printing

Inkjet printing enables the digitally controlled ejection of well-defined volume ink droplets and their precise positioning onto virtually any type of substrate. Traditionally used in text and graphical printing, the ability of inkjet printing of accurately positioning picoliter drops of ink has been more recently exploited to create functional surfaces and devices. Inks with viscosities in the range of 1–20 cps can be typically used with this technology leading to droplets with sizes of tens of micrometers generated at rates up to 20 kHz.[163] Although inkjet printing is a serial process, multiple printheads, each having a large number of nozzles, can be used to pattern surfaces with multiple materials and high throughput, being compatible with R2R production. Advantageously, inkjet printing usually requires minimal postprocessing to obtain the final structure, eliminating the need of wet etching steps typically used in photolithographic techniques.

Typically, a printhead that contains the ink generates a pressure pulse in the fluid, for example, by the sudden deformation of a piezoelectric element in contact with the fluid, which is the responsible of the ejection of a fluid jet through the nozzle (**Figure 14**a). To finally generate well-controlled drops of ink, the jet needs to thin and break up. This jet thinning, driven by surface tension forces, is balanced by viscous and inertial forces. Thus, for sufficiently viscous liquids, surface tension, which tends to squeeze the jet, opposes the viscous stresses within the jet. Contrarily, for low-viscosity fluids, inertia of the fluid within the jet opposes its thinning.[164] This balance of forces is captured by the Ohnesorge number *Oh* given by

$$Oh = \frac{\eta}{\sqrt{\gamma \rho a}} \tag{3}$$

where η is the viscosity, γ is the surface tension, ρ is the density, and a is the nozzle diameter. Experimental studies demonstrate that stable drop formation typically occurs for *Oh* numbers between 0.1 and 1.[165] Besides, energy of the jet should be high enough to have ejection of ink,[166] but not as high as to produce splashing of the ink when reaching the substrate.[167] Once the ink is at the target substrate, it needs to solidify in order to become part of a functional device.

Photopolymerizable materials have been employed in the production of functional patterns and elements by inkjet printing. For example, microlenses with short focal length and large numerical aperture have been successfully generated using this technology enabling better control for in-coupling and out-coupling of light in different devices.[168] Well definition of the optical parameters of the deposited microlenses requires an appropriate selection of the optical properties of the employed material and a fine control of the lens geometry. Inkjet printing enables a large degree of accuracy on all these parameters.[169] As an example, substrates, prepatterned with microplatforms obtained through photolithographic steps, and

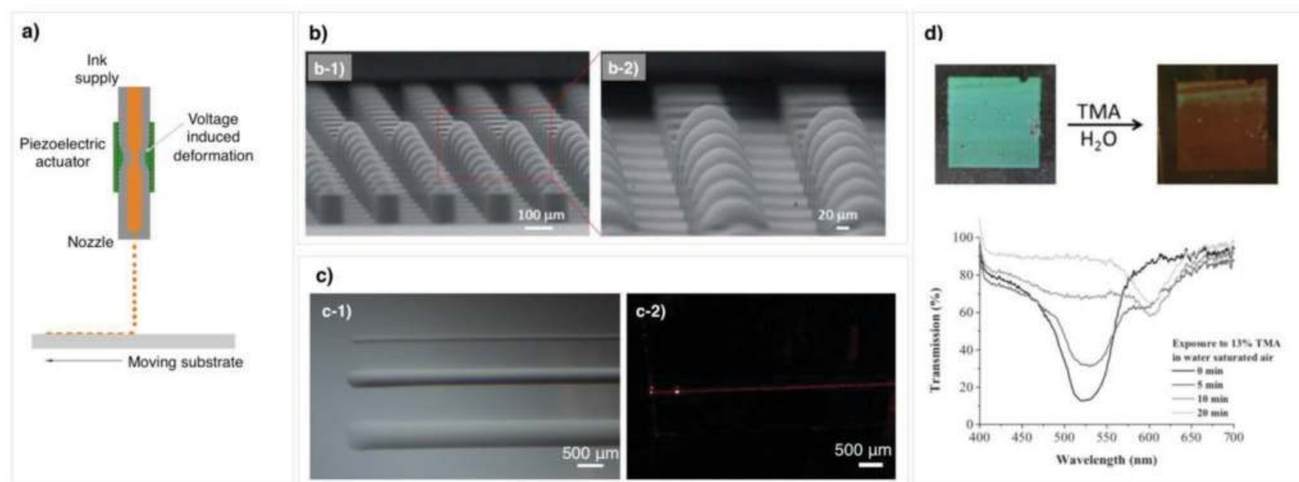

Figure 14. Inkjet printing. a) Schematic illustration of the inkjet printing process (piezoelectric technology). b) Printed microlenses: SEM images of arrays of organic–inorganic hybrid material microlenses fabricated by inkjet printing on 200 µm diameter platforms treated with a fluorosilane. Different number of droplets per platform (from one, at the front, to ten, at the back) lead to different microlens geometries. Reproduced with permission.[169d] Copyright 2013, The Royal Society of Chemistry. c) Printed waveguides: c-1) Channel optical waveguides of different dimensions. c-2) Scattered light streak from an inkjet printed channel waveguide. Reproduced with permission.[171b] Copyright 2018, The Royal Society of Chemistry. d) Response of an inkjet printed cholesteric liquid crystal polymer film to exposure with TMA and water, shifting color from green to red. Transmission spectra changes measured with circularly polarized light after different exposure times of the film to TMA. Reproduced with permission.[173c] Copyright 2014, Wiley-VCH.

© 2019 The Authors. Published by WILEY-VCH Verlag GmbH & Co. KGaA, Weinheim

coated with a fluorosilane, have been used to fabricate arrays of microspherical lenses with well-defined height and radius of curvature. The deposition on the microplatforms of different number of droplets of an organic–inorganic hybrid ink enables, after solvent evaporation and curing, a precise control of the lens characteristics (Figure 14b).[169d]

The ability to digitally pattern lines or areas of material makes inkjet printing also an attractive technique for the fabrication of channel and planar waveguides. Solvent-containing photopolymerizable hybrid organic–inorganic inks have been used for this purpose.[170] To avoid the soft baking steps, needed to evaporate the solvent before photopolymerization, solvent-free inks with suitable viscosity for inkjet printing have also been formulated to prepare printed waveguides. They can be directly printed and photocured immediately after deposition, without the need of further postbaking steps allowing the use of thermally sensitive substrates.[171] As an example, photo-acid-catalyzed organic–inorganic hybrid formulations, based on epoxy and silane monomers, have been successfully prepared as jettable inks for the fabrication of planar and channel waveguides. In the presence of atmospheric water, UV light concomitantly triggers in these systems the photopolymerization of epoxy groups and the hydrolysis and condensation of the silane groups leading to the formation of a cross-linked organic–inorganic polymeric network. Differently from inks based on conventional sol–gel, hydrolysis and condensation are delayed in the absence of actinic light favoring the ink long-term stability. Planar and channel waveguides with propagation losses as low as 0.5 dB cm^{-1} have been prepared with these materials by means of inkjet printing, showing the suitability of these techniques for the preparation of photonic devices (Figure 14c).[171b]

Besides optical applications, inkjet printing of photopolymerizable mesogenic formulations has also been demonstrated to be a powerful tool for the preparation of mechanical actuators,[172] as well as low-cost, battery-free sensors.[173] As an example, thin films based on H-bonded cholesteric LC networks obtained by inkjet printing followed by photopolymerization of reactive mesogens have demonstrated to reversibly change their reflection band in response to humidity or the presence of chemicals such as trimethylamine (TMA), as shown in Figure 14d.[173c]

3.6. Extrusion-Based 3D Printing Techniques

Besides the already mentioned light-assisted 3D fabrication techniques, 3D printing can also be carried out by extruding and selectively depositing materials at digitally defined positions. Many popular commercial printers rely on fused deposition modeling technology that uses a thermoplastic solid filament that feeds a hot extrusion printhead. This selectively deposits molten polymer that immediately solidifies upon deposition, as the material cools down below its glass transition temperature, becoming fixed at the target position.[122a,b] 3D printing can make use of the same basic principle of extrusion and deposition of materials, applied to inks showing viscoelasticity at RT (**Figure 15**a). These materials ideally should have filament formation characteristics on extrusion and the printed lines should present adequate consistency once deposited to guarantee structural integrity of the printed structures and fidelity of the 3D features. These properties are simultaneously found in yield-stress inks that flow when certain threshold of pressure is overcome in the ink reservoir producing an excess of shear stress in the dispensing needle and a drastic decrease of viscosity. Immediately after the material leaves the needle and it is deposited, shear stresses disappear in the ink and this quickly forms a gel leading to filaments with well-defined and self-supporting characteristics, enabling the formation of stable 3D structures.[174] The yield-stress inks can be obtained by including rheology modifiers such as molecular additives, nanoclays, or nanosilicates that can interact with either charged or neutral polymers or even with themselves to form physically cross-linked networks showing the shear-thinning characteristics described earlier.[175] Photopolymerizable materials with this yield-stress feature have been formulated to create 3D printed structures by means of extrusion-based printing. After deposition, the resultant structure can be fixed by exposure to actinic light, this being usually done in a layer-by-layer basis to ensure homogeneous curing of the structure.

As an example, Burdick and coworkers have developed shear-thinning bioinks based on the dual cross-linking of hyaluronic acid (HA)-based hydrogels encompassing guest–host interactions and photo-cross-linking (Figure 15b). When HA is separately modified by coupling with adamantane (Ad) guest and β-cyclodextrin (CD) host moieties, two different hydrogel precursors (Ad-HA and CD-HA, respectively) are obtained. Both precursors supramolecularly assemble through the formation of guest–host pairs, forming a pregel solution upon mixing. These supramolecular guest–host systems (Ad-HA:CD-HA) presents shear-thinning and self-healing characteristics needed to form filaments upon extrusion printing; however, the 3D printed structures tend to collapse after few minutes. If HA is modified only with methacrylate groups leading to a photo-cross-linkable hydrogel precursor (MeHA), the resultant printed hydrogel structures directly collapse just after printing as the materials have no self-assembly characteristics that could stabilize the structure upon deposition. The structural integrity of the supramolecularly cross-linked hydrogel is drastically enhanced by introducing photopolymerizable methacrylate groups onto the adamantane and β-cyclodextrin polymers that can be covalently cross-linked by light just after printing. The removal of shear just after the ink leaves the dispensing needle leads to certain stabilization of the extruded filament due to guest–host interactions; however, fast photopolymerization of the methacrylate groups of the polymers drastically improves the mechanical properties of the hydrogel. The printed HA-based structures were further biofunctionalized with oligopeptides containing the adhesive arginine–glycine–aspartate sequence to support cell adhesion demonstrating the potential of these hydrogel materials and structures as platforms for drug screening and testing, as well as tissue engineering constructs.[176]

Another interesting strategy to preserve the structural integrity of printed filaments, fully relying on the photopolymerization of inks, without limitation on their viscosity, has been recently developed by partially photocuring the ink while it is passing through a light-transmissive dispensing capillary

© 2019 The Authors. Published by WILEY-VCH Verlag GmbH & Co. KGaA, Weinheim

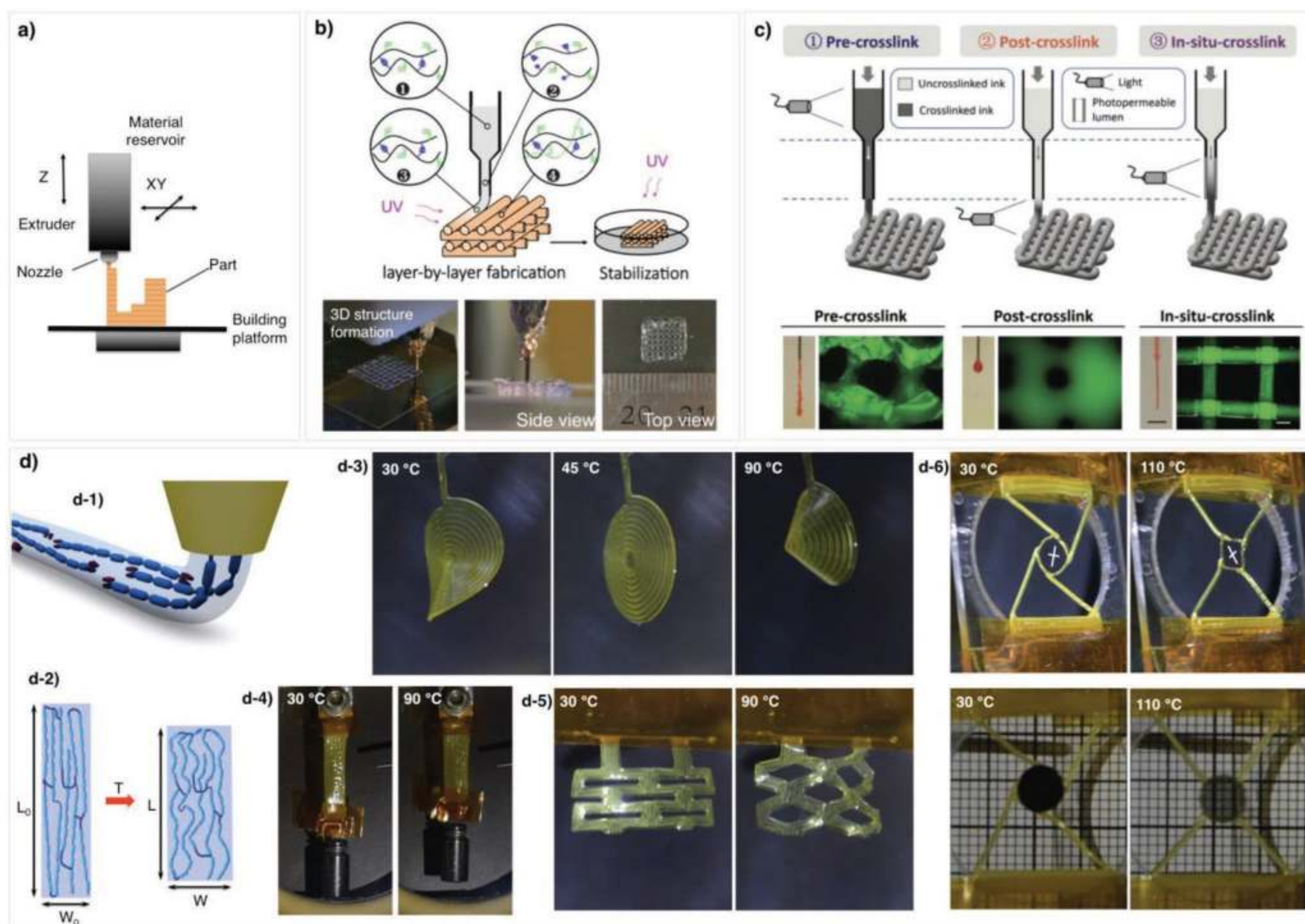

Figure 15. Extrusion-based 3D printing. a) Schematic illustration of the extrusion printing process. b) 3D printing of dual cross-linking hydrogels. Hydrogels are self-assembled in the reservoir through guest–host interactions (1) that are disrupted due to shear in the needle (2). When deposited, hydrogels self-assemble again as no shear is present (3). UV exposure (4) further stabilizes the hydrogels enabling 3D structure formation. Adapted with permission.[176] Copyright 2016, American Chemical Society. Society. c) In situ cross-linking approach: Instead of UV exposure before (pre-cross-link) or after (post-cross-link), partial curing during extrusion (in situ cross-link) by using a photopermeable capillary leads to self-supported structures even when using initially nonviscous formulations. Reproduced with permission.[176] Copyright 2016, Wiley-VCH. d) 4D printing of LCEs. d-1) Schematic view of LC polymer main-chain alignment along the printing direction. d-2) Schematic representation of thermomechanical response of aligned LCEs. d-3) Thermomechanical deformation of a film with spiral-like director texture (8 mm film diameter at 30 °C). d-4) Printed LCE multilayer stripe (25 mm × 6 mm). A weight of 5 is lifted up on heating. d-5) Open structure changing pore shape and size on heating. d-6) Framed chiral structure with inner circle rotating on heating (top). A polarizer piece is rotated by the action of the chiral actuator (bottom). Reproduced with permission.[179b] Copyright 2016, Wiley-VCH.

(Figure 15c).[177] While conventional 3D printing using synthetic acrylate-based macromers, such as PEGDA, leads to filaments that collapse upon deposition, this in situ cross-linking technique enables the 3D printing of distortion-free and self-supported 3D structures up to 10 mm high, using this same precursor.

Besides their use as scaffolds for cell culture, extrusion 3D printed hydrogel structures have been employed in the preparation of stretchable electrical devices as demonstrated by Suo, Vlassak, and coworkers. A photopolymerizable hydrogel precursor, including a hygroscopic salt and a rheological modifier, is 3D printed and later photocured turning into ionically conductive structures with sub-millimeter resolution. These are integrated with polydimethylsiloxane to create soft resistance-based strain sensors with potential applications in soft robotics.[178]

3D printed hydrogels have also been explored as shape-morphing structures. Typically, hydrogel swelling is isotropic in nature; however, Mahadevan, Lewis, and coworkers demonstrated the incorporation of anisotropic mechanical properties in extrusion printed hydrogel structures based on a photopolymerizable ink containing nanofibrillated cellulose.[175b] Upon extrusion, cellulose nanofibrils anisotropically align along the printing direction. This alignment is fixed through photopolymerization carried out just after deposition. The printed filaments show anisotropic mechanical and swelling characteristics that can be controlled through the printing process. This capability to control morphology offers the possibility to design printing paths leading to well-defined alignment patterns that upon swelling morph into prescribed target complex shapes. Through this platform, biomimetic plant-inspired 3D structures have been demonstrated to develop from flat structures in response to humidity.

 © 2019 The Authors. Published by WILEY-VCH Verlag GmbH & Co. KGaA, Weinheim

Extrusion printing has also been extended to mesogenic photopolymerizable materials to generate LCE structures with shape-morphing characteristics as recently demonstrated in three different laboratories.[179] The employed ink basically consists in a main-chain liquid crystalline macromer provided with acrylate end reactive groups together with a photoinitiator. An adequate choice of the printing conditions, mainly ink flux rate, printing speed, and nozzle diameter, leads to alignment of the LC director in the printed material (Figure 15d-1). This alignment can be fixed through photopolymerization at RT. As a result, the printing path determines the LC director pattern of the printed structure and therefore enables the digital programming of stresses upon the right stimuli, temperature in the most simple case (Figure 15d-2).

Figure 15d-3 shows a disk-shaped element printed using this platform. The spiral printing path followed during deposition provides the element with a director profile following this same geometry.[179b] At temperatures close to RT, the system shows a nearly flat shape. Heating of the sample generates stresses within the film inducing deformation. The thermally induced decrease of LC order produces a contraction along the preferential direction of the LC molecules and an expansion along the orthogonal direction. In the particular case of the spiral, the film tends to contract in the azimuthal direction and, at the same time, to expand in the radial one. The system escapes out of the plane to accommodate these stresses, forming a cone as previously predicted by Warner and coworkers.[180] Other robotic functions have been demonstrated such as the artificial muscle of Figure 15d-4 able to lift an object 30 times heavier than itself over a height of 5 mm, just by heating the stripe from 30 to 90 °C. Membrane-type structures that change pore size and shape upon heating have also been implemented (Figure 15d-5). 4D printed LCE chiral structures have also been created, demonstrating their ability to rotate objects. The central ring of the structure, held by four bands, rotates on heating. This function can be used to turn another object, such as a small piece of linear polarizer, as shown in Figure 15d-6.[179b] Overall, this printing platform provides a precise control of the director morphology in the printed structures enabling a precise engineering of the mechanical response in the 4D printed LCE structures.

4. Molecular Alignment Enabled by Light

The generation of soft polymeric structures is most commonly achieved by means of a photoinduced cross-linking process, such as a free-radical or a cycloaddition reaction. The way such a process takes place is intimately linked to the interaction between light and the photosensitive material. For example, the nature of the photosensitive molecule will determine to some extent the energy of the exciting light. Also, radiation intensity is sometimes fixed by the kinetics of the photoinduced reaction. Furthermore, if undesired side reactions occur during light exposure, the dose of the radiation may need to be limited. Besides frequency and intensity, which need to be properly adjusted in any light-enabled structuring process, polarization is another property of radiation that, while not commonly considered in many structuring processes, has important implications in a number of applications, mainly optical ones, but not limited to them. Only a selected group of molecules enables the possibility of fully exploiting the polarization of light for the generation or ordered structures, regardless of whether they are at the nano- or microscale levels. Azobenzenes, cinnamates, and coumarins, presented in Section 2, are some prominent examples of that group of chromophores that enable the generation of anisotropically ordered structures by capturing the information of the polarization state of light. Such ordered structures are typically based on LC phases, and, in many cases, can be inscribed, erased, and selectively reconfigured in a fully reversible manner. This is an interesting feature if applications requiring rewritable materials are to be pursued. This section covers a selection of those polarization-modulated strategies enabling the production of ordered structures and some recent related applications.

In azobenzene-containing materials, the molecular-level process lying at the origin of all subsequent mechanisms and transformations is the *trans–cis* isomerization of azobenzene chromophores that has been covered in Section 2.1. When using LPL of the appropriate wavelength, typically in the blue–green region, azobenzene molecules preferentially align perpendicular to the polarization of the employed light.[18] Photoinduced molecular alignment, which is normally higher in liquid crystalline polymers than in amorphous systems, leads to significant birefringence and dichroism.[5,181] The photoinduced alignment imposed on an azobenzene-containing film can also be transferred, in some cases, through anisotropic interactions to adjacent liquid crystalline materials.[25a,182] In addition to azobenzene materials, side-chain polymers containing cinnamate and coumarin units have also been used for photoalignment of LCs. Exposure of thin films of these materials to UV LPL leads to anisotropically cross-linked systems. Liquid crystals brought in contact with these, so-irradiated, layers align either parallel or perpendicular to the polarization of the actinic light, depending on the material and light dose employed in the cross-linking step.[22,26a,183] Overall, the appropriate design of photoalignment materials and the selection of irradiation conditions, including intensity, dose, and polarization, enable a good control of the anisotropy of the polarization-sensitive material itself as well as that imposed on adjacent liquid crystalline systems.

Due to the large birefringence of mesogenic materials, this patterned control of the morphology has been extensively exploited in the development of different polymeric films for optical applications. Polymeric retarders with orientational patterns have been prepared by photoalignment and used as enhancement foils for liquid crystal displays,[20] or as security elements for valuable documents and goods.[184] These have been obtained, for example, by combining polarization-sensitive cinnamate-containing polymers with a reactive LC. First, a mask-wise irradiation, with different polarizations, of a thin layer of a photoalignment cinnamate-containing polymer is carried out. Second, a thin film of a reactive LC is deposited on top of the photoalignment layer by, for example, spin coating. After being deposited, the reactive LC aligns following the orientation defined during the light exposure step. Finally, the orientation of the reactive LC is fixed by photopolymerization leading to a fully cross-linked and thermally stable optical film with a patterned anisotropic structure.[183a]

© 2019 The Authors. Published by WILEY-VCH Verlag GmbH & Co. KGaA, Weinheim

The ability to locally register anisotropy in polarization-sensitive materials has also enabled the development of a branch of holography, named polarization holography, offering distinctive advantages with respect to conventional holography, such as the ability to reconstruct the registered light field polarization or the achievable 100% efficiency, regardless of the thin or thick character of the hologram.[185] This technique makes use of overlapping, equal intensity beams with different, typically orthogonal, polarizations. As an example, when two circularly polarized beams of orthogonal polarization and equal intensity are made to interfere at small angles of incidence on the film surface, close to the normal, the resultant field in the interference region essentially lies in the plane of the film. Light in this region has constant intensity and a linear polarization that continuously rotates along the grating vector.[185b] Liquid crystalline azobenzene polymers have been extensively investigated as media to register this type of holography. Different chromophores as well as a manifold of polymer architectures have been explored looking for materials able to register stable gratings with high sensitivity for volume holographic recording.[7a,20,21] In addition, polarization gratings have also been used to implement other optical elements and devices such as polarization conversion systems,[186] optical elements to generate beams with orbital angular momentum,[187] and spectropolarimeters capable of characterizing polarimetric parameters of light in real time across different wavelengths with applications in optical remote sensing, biomedical imaging, and telecommunications.[188]

The ability to transfer photoalignment to liquid crystalline materials has also been crucial to achieve control over the shape-morphing capabilities of nematic cross-linked films (**Figure 16**). As already shown in this review, 2D LC network films with a heterogeneous director field have the capability of morphing into 3D shapes.[180] Nematic networks with disclination-type director patterns of different strength were generated by Broer, Schenning, and coworkers by using photoalignment techniques. A photomask with a wedge-shaped opening is used to partly expose to linearly polarized light an LC cell with cinnamate-based photoalignment layers in the inner sides. While the LC cell is being exposed, it slowly rotates under the mask. After a complete rotation, the cell is fully exposed and a complex orientational pattern is registered on the photoalignment inner layers (Figure 16a).[189] The cell is subsequently filled with a reactive mesogen that orients according to the alignment dictated by the light pattern. In the final step, the reactive liquid crystal layer is photopolymerized, thus fixing the LC orientation. Azimuthal or radial director patterns are easily created with this photolithographic platform leading to nematic cross-linked films that deform into conical or saddle-like shape, respectively, upon heating. Using an equivalent procedure, but employing laser light on azobenzene photoalignment layers, disclination-type nematic network films with different defect strengths have been created by White and coworkers (Figure 16b). Photoexcitation of azobenzene dyes included in the nematic network leads to deformation patterns with a symmetry that is coupled to the strength of the inscribed defect.[190]

Other paradigms of deformation have been demonstrated using photoalignment layers and reactive mesogens.[191] As an example, a thin film of nematic polymer network with alternating twisted–nematic regions leads to accordion-like deformations on photoinduced heating.[192] Advancing toward applications, Priimagi and coworkers implemented a self-regulating artificial iris using a cross-linked liquid crystalline polymeric film with a complex orientational profile. Such a profile was achieved by using an LC cell composed of two different layers: a homeotropic orientational layer and a radially aligned azobenzene-based layer—which was obtained by exposing the film to an azimuthally polarized beam (Figure 16c). After filling the cell with a reactive mesogen, a nematic network is formed by photopolymerization. The freestanding film, which contains Disperse Red 1 (DR1), is cut out with 12 petal-like segments that bend up spontaneously to release mechanical stresses leading to the opened up device in the absence of light. Exposure to visible blue light induces continuous *trans–cis–trans* isomerizations of the DR1 units releasing heat to the sample. As a result, due to the defined director profile, the device selfregulates the aperture size in response to the intensity of the incident light.[193]

Pixelated arbitrary director patterns with resolution on the order of 100 µm have also been generated by using a point-by-point focused laser exposure system developed by the group of White.[194] The system controls position, exposure dose, and polarization of the focused beam that digitally modifies an azobenzene photoalignment layer generating the targeted orientational pattern. Additionally, White and coworkers also developed an innovative two-step synthetic procedure to in situ produce patterned LCEs in photopatterned LC cells. First, a low molecular weight nematic diacrylate—which easily aligns according to the commanding layer—is chain extended via an aza-Michael addition in the presence of *n*-butylamine (chain extender). A slight stoichiometric excess of the low molecular weight reactive LC with respect to the chain extender ensures that diacrylate groups remain active at the chain ends of the resulting main-chain LC polymer (LC macromer), which retains the orientation imposed by the commanding layer. The LC macromer is then photopolymerized leading to patterned LCE flat sheets that are capable of morphing into 3D objects when exposed to thermal, chemical, or light stimulation (Figure 16d).[195] A similar strategy has been successfully adapted to thiol–ene/acrylate and thiol–acrylate formulations to prepare LCEs, in this case, through a one-step radical polymerization. The inclusion of a dithiol chain transfer agent reduces the cross-linking via chain transfer and chain extension, leading to LCEs exhibiting reversible strain up to 150%.[196]

Photoinduced alignment of azobenzene molecules can also be transferred to nanoscopic anisotropic structures such as the cylindrical phases found in some photoresponsive block copolymers. With photolithographies approaching resolution closer to the size of typical self-assembled objects, arrangement of these building blocks into well-ordered structures is already a firm candidate for the next generation of nanopatterning techniques.[197] In this sense, photoresponsive self-assembled materials are an exciting platform encompassing the benefits of bottom-up block copolymer lithography and top-down photolithographies. The groups of Seki, Ikeda, and Yu have thoroughly investigated the photoalignment of nanocylinders by employing azobenzene-containing block copolymers. Such materials typically exhibit a microstructure composed of non-photosensitive nanocylinders embedded in a continuous

© 2019 The Authors. Published by WILEY-VCH Verlag GmbH & Co. KGaA, Weinheim

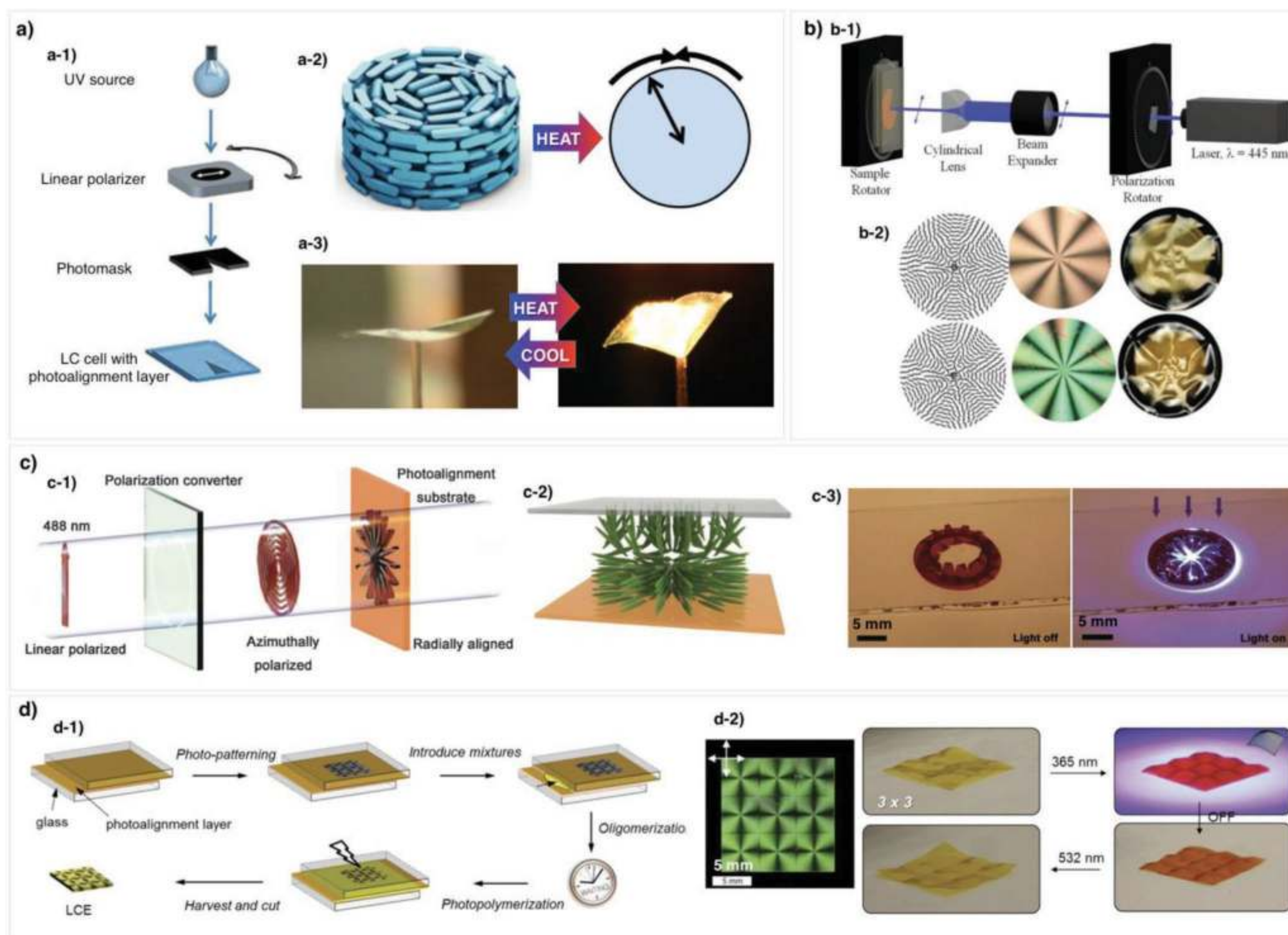

Figure 16. Photoalignment-enabled LC actuators. a) Complex director patterns in the plane: a-1) Schematic illustration of a photolithographic setup for the preparation of patterned alignment LC cells using wedge mask and rotating sample. a-2) Alignment of mesogens in an azimuthal sample and stresses on heating. a-3) Actuation behavior upon heating with an IR lamp. a) Adapted with permission.[189] Copyright 2016, Wiley-VCH. b) Complex director patterns in the plane: b-1) Schematic image of the laser-based setup for point-by-point patterning of LC alignment cells. b-2) Examples of (from left to right) of topological defects director patterns, polarization microscope images, and light-induced deformations in azo-responsive LC networks. Adapted with permission.[190] Copyright 2016, Wiley-VCH. c) Self-regulating iris: c-1) An azimuthally polarized beam is used to expose an azobenzene photoalignment layer and get radial alignment. c-2) Radial to homeotropic alignment of the LC. c-3) The polymerized film is cut out in a circle with 12 petal-like internal segments. In the absence of UV light, the iris is opened and closes upon UV irradiation. Adapted with permission.[193] Copyright 2016, Wiley-VCH. d) LCE with large mechanical response: d-1) Two-step synthetic preparation of LCEs. d-2) Photoresponse of arrays of LCE defects. Adapted with permission.[195] Copyright 2016, Wiley-VCH.

azobenzene LC matrix. Orientation of the nanocylinders, which have a periodicity in the range of tens of nanometers, can be precisely defined on demand, out and in the plane, by changing the polarization of the exciting light and carefully selecting the processing and annealing conditions of the material (**Figure 17**a).[198] Pushing forward to smaller feature definition, Schenning and coworkers have used azobenzene-containing oligo(dimethylsiloxane) mesomorphic materials. These photoresponsive systems self-organize into periodic cylindrical nanostructures with periodicities as small as 3.8 nm. Such morphologies can be aligned in the plane by irradiating the sample with linearly polarized blue light at temperatures just below the isotropization temperature to favor mobility (Figure 17b). The organic–inorganic hybrid nature that favors etch contrast, together with the possibility to combine top-down photolithography to micropattern regions with different morphology orientations, turns these systems into an exciting platform for next-generation nanolithographic processes.[199]

5. Conclusions and Outlook

The ability of light to trigger specific physicochemical changes in resists, polymers, and other reactive systems with a high degree of spatiotemporal control is pivotal to produce well-defined structures, patterns, and morphologies of interest in areas including microelectronics, photonics, biomedicine, and soft robotics. Advances in these areas are the result of interdisciplinary efforts led by chemists, physicists, material scientists, and engineers. These efforts, which include the development of innovative photosensitive materials and novel processing technologies and processes, seek at increasing structure resolution,

© 2019 The Authors. Published by WILEY-VCH Verlag GmbH & Co. KGaA, Weinheim

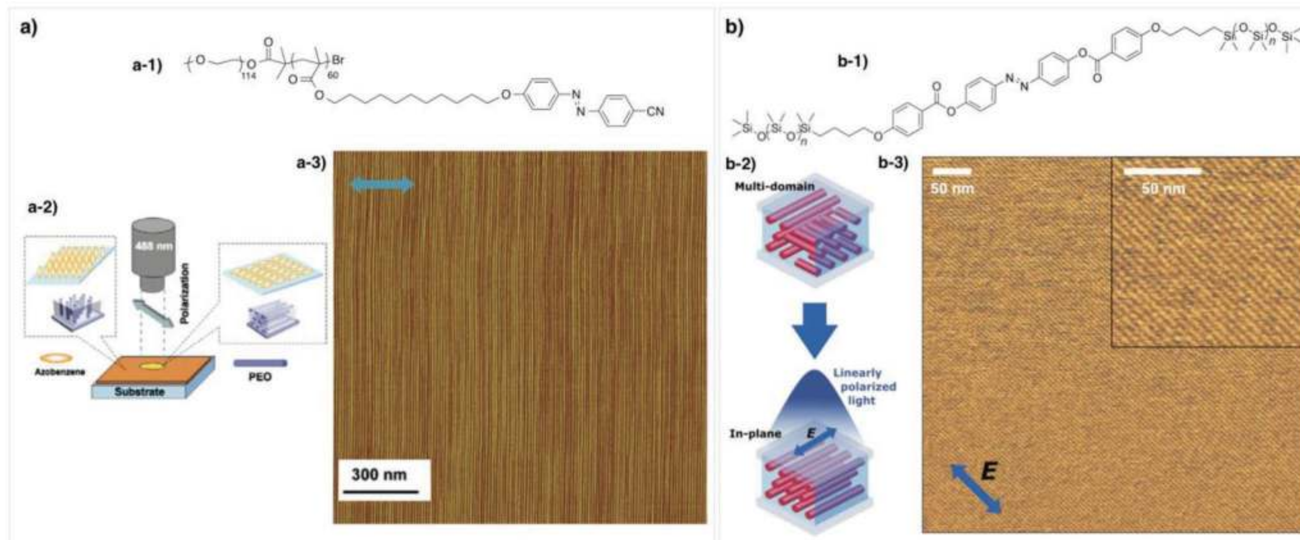

Figure 17. Photoalignment of nanosegregated morphologies. a) Block copolymers. a-1) Chemical structure of a block copolymer leading to poly(ethylene oxide) nanocylinders embedded in an azobenzene-rich LC phase. a-2) Photoinduced alignment of cylinders perpendicular to polarization of light. a-3) Atomic force microscopy (AFM) phase image of an aligned block copolymer film obtained after irradiation and annealing. Arrow indicates the polarization direction of the actinic light. a) Adapted with permission.[198b] Copyright 2016, American Chemical Society. Society. b) Oligo(dimethylsiloxane) for sub-5 nm nanolithography. b-1) Chemical structure of the oligo(dimethylsiloxane) ($n = 5, 9, 13$). b-2) Photoinduced alignment of nanocylinders parallel to polarization. b-3) AFM phase image of an aligned morphology obtained after irradiation. Adapted with permission.[199] Copyright 2016, Wiley-VCH.

lowering manufacturing costs, improving throughput, and enhancing material functionalities.

Progresses in the structuring of light-sensitive polymers have been primarily driven by industrial needs. The insatiable demand for increasingly powerful microelectronic devices has been fueling the progression of the semiconductor industry that tracks Moore's law projections now for more than five decades. This evolution is associated with continuous improvements in materials, photolithographic systems, and processing techniques. Nowadays, DUV 193 nm technology is being pushed to its limits extending its lifetime and reaching astonishing state-of-the-art resolutions of 10 nm. To proceed toward further miniaturization, alternative approaches need to reach industrial production. UV-assisted NIL can beat the current resolution limits of DUV technology and EUV lithography, with light of 13.5 nm, is very well positioned to lead the path toward scaling transistors to smaller nodes. Advanced photolithographic setups and resists for EUV technology are nowadays being developed. With a current target resolution of 7 nm, feature dimension of semiconductors devices is fast approaching the size of the molecules and polymers in these photosensitive materials. Inherently disordered polymeric resists present inhomogeneities at sub-10 nm length scales, leading to defects and structure collapse, being therefore nonideal for this extreme lithography. Thus, alternative systems exhibiting a well-controlled morphology at these dimensions must be developed. Highly ordered molecular systems such as calixarenes or metal oxide–based resists are promising systems for this technology. Inclusion of photoresponsive units, such as azobenzenes, in self-assembled resist materials has also demonstrated great potential to achieve molecular alignment and a higher level of control over feature resolution and orientation. Sub-5 nm features have been reached in these photoaddressable systems by combining top-down and bottom-up patterning strategies.

In parallel to the development of patterning techniques for the mass production of microelectronics, the evolution of AM is shifting the paradigm of fabrication technology itself. AM technologies are key to the fourth industrial revolution in which we are already immersed, and a complete new set of manufacturing techniques is being developed, many of which rely on light-responsive materials. These tools and materials are increasingly sophisticated and have already enabled the production of unprecedented patterns and structures, which are difficult or impossible to create with other processing techniques. However, before AM becomes a player in the arena of industrial applications, many challenges need to be overcome. Broadly, AM techniques would need to improve production speed while keeping resolution in large printed volumes. Recent breakthroughs, such as CLIP, which enables continuous and fast stereolithographic printing of 3D structures, or CAL, allowing the production of structures and parts by tomographic reconstruction, hold the promise to generate new fabrication paradigms and bring AM technologies into mass production. Fast and cost-effective production of structures and devices by these AM technologies will have a huge impact in application areas spanning from engineering, aerospace, automotive, energy to consumer products.

The production of functional polymeric structures with a high level of resolution and performance remains to be one of the major challenges for structuring techniques. There is a need to combine together material architecture and function at different length scales and build a new generation of devices with capabilities that are still a distant dream. Breakthroughs highlighted in this review show the powerful concepts that can be realized by combining light-sensitive materials with advanced

© 2019 The Authors. Published by WILEY-VCH Verlag GmbH & Co. KGaA, Weinheim

manufacturing tools. For example, the development of electrically conductive well-defined structures through light-assisted technologies could change the paradigm of the microelectronics industry and enable the transition from essentially flat 2D microprocessor systems to 3D architectures capable of effectively dissipating heat produced on processing.

On a different arena, light-assisted techniques have enabled the production of biocompatible structures that recreate specific aspects of the ECM of native tissues. Here, there is a challenge that remains, namely, maintaining (bio-)functionality active after processing, which is important to produce ideal synthetic mimics of natural tissues or structures. This will provide more reliable platforms for drug screening, progressively replacing animal models, or suitable constructs for tissue engineering.

In another field of application, there has been a growing interest in the fabrication of responsive structures over the last decade. On one hand, light-based manufacturing techniques enable the preparation of complex structures that can be functionalized with appropriate molecules to be sensitive to specific analytes. Structures can undergo physical changes when a particular chemical substance is present, thus serving as soft sensors in biomedical and environmental applications. On the other hand, stimuli-responsive materials that are capable of delivering mechanical work hold great expectations in a number of fields including biomedicine, automotive, aerospace, or robotics. Achieving a fine control of both the structure and the morphology of stimuli-responsive materials is of paramount importance to control the internal stresses in the material and therefore the mechanical deformation and functions of the resultant structure. Light-responsive photoaddressable surfaces based on azobenzenes or cinnamates have been demonstrated to be a powerful tool to program controlled deformations in thin layers of cross-linked LC polymers. The combination of 3D printing techniques and photopolymerizable stimuli-responsive materials, including high-performance shape memory polymers, hydrogels, and liquid crystalline materials, has now enabled the next generation of 4D printing technologies to fabricate objects that are capable of evolving with time and adapting their shape in response to external agents such as humidity or temperature. Despite these advances, further efforts need to be employed toward the development of functional light-sensitive materials that, in combination with advanced manufacturing tools, will directly lead to structures with controlled morphology and mechanics. Our ability to integrate materials across different length scales, from nano- to macroscale, and simultaneously embed programmed robotic functions in these structures in response to different stimuli will allow to fully deploy the power of 4D printing.

Acknowledgements

J.d.B. acknowledges the MINECO, the FSE, and the FEDER for funding through projects RYC-2015-18471 (Ramón y Cajal program) and CTQ2017-84087. C.S.-S. thanks the Spanish MICINN projects BIO2017-84246-C2-1-R, Gobierno de Aragón, and FEDER (EU).

Conflict of Interest

The authors declare no conflict of interest.

Keywords

photochemical reactions, photosensitive materials, polymeric materials, structuring techniques

Received: April 10, 2019
Revised: May 16, 2019
Published online: June 6, 2019

[1] a) G. M. Wallraff, W. D. Hinsberg, *Chem. Rev.* **1999**, *99*, 1801; b) M. Totzeck, W. Ulrich, A. Göhnermeier, W. Kaiser, *Nat. Photonics* **2007**, *1*, 629; c) M. Waldrop, *Nature* **2016**, *530*, 144.
[2] a) B. D. Gates, Q. B. Xu, M. Stewart, D. Ryan, C. G. Willson, G. M. Whitesides, *Chem. Rev.* **2005**, *105*, 1171; b) M. E. Stewart, C. R. Anderton, L. B. Thompson, J. Maria, S. K. Gray, J. A. Rogers, R. G. Nuzzo, *Chem. Rev.* **2008**, *108*, 494; c) Z. Nie, E. Kumacheva, *Nat. Mater.* **2008**, *7*, 277; d) P. Jonkheijm, D. Weinrich, H. Schröder, C. M. Niemeyer, H. Waldmann. *Angew. Chem., Int. Ed.* **2008**, *47*, 9618; e) S. Tawfick, M. De Volder, D. Copic, S. J. Park, C. R. Oliver, E. S. Polsen, M. J. Roberts, A. J. Hart, *Adv. Mater.* **2012**, *24*, 1628; f) C. Acikgoz, M. A. Hempenius, J. Huskens, G. J. Vancso, *Eur. Polym. J.* **2011**, *47*, 2033; g) Y. Lin, J. Xu, *Adv. Opt. Mater.* **2018**, *6*, 1701359.
[3] a) N. J. Turro, *Modern Molecular Photochemistry*, University Science Books, Sausalito, CA **1991**; b) J. P. Fouassier, J. Lalevée, *Photoinitiators for Polymer Synthesis*, Wiley-VCH, Weinheim, Germany **2012**; c) Y. Yagci, S. Jockusch, N. J. Turro, *Macromolecules* **2010**, *43*, 6245; d) J. V. Crivello, E. Reichmanis, *Chem. Mater.* **2014**, *26*, 533; e) S. Chatani, C. J. Kloxin, C. N. Bowman, *Polym. Chem.* **2014**, *5*, 2187; f) R. Göstl, A. Senf, S. Hecht, *Chem. Soc. Rev.* **2014**, *43*, 1982; g) E. Blasco, M. Wegener, C. Barner-Kowollik, *Adv. Mater.* **2017**, *29*, 1604005.
[4] a) A. Priimagi, C. J. Barrett, A. Shishido, *J. Mater. Chem. C* **2014**, *2*, 7155; b) H. Yu, T. Ikeda, *Adv. Mater.* **2011**, *23*, 2149; c) H. Yu, *Prog. Polym. Sci.* **2014**, *39*, 781; d) T. Seki, *J. Mater. Chem. C* **2016**, *4*, 7895; e) M. O'Neill, S. M. Kelly, *J. Phys. D: Appl. Phys.* **2000**, *33*, R67.
[5] A. Natansohn, P. Rochon, *Chem. Rev.* **2002**, *102*, 4139.
[6] a) J. J. De Lange, J. Monteath Robertson, I. Woodward, *Proc. R. Soc. London, Ser. A* **1939**, *171*, 398; b) C. J. Brown, *Acta Crystallogr.* **1966**, *21*, 146.
[7] a) S. Hvilsted, C. Sánchez, R. Alcalá, *J. Mater. Chem.* **2009**, *19*, 6641; b) A. Priimagi, A. Shevchenko, *J. Polym. Sci., Part B: Polym. Phys.* **2014**, *52*, 163; c) S. L. Oscurato, M. Salvatore, P. Maddalena, A. Ambrosio, *Nanophotonics* **2018**, *7*, 1387; d) A. Priimagi, G. Cavallo, A. Forni, M. Gorynsztejn-Leben, M. Kaivola, P. Metrangolo, R. Milani, A. Shishido, T. Pilati, G. Resnati, G. Terraneo, *Adv. Funct. Mater.* **2012**, *22*, 2572.
[8] a) G. S. Kumar, D. C. Neckers, *Chem. Rev.* **1989**, *89*, 1915; b) P. Weis, S. Wu, *Macromol. Rapid Commun.* **2018**, *39*, 1700220; c) S. T. J. Ryan, J. del Barrio, R. Suardíaz, D. F. Ryan, E. Rosta, O. A. Scherman, *Angew. Chem.* **2016**, *128*, 16330; d) J. del Barrio, E. Blasco, C. Toprakcioglu, A. Koutsioubas, O. A. Scherman, L. Oriol, C. Sánchez-Somolinos, *Macromolecules* **2014**, *47*, 897; e) S. Hernández-Ainsa, R. Alcalá, J. Barberá, M. Marcos, C. Sanchez, J. L. Serrano, *Macromolecules* **2010**, *43*, 2660; f) J. Vapaavuori, C. G. Bazuin, A. Priimagi, *J. Mater. Chem. C* **2018**, *6*, 2168; g) H. K. Bisoyi, Q. Li, *Chem. Rev.* **2016**, *116*, 15089.
[9] H. Rau, in *Photochemistry and Photophysics* (Ed: F. J. Rabeck), CRC, Boca Raton, FL **1990**.
[10] H. M. D. Bandara, S. C. Burdette, *Chem. Soc. Rev.* **2012**, *41*, 1809.
[11] a) G. C. Hampson, J. M. Robertson, *J. Chem. Soc. (Resumed)* **1941**, 409; b) M. Sato, T. Kinoshita, A. Takizawa, Y. Tsujita, *Macromolecules* **1988**, *21*, 1612.

© 2019 The Authors. Published by WILEY-VCH Verlag GmbH & Co. KGaA, Weinheim

[12] a) G. S. Hartley, *Nature* **1937**, *140*, 281; b) G. S. Hartley, R. J. W. Le Fèvre, *J. Chem. Soc.* **1939**, 531.
[13] a) S. Kurihara, T. Ikeda, T. Sasaki, H.-B. Kim, S. Tazuke, *J. Chem. Soc., Chem. Commun.* **1990**, 1751; b) T. Cusati, G. Granucci, M. Persico, *J. Am. Chem. Soc.* **2011**, *133*, 5109.
[14] a) L. Lamarre, C. S. P. Sung, *Macromolecules* **1983**, *16*, 1729; b) T. Naito, K. Horie, I. Mita, *Macromolecules* **1991**, *24*, 2907; c) T. Naito, K. Horie, I. Mita, *Polymer* **1993**, *34*, 4140.
[15] a) E. Sackmann, *J. Am. Chem. Soc.* **1971**, *93*, 7088; b) C. Ruslim, K. Ichimura, *J. Phys. Chem. B* **2000**, *104*, 6529; c) N. Tamaoki, Y. Aoki, M. Moriyama, M. Kidowaki, *Chem. Mater.* **2003**, *15*, 719; d) C. Sánchez, R. Alcalá, S. Hvilsted, P. S. Ramanujam, *J. Appl. Phys.* **2003**, *93*, 4454.
[16] a) T. Buffeteau, F. Lagugné Labarthet, M. Pézolet, C. Sourisseau, *Macromolecules* **1998**, *31*, 7312; b) Z. Sekkat, W. Knoll, *Photoreactive Organic Thin Films*, Academic, San Diego, CA **2002**.
[17] T. Huang, K. H. Wagner, *J. Opt. Soc. Am. A* **1993**, *10*, 306.
[18] F. Weigert, *Verh. Dtsch. Phys. Ges.* **1919**, *21*, 479.
[19] T. Ikeda, O. Tsutsumi, *Science* **1995**, *268*, 1873.
[20] a) A. S. Matharu, S. Jeeva, P. S. Ramanujam, *Chem. Soc. Rev.* **2007**, *36*, 1868; b) M. Ishiguro, D. Sato, A. Shishido, T. Ikeda, *Langmuir* **2007**, *23*, 332; c) M. Häckel, L. Kador, D. Kropp, H. W. Schmidt, *Adv. Mater.* **2007**, *19*, 227.
[21] P. Forcén, L. Oriol, C. Sánchez, F. J. Rodríguez, R. Alcalá, S. Hvilsted, K. Jankova, *Eur. Polym. J.* **2007**, *43*, 3292.
[22] O. Yaroshchuk, Y. Reznikov, *J. Mater. Chem.* **2012**, *22*, 286.
[23] N. Kawatsuki, H. Ono, H. Takatsuka, T. Yamamoto, O. Sangen, *Macromolecules* **1997**, *30*, 6680.
[24] L. M. Minsk, W. P. van Deusen, E. M. Robertson, *US Patent 2 751 296*, **1956**.
[25] a) K. Ichimura, *Chem. Rev.* **2000**, *100*, 1847; b) C. M. Dong, X. Wu, J. Caves, S. S. Rele, B. S. Thomas, E. L. Chaikof, *Jpn. J. Appl. Phys.* **1992**, *31*, 2155; c) C. Zhu, S. R. Kustra, C. J. Bettinger, *Acta Biomater.* **2013**, *9*, 7362; d) M. Schadt, K. Schmitt, V. Kozinkov, V. Chigrinov, *Jpn. J. Appl. Phys.* **1992**, *31*, 2155.
[26] a) M. Obi, S. Morino, K. Ichimura, *Macromol. Rapid Commun.* **1998**, *19*, 643; b) M. O´Neill, S. M. Kelly, *J. Phys. D: Appl. Phys.* **2000**, *33*, R67; c) Q. Fu, L. Cheng, Y. Zhang, W. Shi, *Polymer* **2008**, *49*, 4981; d) C. P. Kabb, C. S. O'Bryan, C. C. Deng, T. E. Angelini, B. S. Sumerlin, *ACS Appl. Mater. Interfaces* **2018**, *10*, 16793; e) A. Concellón, A. P. H. J. Schenning, P. Romero, M. Marcos, J. L. Serrano, *Macromolecules* **2018**, *51*, 2349; f) C. Kim, A. Trajkovska, J. U. Wallace, S. H. Chen, *Macromolecules* **2006**, *39*, 3817.
[27] a) H. D. Becker, *Chem. Rev.* **1993**, *93*, 145; b) H. Bouas-Laurent, J.-P. Desvergne, A. Castellan, R. Lapouyade, *Chem. Soc. Rev.* **2000**, *29*, 43.
[28] J. Van Damme, F. Du Prez, *Prog. Polym. Sci.* **2018**, *82*, 92.
[29] a) T. Ohta, O. Urakawa, Q. Tran-Cong, *Macromolecules* **1998**, *31*, 6845; b) R. D. M. Travasso, O. Kuksenok, A. C. Balazs, *Langmuir* **2005**, *21*, 10912; c) W. Chen, J.-Y. Wang, W. Zhao, L. Li, X. Wei, A. C. Balazs, K. Matyjaszewski, T. P. Russell, *J. Am. Chem. Soc.* **2011**, *133*, 17217.
[30] a) B. L. Feringa, W. F. Jager, B. de Lange, *Tetrahedron* **1993**, *49*, 8267; b) A. S. Dvornikov, E. P. Walker, P. M. Rentzepis, *J. Phys. Chem. A* **2009**, *113*, 13633; c) P. Weis, W. Tian, S. Wu, *Chem. Eur. J.* **2018**, *24*, 6494; d) M. Irie, T. Fukaminato, K. Matsuda, S. Kobatake, *Chem. Rev.* **2014**, *114*, 12174.
[31] a) T. Tsuruoka, R. Hayakawa, K. Kobashi, K. Higashiguchi, K. Matsuda, Y. Wakayama, *Nano Lett.* **2016**, *16*, 7474; b) H. Vijayamohanan, E. F. Palermo, C. K. Ullal, *Chem. Mater.* **2017**, *29*, 4754; c) R. Ji, S. Fu, X. Zhang, X. Han, S. Liu, X. Wang, Y. Liu, *Sci. Rep.* **2018**, *8*, 3818; d) P. Müller, R. Müller, L. Hammer, C. Barner-Kowollik, M. Wegener, E. Blasco, *Chem. Mater.* **2019**, *31*, 1966.
[32] P. Klán, T. Šolomek, C. G. Bochet, A. Blanc, R. Givens, M. Rubina, V. Popik, A. Kostikov, J. Wirz, *Chem. Rev.* **2013**, *113*, 119.
[33] a) P. M. Kharkar, K. L. Kiick, A. M. Kloxin, *Chem. Soc. Rev.* **2013**, *42*, 7335; b) H. Zhao, E. S. Sterner, E. B. Coughlin, P. Theato, *Macromolecules* **2012**, *45*, 1723.
[34] A. M. Kloxin, A. M. Kasko, C. N. Salinas, K. S. Anseth, *Science* **2009**, *324*, 59.
[35] a) D. R. Griffin, A. M. Kasko, *J. Am. Chem. Soc.* **2012**, *134*, 13103; b) D. R. Griffin, J. L. Schlosser, S. F. Lam, T. H. Nguyen, H. D. Maynard, A. M. Kasko, *Biomacromolecules* **2013**, *14*, 1199; c) D. R. Griffin, A. M. Kasko, *ACS Macro Lett.* **2012**, *1*, 1330.
[36] M. A. Azagarsamy, I. A. Marozas, S. Spaans, K. S. Anseth, *ACS Macro Lett.* **2016**, *5*, 19.
[37] a) P. Gumbley, D. Koylu, R. H. Pawle, B. Umezuruike, E. Spedden, C. Staii, S. W. Thomas III, *Chem. Mater.* **2014**, *26*, 1450; b) X. Hu, E. McIntosh, M. G. Simon, C. Staii, S. W. ThomasIII, *Adv. Mater.* **2016**, *28*, 715; c) X. Hu, Z. Qureishi, S. W. ThomasIII, *Chem. Mater.* **2017**, *29*, 2951.
[38] a) M. J. Feeney, X. Hu, R. Srinivasan, N. Van, M. Hunter, I. Georgakoudi, S. W. Thomas III, *Langmuir* **2017**, *33*, 10877; b) M. M. Mahmoodi, S. A. Fisher, R. Y. Tam, P. C. Goff, R. B. Anderson, J. E. Wissinger, D. A. Blank, M. S. Shoichet, M. D. Distefano, *Org. Biomol. Chem.* **2016**, *14*, 8289.
[39] A. del Campo, E. Arzt, *Chem. Rev.* **2008**, *108*, 911.
[40] W. A. Green, *Industrial Photoinitiators: A Technical Guide*, CRC, Boca Raton, FL **2010**.
[41] B. Levrand, A. Herrmann, *Photochem. Photobiol. Sci.* **2002**, *1*, 907.
[42] G. Ullrich, P. Burtscher, U. Salz, N. Moszner, R. Liska, *J. Polym. Sci., Part A: Polym. Chem.* **2006**, *44*, 115.
[43] N. Moszner, T. Hirt, *J. Polym. Sci., Part A: Polym. Chem.* **2012**, *50*, 4369.
[44] E. S. Jönsson, T. Y. Lee, K. Viswanathan, C. E. Hoyle, T. M. Roper, C. A. Guymon, C. Nason, I. V. Khudyakov, *Prog. Org. Coat.* **2005**, *52*, 63.
[45] C. J. Kloxin, T. F. Scott, C. N. Bowman, *Macromolecules* **2009**, *42*, 2551.
[46] a) B. H. Cumpston, S. P. Ananthavel, S. Barlow, D. L. Dyer, J. E. Ehrlich, L. L. Erskine, A. A. Heikal, S. M. Kuebler, I.-Y. S. Lee, D. McCord-Maughon, J. Qin, H. Röckel, M. Rumi, X.-L. Wu, S. R. Marder, J. W. Perry, *Nature* **1999**, *398*, 51; b) R. Nazir, E. Balčiūnas, D. Buczyńska, F. Bourquard, D. Kowalska, D. Gray, S. Maćkowski, M. Farsari, D. T. Gryko, *Macromolecules* **2015**, *48*, 2466; c) R. Whitby, Y. Ben-Tal, R. MacMillan, S. Janssens, S. Raymond, D. Clarke, J. Jin, A. Kay, M. C. Simpson, *RSC Adv.* **2017**, *7*, 13232.
[47] Z. Li, N. Pucher, K. Cicha, J. Torgersen, S. C. Ligon, A. Ajami, W. Husinsky, A. Rosspeintner, E. Vauthey, S. Naumov, T. Scherzer, J. Stampfl, R. Liska, *Macromolecules* **2013**, *46*, 352.
[48] a) J. V. Crivello, *J. Polym. Sci., Part A: Polym. Chem.* **1999**, *37*, 4241; b) J. V. Crivello, K. Dietliker, *Photoinitiators for Free Radical Cationic & Anionic Photopolymerisation*, Wiley, Chichester, UK **1998**.
[49] a) F. D. Saeva, D. T. Breslin, P. A. Martic, *J. Am. Chem. Soc.* **1989**, *111*, 1328; b) F. Hamazu, S. Akashi, T. Koizumi, T. Takata, T. Endo, *J. Polym. Sci., Part A: Polym. Chem.* **1991**, *29*, 1845; c) J. V. Crivello, S. Kong, *J. Polym. Sci., Part A: Polym. Chem.* **2000**, *38*, 1433; d) J. Shao, Y. Huang, Q. Fan, *Polym. Chem.* **2014**, *5*, 4195.
[50] a) J. V. Crivello, M. Sangermano, *J. Polym. Sci., Part A: Polym. Chem.* **2001**, *39*, 343; b) G. Yilmaz, S. Beyazit, Y. Yagci, *J. Polym. Sci., Part A: Polym. Chem.* **2011**, *49*, 1591.
[51] Y. Fukuchi, T. Takahashi, H. Noguchi, M. Saburi, Y. Uchida, *Macromolecules* **1987**, *20*, 2316.
[52] a) C. Kutal, P. A. Grutsch, D. B. Yang, *Macromolecules* **1991**, *24*, 6872; b) Y. Yamaguchi, B. J. Palmer, C. Kutal, T. Wakamatsu, D. B. Yang, *Macromolecules* **1998**, *31*, 5155; c) C. T. Sanderson,

© 2019 The Authors. Published by WILEY-VCH Verlag GmbH & Co. KGaA, Weinheim

B. J. Palmer, A. Morgan, M. Murphy, R. A. Dluhy, T. Mize, I. J. Amster, C. Kutal, *Macromolecules* **2002**, *35*, 9648.
[53] a) N. Arsu, A. Önen, Y. Yagci, *Macromolecules* **1996**, *29*, 8973; b) E. Faggi, J. Aguilera, R. Sáez, F. Pujol, J. Marquet, J. Hernando, R. M. Sebastián, *Macromolecules* **2019**, *52*, 2329.
[54] a) K. Dietliker, R. Hüsler, J. L. Birbaum, S. Ilg, S. Villeneuve, K. Studer, T. Jung, J. Benkhoff, H. Kura, A. Matsumoto, H. Oka, *Prog. Org. Coat.* **2007**, *58*, 146; b) W. Xi, H. Peng, A. Aguirre-Soto, C. J. Kloxin, J. W. Stansbury, C. N. Bowman, *Macromolecules* **2014**, *47*, 6159.
[55] H. C. Kolb, M. G. Finn, K. B. Sharpless, *Angew. Chem., Int. Ed.* **2001**, *40*, 2004.
[56] a) C. W. Tornøe, C. Christensen, M. Meldal, *J. Org. Chem.* **2002**, *67*, 3057; b) V. V. Rostovtsev, L. G. Green, V. V. Fokin, K. B. Sharpless, *Angew. Chem., Int. Ed.* **2002**, *41*, 2596.
[57] S. C. Ritter, B. König, *Chem. Commun.* **2006**, *127*, 4694.
[58] M. A. Tasdelen, Y. Yagci, *Tetrahedron Lett.* **2010**, *51*, 6945.
[59] A. A. Poloukhtine, N. E. Mbua, M. A. Wolfert, G.-J. Boons, V. V. Popik, *J. Am. Chem. Soc.* **2009**, *131*, 15769.
[60] B. J. Adzima, Y. Tao, C. J. Kloxin, C. A. DeForest, K. S. Anseth, C. N. Bowman, *Nat. Chem.* **2011**, *3*, 256.
[61] a) T. Gong, B. J. Adzima, N. H. Baker, C. N. Bowman, *Adv. Mater.* **2013**, *25*, 2024; b) A. A. Alzahrani, A. H. Erbse, C. N. Bowman, *Polym. Chem.* **2014**, *5*, 1874; c) A. U. Shete, B. M. El-Zaatari, J. M. French, C. J. Kloxin, *Chem. Commun.* **2016**, *52*, 10574; d) T. Gong, B. J. Adzima, C. N. Bowman, *Chem. Commun.* **2013**, *49*, 7950; e) A. Baranek, H. B. Song, M. McBride, P. Finnegan, C. N. Bowman, *Macromolecules* **2016**, *49*, 1191; f) H. B. Song, A. Baranek, C. N. Bowman, *Polym. Chem.* **2016**, *7*, 603; g) H. B. Song, A. Baranek, B. T. Worrell, W. D. Cook, C. N. Bowman, *Adv. Funct. Mater.* **2018**, *28*, 1801095; h) S. Liang, Y. Guan, Y. Zhang, *ACS Omega* **2019**, *4*, 5650.
[62] C. E. Hoyle, C. N. Bowman, *Angew. Chem., Int. Ed.* **2010**, *49*, 1540.
[63] N. B. Cramer, J. P. Scott, C. N. Bowman, *Macromolecules* **2002**, *35*, 5361.
[64] a) H. Lu, J. A. Carioscia, J. W. Stansbury, C. N. Bowman, *Dent. Mater.* **2005**, *21*, 1129; b) S. C. Ligon-Auer, M. Schwentenwein, C. Gorsche, J. Stampfl, R. Liska, *Polym. Chem.* **2016**, *7*, 257.
[65] a) N. B. Cramer, T. Davies, A. K. O'Brien, C. N. Bowman, *Macromolecules* **2003**, *36*, 4631; b) Y. W. Yi, V. Khire, C. N. Bowman, J. E. Maclennan, N. A. Clark, *J. Appl. Phys.* **2008**, *103*, 093518.
[66] V. S. Khire, Y. Yi, N. A. Clark, C. N. Bowman, *Adv. Mater.* **2008**, *20*, 3308.
[67] a) J. F. Ashley, N. B. Cramer, R. H. Davis, C. N. Bowman, *Lab Chip* **2011**, *11*, 2772; b) C. F. Carlborg, T. Haraldsson, K. Öberg, M. Malkoch, W. van der Wijngaart, *Lab Chip* **2011**, *11*, 3136; c) A. S. Quick, J. Fischer, B. Richter, T. Pauloehrl, V. Trouillet, M. Wegener, C. Barner-Kowollik, *Macromol. Rapid Commun.* **2013**, *34*, 335; d) T. Griesser, A. Wolfberger, U. Daschiel, V. Schmidt, A. Fian, A. Jerrar, C. Teichert, W. Kern, *Polym. Chem.* **2013**, *4*, 1708; e) A. R. Davis, K. R. Carter, *Macromolecules* **2015**, *48*, 1711; f) P. M. Kharkar, M. S. Rehmann, K. M. Skeens, E. Maverakis, A. M. Kloxin, *ACS Biomater. Sci. Eng.* **2016**, *2*, 165; g) M. M. Zieger, P. Müller, E. Blasco, C. Petit, V. Hahn, L. Michalek, H. Mutlu, M. Wegener, C. Barner-Kowollik, *Adv. Funct. Mater.* **2018**, *28*, 1801405.
[68] B. D. Fairbanks, T. F. Scott, C. J. Kloxin, K. S. Anseth, C. N. Bowman, *Macromolecules* **2009**, *42*, 211.
[69] H. Y. Park, C. J. Kloxin, T. F. Scott, C. N. Bowman, *Macromolecules* **2010**, *43*, 10188.
[70] a) A. B. Lowe, C. E. Hoyle, C. N. Bowman, *J. Mater. Chem.* **2010**, *20*, 4745; b) M. Lomba, L. Oriol, R. Alcalá, C. Sánchez, M. Moros, V. Grazú, J. Luis Serrano, J. M. de la Fuente, *Macromol. Biosci.* **2011**, *11*, n/a; c) D. Martella, C. Parmeggiani, D. S. Wiersma, M. Piñol, L. Oriol, *J. Mater. Chem. C* **2015**, *3*, 9003; d) H. Peng, C. Wang, W. Xi, B. A. Kowalski, T. Gong, X. Xie, W. Wang, D. P. Nair, R. R. McLeod, C. N. Bowman, *Chem. Mater.* **2014**, *26*, 6819; e) Z. Liu, J. Ou, H. Lin, H. Wang, Z. Liu, J. Dong, H. Zou, *Anal. Chem.* **2014**, *86*, 12334; f) R. Cervera-Procas, C. Sánchez-Somolinos, J. L. Serrano, A. Omenat, *Macromol. Rapid Commun.* **2013**, *34*, 498.
[71] J. A. Norton, *Chem. Rev.* **1942**, *31*, 319.
[72] Y.-L. Liu, T.-W. Chuo, *Polym. Chem.* **2013**, *4*, 2194.
[73] B. J. Adzima, C. J. Kloxin, C. A. DeForest, K. S. Anseth, C. N. Bowman, *Macromol. Rapid Commun.* **2012**, *33*, 2092.
[74] T. Gruendling, K. K. Oehlenschlaeger, E. Frick, M. Glassner, C. Schmid, C. Barner-Kowollik, *Macromol. Rapid Commun.* **2011**, *32*, 807.
[75] a) B. Richter, T. Pauloehrl, J. Kaschke, D. Fichtner, J. Fischer, A. M. Greiner, D. Wedlich, M. Wegener, G. Delaittre, C. Barner-Kowollik, M. Bastmeyer, *Adv. Mater.* **2013**, *25*, 6117; b) A. S. Quick, H. Rothfuss, A. Welle, B. Richter, J. Fischer, M. Wegener, C. Barner-Kowollik, *Adv. Funct. Mater.* **2014**, *24*, 3571; c) E. Blasco, B. Yameen, A. S. Quick, P. Krolla-Sidenstein, A. Welle, M. Wegener, C. Barner-Kowollik, *Macromolecules* **2015**, *48*, 8718; d) T. K. Claus, B. Richter, V. Hahn, A. Welle, S. Kayser, M. Wegener, M. Bastmeyer, G. Delaittre, C. Barner-Kowollik, *Angew. Chem.* **2016**, *128*, 3882; e) A. Kerbs, P. Mueller, M. Kaupp, I. Ahmed, A. S. Quick, D. Abt, M. Wegener, C. M. Niemeyer, C. Barner-Kowollik, L. Fruk, *Chem. Eur. J.* **2017**, *23*, 4990.
[76] H. J. Levinson, *Principles of Lithography*, SPIE, Bellingham, WA **2011**.
[77] L. Li, X. Liu, S. Pal, S. Wang, C. K. Ober, E. P. Giannelis, *Chem. Soc. Rev.* **2017**, *46*, 4855.
[78] G. E. Moore, *Electron* **1965**, *38*, 114.
[79] B. J. Lin, *Optical Lithography: Here Is Why*, SPIE, Bellingham, WA **2011**.
[80] M. Dusa, B. Arnold, A. Fumar-Pici, in *Proc. IEEE Int. Symp. Semiconductor Manufturing (ISSM 2005)*, IEEE, San Jose, CA, USA, September **2005**, p. 177.
[81] M. D. Levenson, N. S. Viswanathan, R. A. Simpson, *IEEE Trans. Electron Devices* **1982**, *29*, 1828.
[82] R. van Es, M. A. van de Kerkhof, A. W. E. Minnaert, G. Fisser, J. W. de Klerk, J. Smits, R. Moors, E. Verhoeven, L. Levasier, R. Peeters, M. Pieters, H. Meiling, *Proc. SPIE* **2018**, *10583*, 105830H.
[83] a) J. M. Shaw, J. D. Gelorme, N. C. LaBianca, W. E. Conley, S. J. Holmes, *IBM J. Res. Dev.* **1997**, *41*, 81; b) M. Hepher, H. M. Wagner, *US Patent 2* 852 379, **1955**; c) W. M. Moreau, *Semiconductor Lithography. Principles, Practices, and Materials*, Plenum, New York **1988**.
[84] I. A. Barker, A. P. Dove, *Chem. Commun.* **2013**, *49*, 1205.
[85] A. D. Campo, C. Greiner, *J. Micromech. Microeng.* **2007**, *17*, R81.
[86] a) J. M. J. Frechet, H. Ito, C. G. Willson, *Proc. Microcircuit Eng.* **1982**, *82*, 260; b) H. Ito, C. G. Willson, *Polym. Eng. Sci.* **1983**, *23*, 1012.
[87] a) T. Fujii, S. Matsumaru, T. Yamada, Y. Komuro, D. Kawana, K. Ohmori, *Proc. SPIE* **2016**, *9776*, 97760Y; b) T. Nagai, H. Nakagawa, T. Naruoka, S. Tagawa, A. Oshima, S. Nagahara, G. Shiraishi, K. Yoshihara, Y. Terashita, Y. Minekawa, E. Buitrago, Y. Ekinci, O. Yildirim, M. Meeuwissen, R. Hoefnagels, G. Rispens, C. Verspaget, R. Maas, *Proc. SPIE* **2016**, *9779*, 977908.
[88] a) D. P. Green, V. Jain, B. Bailey, M. Wagner, M. B. Clark, D. Valeri, S. Lakso, *Proc. SPIE* **2013**, *8679*, 867912; b) L. Li, S. Chakrabarty, J. Jiang, B. Zhang, C. Ober, E. P. Giannelis, *Nanoscale* **2016**, *8*, 1338.
[89] a) H. H. Gatzen, V. Saile, J. Leuthold, *Micro and Nano Fabrication*, Springer, Berlin, Germany **2015**; b) S. Franssila, *Introduction to Microfabrication*, Wiley, Chichester, UK **2010**; c) S. Cabrini, S. Kawata, *Nanofabrication Handbook*, CRC, Boca Raton, FL **2012**.
[90] J. C. Love, D. B. Wolfe, H. O. Jacobs, G. M. Whitesides, *Langmuir* **2001**, *17*, 6005.

© 2019 The Authors. Published by WILEY-VCH Verlag GmbH & Co. KGaA, Weinheim

[91] a) D. C. Duffy, J. C. McDonald, O. J. A. Schueller, G. M. Whitesides, *Anal. Chem.* **1998**, *70*, 4974; b) E. Mitri, G. Birarda, L. Vaccari, S. Kenig, M. Tormen, G. Grenci, *Lab Chip* **2014**, *14*, 210; c) D. I. Walsh III, D. S. Kong, S. K. Murthy, P. A. Carr, *Trends Biotechnol.* **2017**, *35*, 383; d) D. Ha, J. Hong, H. Shin, T. Kim, *Lab Chip* **2016**, *16*, 4296; f) D. Liu, D. J. Broer, *Langmuir* **2014**, *30*, 13499.
[92] a) H. Zappe, *Fundamentals of Micro-Optics*, 1st ed., Cambridge University Press, Cambridge, UK **2010**; b) E. Peeters, J. Lub, J. A. M. Steenbakkers, D. J. Broer, *Adv. Mater.* **2006**, *18*, 2412; c) B. van der Zande, C. Doornkamp, S. J. Roosendaal, J. Steenbakkers, A. O. Hoog, J. Osenga, J. J. Van Glabbeek, L. Stofmeel, J. Lub, M. Shibazaki, K. Asahara, T. Inada, M. Yoshiga, S. Kawata, *J. SID* **2005**, *13*, 627; d) J. Lub, D. J. Broer, R. T. Wegh, E. Peeters, B. M. I. van der Zande, *Mol. Cryst. Liq. Cryst.* **2005**, *429*, 77; e) C. de Witz, D. J. Broer, *Polym. Prepr. (Am. Chem. Soc., Div. Polym. Chem.)* **2003**, *44*, 236; f) C. Sánchez, B. J. de Gans, D. Kozodaev, A. Alexeev, M. J. Escuti, C. van Heesch, T. Bel, U. S. Schubert, C. W. M. Bastiaansen, D. J. Broer, *Adv. Mater.* **2005**, *17*, 2567.
[93] J. Patterson, M. M. Martino, J. A. Hubbell, *Mater. Today* **2010**, *13*, 14.
[94] N. M. Alves, I. Pashkuleva, R. L. Reis, J. F. Mano, *Small* **2010**, *6*, 2208.
[95] C. M. Kirschner, K. S. Anseth, *Small* **2013**, *9*, 578.
[96] a) S. Nemir, H. N. Hayenga, J. L. West, *Biotechnol. Bioeng.* **2010**, *105*, 636; b) R. A. Marklein, J. A. Burdick, *Soft Matter* **2010**, *6*, 136.
[97] a) P. A. Janmey, R. T. Miller, *J. Cell Sci.* **2011**, *124*, 9; b) O. Chaudhuri, S. T. Koshy, C. Branco da Cunha, J.-W. Shin, C. S. Verbeke, K. H. Allison, D. J. Mooney, *Nat. Mater.* **2014**, *13*, 970.
[98] a) S. A. Fisher, P. N. Anandakumaran, S. C. Owen, M. S. Shoichet, *Adv. Funct. Mater.* **2015**, *25*, 7163; b) A. D. Arya, P. M. Hallur, A. G. Karkisaval, A. Gudipati, S. Rajendiran, V. Dhavale, B. Ramachandran, A. Jayaprakash, N. Gundiah, A. Chaubey, *ACS Appl. Mater. Interfaces* **2016**, *8*, 22005; c) K. Uto, J. H. Tsui, C. A. DeForest, D.-H. Kim, *Prog. Polym. Sci.* **2017**, *65*, 53; d) E. R. Ruskowitz, C. A. DeForest, *Nat. Rev. Mater.* **2018**, *3*, 17087.
[99] a) J. Kim, J. A. Hanna, M. Byun, C. D. Santangelo, R. C. Hayward, *Science* **2012**, *335*, 1201; b) D. Liu, C. W. M. Bastiaansen, J. M. J. den Toonder, D. J. Broer, *Soft Matter* **2013**, *9*, 588.
[100] Z. L. Wu, M. Moshe, J. Greener, H. Therien-Aubin, Z. Nie, E. Sharon, E. Kumacheva, *Nat. Commun.* **2013**, *4*, 1586.
[101] M. E. Sousa, D. J. Broer, C. W. M. Bastiaansen, L. B. Freund, G. P. Crawford, *Adv. Mater.* **2006**, *18*, 1842.
[102] a) D. Liu, C. W. M. Bastiaansen, J. M. J. den Toonder, D. J. Broer, *Angew. Chem., Int. Ed.* **2012**, *51*, 892; b) D. Liu, *Liq. Cryst.* **2016**, *43*, 2136.
[103] a) M. Campbell, D. N. Sharp, M. T. Harrison, R. G. Denning, A. J. Turberfield, *Nature* **2000**, *404*, 53; b) S. Yang, M. Megens, J. Aizenberg, P. Wiltzius, P. M. Chaikin, W. B. Russel, *Chem. Mater.* **2002**, *14*, 2831.
[104] a) J. De Boor, N. Geyer, U. Gösele, V. Schmidt, *Opt. Lett.* **2009**, *34*, 1783; b) M. Vala, J. Homola, *Opt. Express* **2014**, *22*, 18778.
[105] a) T. Y. M. Chan, O. Toader, S. John, *Phys. Rev. E* **2006**, *73*, 2736; b) Y. Lin, A. Harb, D. Rodriguez, K. Lozano, D. Xu, K. P. Chen, *Opt. Express* **2008**, *16*, 9165.
[106] S. Behera, M. Kumar, J. Joseph, *Opt. Lett.* **2016**, *41*, 1893.
[107] D. A. Bacon-Brown, P. V. Braun, *Adv. Opt. Mater.* **2018**, *6*, 1701049.
[108] I. Wathuthanthri, Y. Liu, K. Du, W. Xu, C.-H. Choi, *Adv. Funct. Mater.* **2013**, *23*, 608.
[109] R. H. Siddique, R. Hünig, A. Faisal, U. Lemmer, H. Hölscher, *Opt. Mater. Express* **2015**, *5*, 996.
[110] H. Ning, J. H. Pikul, R. Zhang, X. Li, S. Xu, J. Wang, J. A. Rogers, W. P. King, P. V. Braun, *Proc. Natl. Acad. Sci. USA* **2015**, *112*, 6573.
[111] a) H. C. Jeon, S.-G. Park, S. Cho, S.-M. Yang, *J. Mater. Chem.* **2012**, *22*, 23650; b) S. Bagheri, N. Strohfeldt, F. Sterl, A. Berrier, A. Tittl, H. Giessen, *ACS Sens.* **2016**, *1*, 1148.
[112] N. Jiang, H. Butt, Y. Montelongo, F. Liu, S. Afewerki, G. L. Ying, Q. Dai, S. H. Yun, A. K. Yetisen, *Adv. Funct. Mater.* **2018**, *28*, 1702715.
[113] a) S.-G. Park, S.-K. Lee, J. H. Moon, S.-M. Yang, *Lab Chip* **2009**, *9*, 3144; b) L. L. Yuan, P. R. Herman, *Sci. Rep.* **2016**, *6*, 1; c) J. Park, K.-I. Kim, K. Kim, D.-C. Kim, D. Cho, J. H. Lee, S. Jeon, *Adv. Mater.* **2015**, *27*, 8000.
[114] a) B. Richards, E. Wolf, *Proc. R. Soc. London, Ser. A* **1959**, *253*, 358; b) R. Dorn, S. Quabis, G. Leuchs, *Phys. Rev. Lett.* **2003**, *91*, 358.
[115] G. A. Lester, S. J. Coulston, A. M. Strudwick, *Appl. Opt.* **2006**, *45*, 110.
[116] a) J. S. Miller, M. I. Béthencourt, M. Hahn, T. R. Lee, J. L. West, *Biotechnol. Bioeng.* **2006**, *93*, 1060; b) M. G. Ivan, J.-B. Vaney, D. Verhaart, E. Meinders, *Proc. SPIE* **2009**, *7271*, 72711S.
[117] a) M. S. Hahn, J. S. Miller, J. L. West, *Adv. Mater.* **2005**, *17*, 2939; b) M. Lomba, L. Oriol, C. Sánchez, V. Grazú, B. S. Gutiérrez, J. L. Serrano, J. M. De la Fuente, *Carbohydr. Polym.* **2012**, *90*, 419; c) M. Lomba, L. Oriol, C. Sánchez-Somolinos, V. Grazú, M. Moros, J. L. Serrano, J. Martínez De la Fuente, *React. Funct. Polym.* **2013**, *73*, 499; d) A. Concellón, L. Asín, S. González-Lana, J. M. de la Fuente, C. Sánchez-Somolinos, M. Piñol, L. Oriol, *Polymer* **2017**, *117*, 259.
[118] C. W. Hull, *US Patent 4 575 330*, **1986**.
[119] K. C. Hribar, P. Soman, J. Warner, P. Chung, S. Chen, *Lab Chip* **2014**, *14*, 268.
[120] J. R. Tumbleston, D. Shirvanyants, N. Ermoshkin, R. Janusziewicz, A. R. Johnson, D. Kelly, K. Chen, R. Pinschmidt, J. P. Rolland, A. Ermoshkin, E. T. Samulski, J. M. DeSimone, *Science* **2015**, *347*, 1349.
[121] B. E. Kelly, I. Bhattacharya, H. Heidari, M. Shusteff, C. M. Spadaccini, H. K. Taylor, *Science* **2019**, *363*, 1075.
[122] a) S. A. M. Tofail, E. P. Koumoulos, A. Bandyopadhyay, S. Bose, L. O'Donoghue, C. Charitidis, *Mater. Today* **2018**, *21*, 22; b) R. L. Truby, J. A. Lewis, *Nature* **2016**, *540*, 371; c) E. MacDonald, R. Wicker, *Science* **2016**, *353*, aaf2093; d) M. Hofmann, *ACS Macro Lett.* **2014**, *3*, 382; e) N. Bhattacharjee, C. Parra-Cabrera, Y. T. Kim, A. P. Kuo, A. Folch, *Adv. Mater.* **2018**, *30*, 1800001; f) A. Camposeo, L. Persano, M. Farsari, D. Pisignano, *Adv. Opt. Mater.* **2019**, *7*, 1800419.
[123] a) A. P. Zhang, X. Qu, P. Soman, K. C. Hribar, J. W. Lee, S. Chen, S. He, *Adv. Mater.* **2012**, *24*, 4266; b) R. Gauvin, Y.-C. Chen, J. W. Lee, P. Soman, P. Zorlutuna, J. W. Nichol, H. Bae, S. Chen, A. Khademhosseini, *Biomaterials* **2012**, *33*, 3824; c) V. B. Morris, S. Nimbalkar, M. Younesi, P. McClellan, O. Akkus, *Ann. Biomed. Eng.* **2017**, *45*, 286.
[124] K. Kim, A. Yeatts, D. Dean, J. P. Fisher, *Tissue Eng., Part B* **2010**, *16*, 523.
[125] F. P. W. Melchels, J. Feijen, D. W. Grijpma, *Biomaterials* **2009**, *30*, 3801.
[126] S. Schüller-Ravoo, S. M. Teixeira, J. Feijen, D. W. Grijpma, A. A. Poot, *Macromol. Biosci.* **2013**, *13*, 1711.
[127] C. Huang, L. Chen, *Adv. Mater.* **2016**, *28*, 8079.
[128] a) D. Y. Fozdar, P. Soman, J. W. Lee, L.-H. Han, S. Chen, *Adv. Funct. Mater.* **2011**, *21*, 2712; b) P. Soman, D. Y. Fozdar, J. W. Lee, A. Phadke, S. Varghese, S. Chen, *Soft Matter* **2012**, *8*, 4946.
[129] a) S. Tibbits, https://www.ted.com/talks/skylar_tibbits_the_emergence_of_4d_printing (accessed: February 2019); b) S. Tibbits, *Archit. Des.* **2014**, *84*, 116.
[130] L. Huang, R. Jiang, J. Wu, J. Song, H. Bai, B. Li, Q. Zhao, T. Xie, *Adv. Mater.* **2017**, *29*, 1605390.
[131] M. Zarek, M. Layani, I. Cooperstein, E. Sachyani, D. Cohn, S. Magdassi, *Adv. Mater.* **2016**, *28*, 4449.
[132] Q. Ge, A. H. Sakhaei, H. Lee, C. K. Dunn, N. X. Fang, M. L. Dunn, *Sci. Rep.* **2016**, *6*, 31110.
[133] a) *Multiphoton Lithography: Techniques, Materials, and Applications* (Eds.: J. Stampfl, R. Liska, A. Ovsianikov), Wiley-VCH, Weinheim, Germany **2016**. (b) C. Barner-Kowollik, M. Bastmeyer, E. Blasco,

© 2019 The Authors. Published by WILEY-VCH Verlag GmbH & Co. KGaA, Weinheim

G. Delaittre, P. Müller, B. Richter, M. Wegener, *Angew. Chem., Int. Ed.* **2017**, *56*, 15828.
[134] S. Kawata, H. B. Sun, T. Tanaka, K. Takada, *Nature* **2001**, *412*, 697.
[135] a) S. Maruo, O. Nakamura, S. Kawata, *Opt. Lett.* **1997**, *22*, 132.
[136] a) K. K. Seet, V. Mizeikis, S. Matsuo, S. Juodkazis, H. Misawa, *Adv. Mater.* **2005**, *17*, 541; b) S. Hengsbach, A. D. Lantada, *Smart Mater. Struct.* **2014**, *23*, 085033.
[137] a) J. Serbin, A. Egbert, A. Ostendorf, B. N. Chichkov, R. Houbertz, G. Domann, J. Schulz, C. Cronauer, L. Fröhlich, M. Popall, *Opt. Lett.* **2003**, *28*, 301; b) J. Serbin, A. Ovsianikov, B. Chichkov, *Opt. Express* **2004**, *12*, 5221.
[138] A. S. Quick, A. de los Santos Pereira, M. Bruns, T. Bückmann, C. Rodriguez-Emmenegger, M. Wegener, C. Barner-Kowollik, *Adv. Funct. Mater.* **2015**, *25*, 3735.
[139] D. Gräfe, A. Wickberg, M. M. Zieger, M. Wegener, E. Blasco, C. Barner-Kowollik, *Nat. Commun.* **2018**, *9*, 1.
[140] M. Deubel, G. von Freymann, M. Wegener, S. Pereira, K. Busch, C. M. Soukoulis, *Nat. Mater.* **2004**, *3*, 444.
[141] a) J.-J. Park, X. Bulliard, J. M. Lee, J. Hur, K. Im, J.-M. Kim, P. Prabhakaran, N. Cho, K.-S. Lee, S.-Y. Min, T.-W. Lee, S. Yong, D.-Y. Yang, *Adv. Funct. Mater.* **2010**, *20*, 2296; b) E. Blasco, J. Müller, P. Müller, V. Trouillet, M. Schön, T. Scherer, C. Barner-Kowollik, M. Wegener, *Adv. Mater.* **2016**, *28*, 3592.
[142] M. Hippler, E. D. Lemma, S. Bertels, E. Blasco, C. Barner-Kowollik, M. Wegener, M. Bastmeyer, *Adv. Mater.* **2019**, 1808110.
[143] A. Marino, G. Ciofani, C. Filippeschi, M. Pellegrino, M. Pellegrini, P. Orsini, M. Pasqualetti, V. Mattoli, B. Mazzolai, *ACS Appl. Mater. Interfaces* **2013**, *5*, 13012.
[144] a) P. Tayalia, C. R. MendonCa, T. Baldacchini, D. J. Mooney, E. Mazur, *Adv. Mater.* **2008**, *20*, 4494; b) A. M. Greiner, F. Klein, T. Gudzenko, B. Richter, T. Striebel, B. G. Wundari, T. J. Autenrieth, M. Wegener, C. M. Franz, M. Bastmeyer, *Biomaterials* **2015**, *69*, 121; c) A. Ovsianikov, S. Mühleder, J. Torgersen, Z. Li, X.-H. Qin, S. Van Vlierberghe, P. Dubruel, W. Holnthoner, H. Redl, R. Liska, J. Stampfl, *Langmuir* **2014**, *30*, 3787; d) X.-H. Qin, X. Wang, M. Rottmar, B. J. Nelson, K. Maniura-Weber, *Adv. Mater.* **2018**, *30*, 1705564; e) R. Y. Tam, L. J. Smith, M. S. Shoichet, *Acc. Chem. Res.* **2017**, *50*, 703.
[145] W. Zhang, P. Soman, K. Meggs, X. Qu, S. Chen, *Adv. Funct. Mater.* **2013**, *23*, 3226.
[146] H. Zeng, D. Martella, P. Wasylczyk, G. Cerretti, J.-C. G. Lavocat, C.-H. Ho, C. Parmeggiani, D. S. Wiersma, *Adv. Mater.* **2014**, *26*, 2319.
[147] M. Hippler, E. Blasco, J. Qu, M. Tanaka, C. Barner-Kowollik, M. Wegener, M. Bastmeyer, *Nat. Commun.* **2019**, *10*, 1.
[148] a) J. Haisma, M. Verheijen, K. vandenHeuvel, J. vandenBerg, *J. Vac. Sci. Technol. B* **1996**, *14*, 4124; b) M. Colburn, S. C. Johnson, M. D. Stewart, S. Damle, T. C. Bailey, B. Choi, M. Wedlake, T. B. Michaelson, S. V. Sreenivasan, J. G. Ekerdt, C. G. Willson, *Proc. SPIE* **1999**, *3676*, 379; c) M. C. Traub, W. Longsine, V. N. Truskett, *Annu. Rev. Chem. Biomol. Eng.* **2016**, *7*, 583.
[149] M. D. Austin, H. Ge, W. Wu, M. Li, Z. Yu, D. Wasserman, S. A. Lyon, S. Y. Chou, *Appl. Phys. Lett.* **2004**, *84*, 5299.
[150] P. Ruchhoeft, M. Colburn, B. Choi, H. Nounu, S. Johnson, T. Bailey, S. Damle, M. Stewart, J. Ekerdt, S. V. Sreenivasan, J. C. Wolfe, C. G. Willson, *J. Vac. Sci. Technol. B* **1999**, *17*, 2965.
[151] a) N. Kooy, K. Mohamed, L. T. Pin, O. S. Guan, *Nanoscale Res. Lett.* **2014**, *9*, 320; b) S. H. Ahn, L. J. Guo, *Adv. Mater.* **2008**, *20*, 2044; c) H. Yoshikawa, J. Taniguchi, G. Tazaki, T. Zento, *Microelectron. Eng.* **2013**, *112*, 273.
[152] S. C. Ligon, B. Husár, H. Wutzel, R. Holman, R. Liska, *Chem. Rev.* **2014**, *114*, 557.
[153] A. Mihi, F. J. Beck, T. Lasanta, A. K. Rath, G. Konstantatos, *Adv. Mater.* **2014**, *26*, 443.
[154] a) E. C. Hagberg, M. Malkoch, Y. Ling, C. J. Hawker, K. R. Carter, *Nano Lett.* **2007**, *7*, 233; b) H. Lin, X. Wan, X. Jiang, Q. Wang, J. Yin, *Adv. Funct. Mater.* **2011**, *21*, 2960.
[155] Y. Takabayashi, M. Hiura, H. Morohoshi, N. Kodachi, T. Hayashi, A. Kimura, T. Yoshida, K. Mishima, Y. Suzaki, J. Choi, *Proc. SPIE* **2017**, *10144*, 1014405.
[156] a) V. A. Schulte, M. Díez, M. Möller, M. C. Lensen, *Biomacromolecules* **2009**, *10*, 2795; b) J.-Y. Li, Y.-C. Ho, Y.-C. Chung, F.-C. Lin, W.-L. Liao, W.-B. Tsai, *Biofabrication* **2013**, *5*, 035003.
[157] M. Mühlberger, M. Rohn, J. Danzberger, E. Sonntag, A. Rank, L. Schumm, R. Kirchner, C. Forsich, S. Gorb, B. Einwögerer, E. Trappl, D. Heim, H. Schift, I. Bergmair, *Microelectron. Eng.* **2015**, *141*, 140.
[158] S. Choo, H.-J. Choi, H. Lee, *Mater. Lett.* **2014**, *121*, 170.
[159] M. Cottat, N. Lidgi-Guigui, I. Tijunelyte, G. Barbillon, F. Hamouda, P. Gogol, A. Aassime, J.-M. Lourtioz, B. Bartenlian, M. L. de la Chapelle, *Nanoscale Res. Lett.* **2014**, *9*, 623.
[160] S. Ahn, J. Yang, M. Miller, M. Ganapathisubramanian, M. Menezes, J. Choi, F. Xu, D. J. Resnick, S. V. Sreenivasan, *Proc. SPIE* **2013**, *8680*, 86800W.
[161] a) C.-H. Chuang, D.-M. Lu, P.-H. Wang, W.-Y. Lee, M. O. Shaikh, *Microsyst. Technol.* **2018**, *24*, 389; b) N. B. A. T. A. Yusof, J. Taniguchi, *Microelectron. Eng.* **2013**, *110*, 163.
[162] a) C. Battaglia, J. Escarré, K. Söderström, L. Erni, L. Ding, G. Bugnon, A. Billet, M. Boccard, L. Barraud, S. De Wolf, F.-J. Haug, M. Despeisse, C. Ballif, *Nano Lett.* **2011**, *11*, 661; b) F. Jiao, Q. Huang, W. Ren, W. Zhou, F. Qi, Y. Zheng, J. Xie, *Microelectron. Eng.* **2013**, *103*, 126; c) F. Back, M. Bockmeyer, E. Rudigier-Voigt, P. Löbmann, *Thin Solid Films* **2014**, *562*, 274; d) J.-Y. Chen, M.-H. Yu, C.-Y. Chang, Y.-H. Chao, K. W. Sun, C.-S. Hsu, *ACS Appl. Mater. Interfaces* **2014**, *6*, 6164.
[163] a) B. Derby, *Annu. Rev. Mater. Res.* **2010**, *40*, 395; b) J. Alamán, R. Alicante, J. Peña, C. Sánchez-Somolinos, *Materials* **2016**, *9*, 910.
[164] a) C. Clasen, P. M. Phillips, L. Palangetic, A. J. Vermant, *AIChE J.* **2012**, *58*, 3242; b) R. F. Day, E. J. Hinch, J. R. Lister, *Phys. Rev. Lett.* **1998**, *80*, 704.
[165] B. Derby, N. Reis, K. Seerden, P. S. Grant, J. Evans, *MRS Proc.* **2000**, *625*, 195.
[166] P. C. Duineveld, M. M. De Kok, M. Buechel, A. H. Sempel, K. A. H. Mutsaers, P. Van de Weijer, I. G. J. Camps, T. J. M. Van den Biggelaar, J. E. J. M. Rubingh, E. I. Haskal, *Proc. SPIE* **2002**, *4464*, 59.
[167] a) R. Bhola, S. Chandra, *J. Mater. Sci.* **1999**, *34*, 4883; b) C. D. Stow, M. G. Hadfield, *Proc. R. Soc. A* **1981**, *373*, 419.
[168] a) W. R. Cox, C. Guan, D. J. Hayes, *Proc. SPIE* **2000**, *3952*, 400; b) M.-W. Wang, D.-C. Pang, Y.-E. Tseng, C.-C. Tseng, *J. Taiwan Inst. Chem. Eng.* **2014**, *45*, 1049.
[169] a) L. Jacot-Descombes, M. R. Gullo, V. J. Cadarso, J. Brugger, *J. Micromech. Microeng.* **2012**, *22*, 074012; b) V. J. Cadarso, J. Perera-Nunez, L. Jacot-Descombes, K. Pfeiffer, U. Ostrzinski, A. Voigt, A. Llobera, G. Gruetzer, J. Brugger, *Opt. Express* **2011**, *19*, 18665; c) M. Blattmann, M. Ocker, H. Zappe, A. Seifert, *Opt. Express* **2015**, *23*, 24525; d) J. Y. Kim, C. Martin-Olmos, N. S. Baek, J. Brugger, *J. Mater. Chem. C* **2013**, *1*, 2152.
[170] a) T. Wolfer, P. Bollgruen, D. Mager, L. Overmeyer, J. G. Korvink, *Procedia Technol.* **2014**, *15*, 521; b) T. Wolfer, P. Bollgruen, D. Mager, L. Overmeyer, J. G. Korvink, *Mechatronics* **2016**, *34*, 119.
[171] a) P. Bollgruen, T. Wolfer, U. Gleissner, D. Mager, C. Megnin, L. Overmeyer, T. Hanemann, J. G. Korvink, *Flexible Printed Electron.* **2017**, *2*, 045003; b) J. Alamán, M. López-Valdeolivas, R. Alicante, F. J. Medel, J. Silva-Treviño, J. I. Peña, C. Sánchez-Somolinos, *J. Mater. Chem. C* **2018**, *6*, 3882.
[172] C. L. van Oosten, C. W. M. Bastiaansen, D. J. Broer, *Nat. Mater.* **2009**, *8*, 677.

 © 2019 The Authors. Published by WILEY-VCH Verlag GmbH & Co. KGaA, Weinheim

[173] a) N. Herzer, H. Guneysu, D. J. D. Davies, D. Yildirim, A. R. Vaccaro, D. J. Broer, C. W. M. Bastiaansen, A. P. H. J. Schenning, *J. Am. Chem. Soc.* **2012**, *134*, 7608; b) D. J. D. Davies, A. R. Vaccaro, S. M. Morris, N. Herzer, A. P. H. J. Schenning, C. W. M. Bastiaansen, *Adv. Funct. Mater.* **2013**, *23*, 2723; c) J. E. Stumpel, C. Wouters, N. Herzer, J. Ziegler, D. J. Broer, C. W. M. Bastiaansen, A. P. H. J. Schenning, *Adv. Opt. Mater.* **2014**, *2*, 459.

[174] a) B. G. Compton, J. A. Lewis, *Adv. Mater.* **2014**, *26*, 5930; b) D. J. Lorang, D. Tanaka, C. M. Spadaccini, K. A. Rose, N. J. Cherepy, J. A. Lewis, *Adv. Mater.* **2011**, *23*, 5055.

[175] a) J. R. Xavier, T. Thakur, P. Desai, M. K. Jaiswal, N. Sears, E. Cosgriff-Hernandez, R. Kaunas, A. K. Gaharwar, *ACS Nano* **2015**, *9*, 3109; b) A. Sydney Gladman, E. A. Matsumoto, R. G. Nuzzo, L. Mahadevan, J. A. Lewis, *Nat. Mater.* **2016**, *15*, 413; c) C. B. Highley, C. B. Rodell, J. A. Burdick, *Adv. Mater.* **2015**, *27*, 5075.

[176] L. Ouyang, C. B. Highley, C. B. Rodell, W. Sun, J. A. Burdick, *ACS Biomater. Sci. Eng.* **2016**, *2*, 1743.

[177] L. Ouyang, C. B. Highley, W. Sun, J. A. Burdick, *Adv. Mater.* **2017**, *29*, 1604983.

[178] K. Tian, J. Bae, S. E. Bakarich, C. Yang, R. D. Gately, G. M. Spinks, M. in het Panhuis, Z. Suo, J. J. Vlassak, *Adv. Mater.* **2017**, *29*, 1604827.

[179] a) C. P. Ambulo, J. J. Burroughs, J. M. Boothby, H. Kim, M. R. Shankar, T. H. Ware, *ACS Appl. Mater. Interfaces* **2017**, *9*, 37332; b) M. López-Valdeolivas, D. Liu, D. J. Broer, C. Sánchez-Somolinos, *Macromol. Rapid Commun.* **2018**, *39*, 1700710; c) A. Kotikian, R. L. Truby, J. W. Boley, T. J. White, J. A. Lewis, *Adv. Mater.* **2018**, *30*, 1706164.

[180] C. D. Modes, K. Bhattacharya, M. Warner, *Phys. Rev. E* **2010**, *81*, 6911091.

[181] a) M. Eich, J. H. Wendorff, B. Reck, H. Ringsdorf, *Makromol. Chem., Rapid Commun.* **1987**, *8*, 59; b) S. Hvilsted, F. Andruzzi, C. Kulinna, H. W. Siesler, P. S. Ramanujam, *Macromolecules* **1995**, *28*, 2172.

[182] a) K. Ichimura, Y. Suzuki, T. Seki, A. Hosoki, K. Aoki, *Langmuir* **1988**, *4*, 1214; b) W. M. Gibbons, P. J. Shannon, S.-T. Sun, B. J. Swetlin, *Nature* **1991**, *351*, 49.

[183] a) M. Schadt, H. Seiberle, A. Schuster, S. M. Kelly, *Jpn. J. Appl. Phys.* **1995**, *34*, 3240; b) V. G. Chigrinov, V. M. Kozenkov, H.-S. Kwok, *Photoalignment of Liquid Crystalline Materials: Physics and Applications*, Wiley, Chichester, UK **2008**.

[184] F. Moia, *Proc. SPIE* **2002**, *4677*, 194.

[185] a) Sh. D. Kakichashvili, *Opt. Spectrosk.* **1972**, *33*, 324; b) L. Nikolova, T. Todorov, *Opt. Acta: Int. J. Opt.* **1984**, *31*, 579.

[186] J. Kim, R. K. Komanduri, K. F. Lawler, M. J. Escuti, D. J. Kekas, *Appl. Opt.* **2012**, *51*, 4852.

[187] Y. Li, J. Kim, M. J. Escutii, *Appl. Opt.* **2012**, *51*, 8236.

[188] a) T. Todorova, L. Nikolova, *Opt. Lett.* **1992**, *17*, 358; b) M. J. Escuti, C. Oh, C. Sánchez, C. Bastiaansen, D. J. Broer, *Proc. SPIE* **2006**, *6302*, 630207.

[189] L. T. de Haan, C. Sánchez-Somolinos, C. M. W. Bastiaansen, A. P. H. J. Schenning, D. J. Broer, *Angew. Chem., Int. Ed.* **2012**, *51*, 12469.

[190] M. E. McConney, A. Martinez, V. P. Tondiglia, K. M. Lee, D. Langley, I. I. Smalyukh, T. J. White, *Adv. Mater.* **2013**, *25*, 5880.

[191] a) C. D. Modes, M. Warner, C. Sánchez-Somolinos, L. T. de Haan, D. Broer, *Phys. Rev. E* **2012**, *86*, 2975; b) C. D. Modes, M. Warner, C. Sánchez-Somolinos, L. T. de Haan, D. Broer, *Proc. R. Soc. A* **2013**, *469*, 20120631.

[192] L. T. de Haan, V. Gimenez-Pinto, A. Konya, T.-S. Nguyen, J. M. N. Verjans, C. Sánchez-Somolinos, J. V. Selinger, R. L. B. Selinger, D. J. Broer, A. P. H. J. Schenning, *Adv. Funct. Mater.* **2014**, *24*, 1251.

[193] H. Zeng, O. M. Wani, P. Wasylczyk, R. Kaczmarek, A. Priimagi, *Adv. Mater.* **2017**, *29*, 1701814.

[194] T. H. Ware, M. E. McConney, J. J. Wie, V. P. Tondiglia, T. J. White, *Science* **2015**, *347*, 982.

[195] S.-K. Ahn, T. H. Ware, K. M. Lee, V. P. Tondiglia, T. J. White, *Adv. Funct. Mater.* **2016**, *26*, 5819.

[196] a) T. H. Ware, Z. P. Perry, C. M. Middleton, S. T. Iacono, T. J. White, *ACS Macro Lett.* **2015**, *4*, 942; b) T. Guin, M. J. Settle, B. A. Kowalski, A. D. Auguste, R. V. Beblo, G. W. Reich, T. J. White, *Nat. Commun.* **2018**, *9*, 2531.

[197] K. Nickmans, A. P. H. J. Schenning, *Adv. Mater.* **2018**, *30*, 1703713.

[198] a) Y. Morikawa, S. Nagano, K. Watanabe, K. Kamata, T. Iyoda, T. Seki, *Adv. Mater.* **2006**, *18*, 883; b) H. Yu, T. Iyoda, T. Ikeda, *J. Am. Chem. Soc.* **2006**, *128*, 11010; c) Y. Morikawa, T. Kondo, S. Nagano, T. Seki, *Chem. Mater.* **2007**, *19*, 1540; d) S. Nagano, Y. Koizuka, T. Murase, M. Sano, Y. Shinohara, Y. Amemiya, T. Seki, *Angew. Chem., Int. Ed.* **2012**, *51*, 5884; e) M. Sano, S. Nakamura, M. Hara, S. Nagano, Y. Shinohara, Y. Amemiya, T. Seki, *Macromolecules* **2014**, *47*, 7178.

[199] K. Nickmans, G. M. Bögels, C. Sánchez-Somolinos, J. N. Murphy, P. Leclère, I. K. Voets, A. P. H. J. Schenning, *Small* **2017**, *13*, 1701043.

© 2019 The Authors. Published by WILEY-VCH Verlag GmbH & Co. KGaA, Weinheim